Inline Analytical Supported Process Development Towards Alternative Bio-based Plasticizers

Vom Promotionsausschuss der
Technischen Universität Hamburg

zur Erlangung des akademischen Grades

Doktor-Ingenieur (Dr.-Ing.)

genehmigte Dissertation

von

Robert Hiessl

aus

Karlsruhe

2021

1. Gutachter:	Prof. Dr. rer. nat. Andreas Liese
2. Gutachter:	Prof. Dr.-Ing. Kerstin Kuchta
Prüfungsvorsitz:	Prof. Dr.-Ing. Michael Schlüter

Tag der mündlichen Prüfung: 01.07.2021

First of all I would like to thank Prof. Andreas Liese for the opportunity to do my PhD at his institute and also his unlimited support during this time.

In addition, I would like to thank Prof. Kerstin Kuchta for reviewing my thesis as second examiner and Prof. Michael Schlüter for doing the examination chair.

Additionally, I am very grateful to my group leaders at the Institute of Technical Biocatalysis, Dr. Joscha Kleber, Dr. Christian Scherkus and Dr. Stefan Wahlefeld, for their critical review and all the discussions we had.

I also would like to thank the project partners at the University of Bielefeld, Prof. Harald Gröger, Dr. Carmen Plass and Niklas Adebar and also the project partners at the BASF, Dr. Rainer Otter, Dr. Angelika Langsch and Dr. Axel Grimm for the very good cooperation and the interesting project meetings.

Furthermore, I want to express my gratitude to all my students for their excellent work: Yvonne Schade, Sophie Wardin, Laura Vega Fernández, Sofia Chacón Vargas, Leon Hennecke, Jan-Ole Kundoch, Victoria Bueschler and Fernando Lopez Haro.

As well I want to thank Prof. Garabed Antranikian and Dr. Barbara Klippel from the Institute of Technical Microbiology for the cooperation regarding the screening of enzymes.

I also want to thank Dr. Claudia Engelmann and Frederic Perz for the nice discussions and ideas at or after work, Jannis Alexander Reich for his great support regarding Matlab and also the whole team at the Institute of Technical Biocatalysis for all the help during these years.

Concluding, I would like to say thank you to my family for their support throughout my studies in the north of Germany and finally to my wife Gesche for giving me motivation whenever needed.

Abstract

Polyvinyl chloride (PVC) is nowadays the third most applied polymer with approximately 41 million tons produced in 2017. Plasticizers are added to the PVC polymer to increase the flexibility. The most common class of plasticizers are *ortho*-phthalic acid esters (phthalates). In the last years, the application of some of the latter was restricted due to health concerns. Therefore, the need for non-harmful alternatives arises. Additionally, bio-based plasticizer are a promising approach, since these will decrease the overall carbon footprint of the plasticized polymer.

In this thesis, a three-step process is developed to produce bio-based plasticizers in a multi-gram scale using renewable resources as basis. Starting from 2-methylfuran and maleic acid anhydride, in a Diels-Alder reaction, a cyclic 6-membered ring intermediate for the plasticizing building block (1st step) is synthesized. This instable intermediate tends to undergo a *retro*-Diels-Alder reaction and need to be stabilized *via* hydrogenation prior to further reaction steps avoiding the backwards reaction (2nd step). In a 3rd step, the cyclic plasticizer building block was successfully esterified at its acid groups in *ortho*-position. Here, 2-ethylhexanol, a standard alcohol applied in the synthesis of various plasticizers, is used. Additionally, the applicability of more than 80 enzymes for a biocatalytic esterification step was investigated. Throughout this work, inline analytic was employed for the characterization of the respective reaction steps. In detail, Fourier-transformed Infrared spectroscopy (FTIR) equipped with Attenuated Total Reflection (ATR) probes was implemented. These probes enable a non-destructive analysis directly inside the reactor vessel. To derive the respective concentrations from the recorded vibrational spectra, chemometric models were developed. In this work, the Indirect Hard Modeling (IHM) as a physically motivated hard modeling approach was applied. Besides using these established inline analytical methods in terms of process characterization, the inline measured data were used to set up kinetic models describing the each single reaction step. For this reason, the inline data were fitted to inline measured concentration profiles yielding the respective reaction rate constants.

Concluding, in this thesis a promising approach for inline analytical-supported process development towards bio-based plasticizer is presented. Moreover, this approach can be transferred to other potential plasticizer candidates helping to reduce the time needed for the process development.

Zusammenfassung

Polyvinylchlorid (PVC) ist heute das dritthäufigste verwendete Polymer, von welchem im Jahr 2017 41 Millionen Tonnen weltweit produziert wurden. Für viele Anwendungen von PVC werden Weichmacher zugegeben, um die Flexibilität des PVC-Kunststoffs zu erhöhen. Die häufig verwendeten Weichmacher *ortho*-Phthalsäureester (Phthalate) zeigen jedoch auch negative Auswirkungen auf den menschlichen Organismus, weshalb deren Einsatz in den letzten Jahren gesetzlich eingeschränkt wurde. Hieraus ergibt sich der Bedarf an gesundheitlich unbedenklichen Alternativen, welche in dieser Arbeit mit dem Ansatz der Herstellung eines bio-basierten Weichmachers verbunden wurde um damit die CO_2-Bilanz von Weich-PVC zu verringern.

In dieser Arbeit wurde, beginnend bei Molekülen die aus nachwachsenden Rohstoffen hergestellt werden können, ein dreistufiger Herstellungsprozess von bio-basierten Weichmachern im Gramm-Maßstab entwickelt. Im ersten Schritt wird in einer reversiblen und lösungsmittelfreien Diels-Alder Reaktion aus 2-Methylfuran und Maleinsäure Anhydrid ein zyklischer 6-Ring-Grundbaustein synthetisiert. Dieses in Lösung zur *retro*-Diels-Alder Reaktion neigende Intermediat wurde im zweiten Schritt mittels Hydrierung stabilisiert. Im letzten Reaktionsschritt wurde dieser hydrierte Grundbaustein an den *ortho*-Säuregruppen mit dem Alkohol 2-Ethylhexanol erfolgreich Säure-katalysiert verestert. Parallel wurden mehr als 80 Enzyme als möglicher Biokatalysator für diese Veresterung untersucht. Die Charakterisierung der einzelnen Reaktionsschritte erfolgte mittels Inlineanalytik. Es wurde Fourier-Transformierte Infrarotspektroskopie (FTIR) mittels Sonden nach dem Prinzip der abgeschwächten Totalreflektion (ATR) im Reaktor für zerstörungsfreie, nicht-invasive *inline* Messungen implementiert. Aus den Schwingungs-Absorptionsspektren wurden mittels Indirect Hard Modeling (IHM), einem physikalisch motiviertem, chemometrischem Modellansatz, die entsprechenden Konzentrationen berechnet. Neben der Prozesscharakterisierung wurden die Inlinedaten auch zur Erstellung von kinetischen Modellen zur Beschreibung der einzelnen Reaktionsschritte verwendet.

Zusammenfassend stellt diese Arbeit einen vielversprechenden Ansatz zur inline-analytisch-unterstützten Prozessentwicklung hin zu einem bio-basierten Weichmacher vor. Der untersuchte Ansatz kann auf andere Weichmacherkandidaten übertragen werden und somit dabei helfen die Entwicklungsdauer der Prozesse zu reduzieren.

Content

List of Abbreviations and Symbols

Table 1: List of abbreviations used along with their meaning.

Abbreviation	Meaning
PVC	Polyvinyl chloride
GWP	Global warming potential
PLA	Polylactic acid
FTIR	Fourier-transformed infrared spectroscopy
ATR	Attenuated total reflection
IHM	Indirect Hard Modeling
VCM	Vinyl chloride monomer
PE	Polyethylene
PP	Polypropylene
PET	Polyethylene terephthalate
PC	Polycarbonate
DEHP	Diethylhexyl pthalate
NMR	Nuclear magnetic resonance
UV/VIS	Ultraviolet/visible
MIR	Middle infrared
NIR	Near infrared
GC	Gas chromatography
PLS	Partial least squares
RMSECV	Root mean square error of cross validation
RMSEP	Root mean square error of prediction
2MF	2-Methylfuran
MAA	Maleic acid anhydride
DAP	4-Methyl-3a,4,7,7a-tetrahydro-4,7-epoxyisobenzofuran-1,3-dione
HPLC	High performance liquid chromatography
NRTL	Non-random two-liquid model
IRM	Initial rate method
Pt	Platinum
Pd	Palladium
Rh	Rhodium
Ru	Ruthenium
Pd/C	Palladium on charcoal
2MeTHF	2-Methyltetrahydrofuran
BSA	Succinic acid anhydride
DAPH	4-Methylhexahydro-4,7-epoxyisobenzofuran-1,3-dione
2EH	2-Ethylhexanol
DAPHE	Bis(2-ethylhexyl)-1-methyl-7-oxabicyclo[2.2.1]heptane-2,3-dicarboxylate
DAPHME	Monoester of DAPH and 2EH
FID	Flame ionization detector
DoE	Design of experiments
RSM	Response surface design
GC-MS	Gas chromatography coupled with mass spectroscopy
EC	Enzyme class

Table 2: List of symbols used along with their meaning and respective unit.

Symbol	Meaning	Unit
A	Absorbance	arbitrary unit a.u.
$\boldsymbol{\lambda_0}$	Wavelength in vacuum	nm
n	Refractive index	-
$\tilde{\boldsymbol{\nu}}$	Wavenumber	cm^{-1}
w	Peak position	cm^{-1}
$\boldsymbol{\alpha}$	Maximum intensity	arbitrary unit a.u.
$\boldsymbol{\beta}$	Fractional parameter	-
$\boldsymbol{\gamma}$	Half width with half height	arbitrary unit a.u.
$\boldsymbol{\psi_i}$	IHM Model parameters	-
$\boldsymbol{\theta}$	Model parameter vector	-
j	Total number of measurements	-
$\boldsymbol{\hat{y}_i}$	Concentration measured with IR	$mol\ L^{-1}$
$\boldsymbol{y_i}$	Reference concentration	$mol\ L^{-1}$
x	Mass fraction	$g\ g^{-1}$
k	Reaction rate constant	dependent on reaction order
E_A	Energy of activation	$kJ\ mol^{-1}$
R	Universal gas constant	$J\ mol^{-1}\ K^{-1}$
T	Temperature	K or °C
$\boldsymbol{P_{obs}}$	Observed productivity	$mmol\ L^{-1}$
$\boldsymbol{P_{sp}}$	Specific productivity	$mmol\ L^{-1}\ g_{catalyst}^{-1}\ bar_{H2}^{-1}$
$\boldsymbol{S_{app}}$	Apparent selectivity	-
$\boldsymbol{X_{app}}$	Apparent conversion	-
t	time	min or s

List of Figures

List of Tables

1 Introduction

1.1 PVC and Plasticizers

1.1.1 PVC

Polyvinyl chloride (PVC) is an important amorphous and crystalline thermoplastic polymer with a broad range of applications, its structure is shown in Figure 1. PVC was first discovered by HENRI VICTOR REGNAULT in 1838. He synthesized the monomer vinyl chloride, which polymerized by the exposure to sunlight. The same was observed by EUGEN BAUMANN in 1872. However, both of them did not continue their work. Later in 1912, the German chemist FRITZ KLATTE was able to claim the first patent on the polymerization of PVC using sunlight which can be seen as the starting point of the rise of PVC. In 1926, when the patent was expiring, WALDO SEMON started working for the rubber producer BF Goodrich. While trying to find a suitable adhesive binding rubber to metals, he was experimenting with PVC and different additives. Thereby, he found a soft and flexible polymer with outstanding properties. Together with Union Carbide, BF Goodrich produced the first products PVC in a commercial scale. This paved the way for today's third most applied polymer.

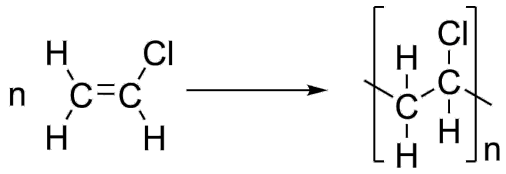

Figure 1: Synthesis of polyvinyl chloride (PVC) from vinyl chloride monomers (VCM).

PVC is produced by radical polymerization starting from vinyl chloride monomers (VCM) in reactors up to 200 m³ (Wypych, 2017). Mostly, suspension polymerization is applied, yielding particles with a size of 100 to 180 µm, similar compared to mass polymerization. Besides suspension and mass (or bulk) polymerization, the reaction can also be performed in emulsion leading to much smaller particle sizes of 0.1 – 3.0 µm. The radical polymerization is started by addition of an initiator or by free radicals (Allsopp, Vianello, 2010). As initiator, often peroxides, like for examples di-benzoyl peroxides are applied (Búcsi, Szőcs, 2000). Beside peroxides, also azo components can be applied (Braun, 2005). The reaction is highly exothermic, with 1540 kJ kg^{-1} heat of reaction released and is usually carried out between 35 and 70 °C, depending on the chain length desired (Semeijn, Schur, 2020). In most cases, the heat removal from the reactor determines the reaction rate (Wypych, 2017). After the chain

length exceeds six VCM, the polymer becomes insoluble and starts precipitating from the reaction solution (Allsopp, Vianello, 2010).

Already in the 1930s, a broad range of products was produced from PVC. The production capacity increased fast and today PVC is the third most used polymer after polyethylene (PE) and polypropylene (PP). In the year 2017, 41 million tons of PVC were produced worldwide, the capacities are still increasing with about 4% per year (Wypych, 2017). In the same year, only about 16 million tons of waste PVC were generated. This difference can be explained with many long-lasting applications of this polymer (Geyer, 2020).

Today a large number of different products is made of PVC, like for example piping, floorings, flame resistant coatings or shower curtains, but also cables, rubber boots or blood bags are available. About two thirds of the PVC produced are applied for construction purposes (pipings, roofing, cables), the remaining third is used for example for medical single use equipment or packaging foils (Geyer, 2020).

In Figure 2, the Global Warming Potential (GWP) for different polymers is visualized by the relative size of the respective carbon footprint. For one kg of PVC, about 2.6 kg of CO_2 equivalents are produced, which is lower compared to other fossil-based polymers, like for example PE, polyethylene terephthalate (PET) and polycarbonate (PC). Only for bio-based solutions like polylactic acid (PLA), lower amounts of CO_2 (2.2 kg CO_2 eq. kg^{-1} polymer) are generated during production and incineration after the products lifespan ended. The high difference in the GWP of PVC versus other fossil-based polymers, can partly be associated to the high amount of chlorine per mass within the polymer.

According to the Principles of Green Chemistry (Anastas, Zimmerman, 2003), and more recently also to the UN Sustainable Development Goals (United Nations, 2015), the production of polymers like PVC is crucial in a sustainable future. Besides using renewable resources, energy should be employed efficiently and generated waste should be recycled. In 2011, the VinylPlus® programme was started by the European PVC industry with the aim of increasing the polymers sustainability. Since then, the recycling PVC industry is growing every year, with about 770,000 tons of recycled PVC in 2019 (VinylPlus, 2020). In the same year, the company INOVYN launched the first fossil-free PVC produced from bio-based ethylene (INOVYN, 2019). Along with bio-based additives, this highlights the possibility to transfer this long-term, non-

biodegradable polymer into a circular economy with a further reduction of its carbon footprint.

Depending on the application of PVC, additives like heat stabilizers, lubricants and/or plasticizers are added to the polymer to obtain certain PVC properties. By the addition of plasticizers, a soft and flexible product is obtained. The plasticizing mechanism and some industrial important examples are discussed in the next section.

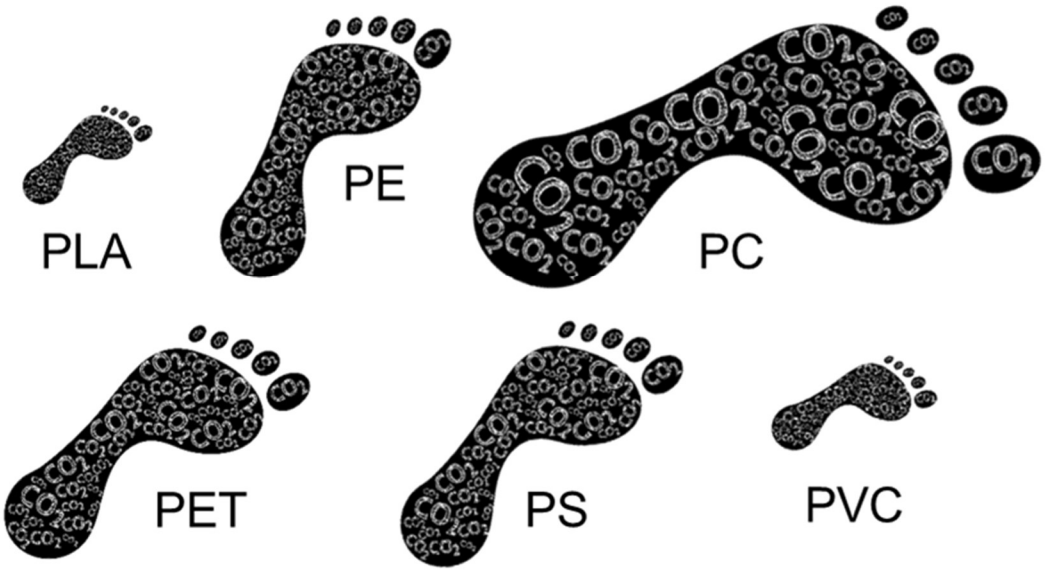

Figure 2: Global Warming Potential for various polymers after production and incineration. PLA: Polylactic acid: 2.2 kg CO_2 eq. kg^{-1} polymer; PE: Polyethylene 4.9 kg CO_2 eq. kg^{-1} polymer; PC: Polycarbonate 8.8 kg CO_2 eq. kg^{-1} polymer; PET: Polyethylene terephthalate 5.2 kg CO_2 eq. kg^{-1} polymer; PS: Polystyrene 5.1 kg CO_2 eq. kg^{-1} polymer; PVC: Polyvinyl chloride 2.6 kg CO_2 eq. kg^{-1} polymer. Numbers taken from Groot (Groot, Borén, 2010).

1.1.2 Plasticizers

Since the early beginning of the rise of PVC, plasticizers are applied for increasing the polymer's flexibility. In the first patent by FRIEDRICH KLATTE, different plasticizers were included (Wypych, 2015). However, these were not the earliest plasticizers mentioned. After the development of cellulose nitrate in 1846, ALEXANDER PARKES investigated the effect of cottonseed and castor oils within the cellulose nitrate and invented a new material, which was patented in 1865 and named Parkesine. The newly developed polymer was unstable, the plasticizers evaporated and the material was shrinking. In 1870, JOHN WESLEY HYATT was the first to patent camphor as plasticizer. Along with cellulose nitrate, the first large-scale plasticized polymer Celluloid was produced. 40 years later, the Celluloid Company launched a less flammable polymer made from

cellulose acetate and triphenyl phosphate as plasticizer. The fire retarding effect of phosphate based plasticizers is still applied nowadays, which is achieved already with 8 wt% within the polymer (Wilkes *et al.*, 2005).

Polymers can be plasticized in two different ways, internally or externally. Internal plasticizers are covalently bound to the monomer before polymerization and are therefore included in the produced copolymer. However, most commonly external plasticizers are used. These are mixed with the polymer to solvate the amorphous parts of the polymer (Daniels, 2009). A plasticizer changes the physico-mechanical properties of the polymer, which is brittle and stiff without their addition. First, they lower the glass transition temperature, describing the temperature at which amorphous polymers change from a hard and brittle state into a soft and viscous state. The plasticizer is partly solvating the polymer chains and therefore decreasing the friction and reducing the viscosity (Wypych, 2015).

The plasticizing mechanism was unclear during the development of these first examples of plasticized polymers. In the 50s of the last century, different theories were developed to describe the plasticization effect, which are summarized in Figure 3. The lubricity theory explains the obtained flexibility of the polymer by the plasticizer acting as molecular lubricant between the polymer chains. Non-plasticized polymer chains are expected to be unable to move freely. Another explanation was provided by the gel theory which states, that the polymer chains are loosely associated at varied intervals by weak secondary bonding forces, for example hydrogen bonds. Here, the plasticizer is increasing the flexibility between the loose chains. This theory can additionally describe the differences observed in external and internal plasticization. The free volume theory tries to explain the plasticizing effect along with the decrease of the glass transition temperature. When plasticizers are added into the polymer matrix, the volume is decreasing linearly until the glass transition temperature is reached. Below the glass transition temperature, this decrease in volume is slowed down. This reduction of the specific volume above the glass transition temperature is attributed to the free volume/space between the polymer chains (Daniels, 2009, Reinecke *et al.*, 2004).

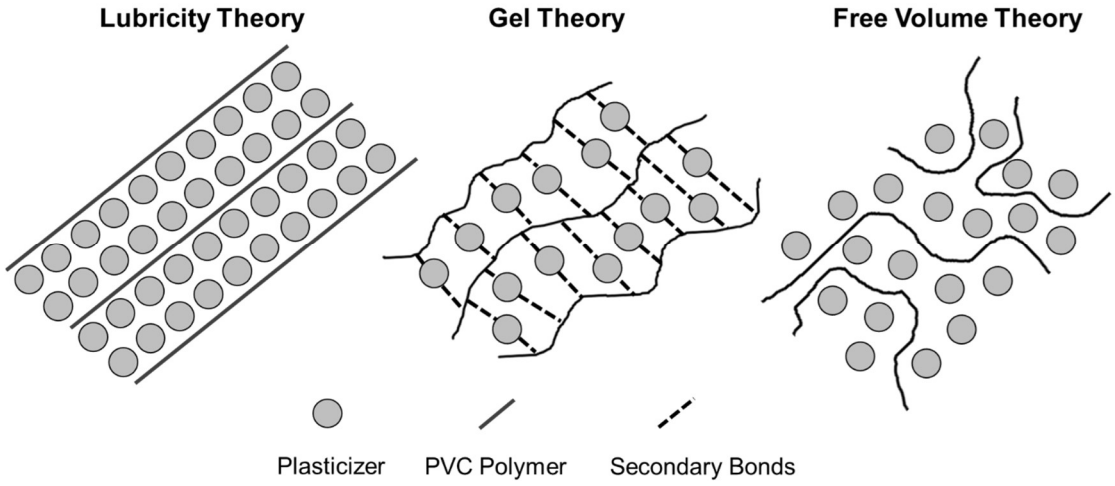

Figure 3: Schematic overview of different plasticization theories. Adapted from Bocqué (Bocqué et al., 2016).

Plasticizer consist of different building blocks: a compatibilizer is needed for granting stability and compability within the polymer. In the case of phthalates this is achieved by the aromatic ring. To ensure the plasticizer and the polymer are sticking together, polar ester groups are used as cohesive blocks. Furthermore, spacers are needed for increasing the distance between the polymer chains. Here, the aliphatic chains bound to the ester group are responsible for the increased flexibility (Bocqué *et al.*, 2016).

Today (2020), nearly 10 million tons of plasticizers are produced. A large variety of about 500 different plasticizer types is available. Between 80 and 90% of the produced plasticizers are applied for the production of soft/plasticized PVC (Kumar, 2019). Other important applications are found in the field of adhesives and sealants (Breitscheidel, 2013). The remaining are employed for applications like concrete (Nagrockiene *et al.*, 2013), paintings (Koleske *et al.*, 2012) or rocket fuels (Libardi *et al.*, 2009). Plasticizers can be classified depending on their chemical structure, which is shown in Figure 4.

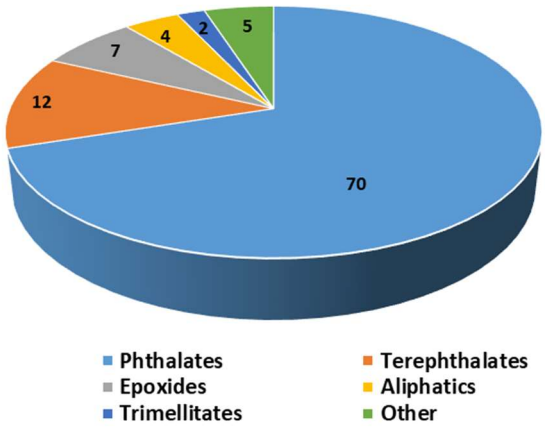

Figure 4: Plasticizer consumption in 2014 divided on their chemical structure, 8 million tons of plasticizers used in total (Tullo, 2015).

In 2014, with 70% the biggest share of plasticizers produced were (*ortho*-) phthalates. Besides, also terephthalates and epoxides are applied with higher amounts. The rest of the plasticizer market consist of trimellitates, aliphatics like cyclohexanoates or adipin-based and phosphate plasticizers. There are primary and secondary plasticizers available. The primary ones can be used without further additives, while the secondary can only be applied in conjunction with a primary one due to their limited compatibility, like in the case of epoxidized soy bean oil. Secondary plasticizers are mainly added for reasons of cost reductions and to improve certain performance properties (Sears *et al.*, 1985).

Plasticizers can not only be classified according to their chemical structure but also depending on the resources used for their synthesis (bio- or fossil-based) or their capability of being biodegraded. Another common grouping for different plasticizer is the differentiation between phthalates and non-phthalates (Wypych, 2017).

For the production of plasticized PVC products, mostly phthalates were employed in the past and are still a large fraction of all plasticizer applied. The most prominent example of this group is diethylhexylphthalate (DEHP), which was added in various soft PVC products, toys or packaging foils. Interestingly, besides its efficient plasticizing properties, an additional stabilizing effect of DEHP on red blood cells within blood bags made from PVC was shown (Melzak *et al.*, 2018). This allowed a significant increase of the storage time of the blood of up to 49 days (Lozano, Cid, 2013).

On the other side, DEHP and other plasticizers from the group of *ortho*-phthalates act as endocrine disruptor (Christen *et al.*, 2012). In addition, reproductive toxicity of certain phthalates was shown (Martino-Andrade, Chahoud, 2010). Due to these

concerns, the application of DEHP and various other phthalates was restricted in Europe (Erickson, 2018) as well in the US (Hogue, 2017). Therefore, the need for suitable substitutions showing similar good performance properties without posing health risks is clear.

After about 100 years of phthalates dominating the plasticizer market, especially in the last decades, a large variety of different new plasticizers rose in the focus of research and development. An example, produced at large scale, is Hexamoll® DINCH, which was developed as a replacement for DEHP. Its synthesis is based on a hydrogenation of diisononylphthalate yielding a cyclohexane backbone instead of the aromatic ring (Wadey, 2003). Recently, a new variety of Hexamoll® DINCH based on a renewable raw material basis using a biomass balance approach is available (BASF SE, 2021). This plasticizer is applied in different sensitive applications like food packaging or medical single use equipment (Umweltbundesamt, 2014). In the group of aliphatics, different plasticizers can also be prepared on the basis of renewable resources. Large effort was put into the development of new plasticizers based on epoxidized vegetable oils. Vegetable oils are obtained by extraction from the respective plants and, therefore, are an example for renewable resources. The unsaturated bonds in the fatty acids of the plant oil are epoxidized to obtain a bio-based plasticizer. Here, for example, soy bean (Jia *et al.*, 2016), sunflower (Bouchareb, Benaniba, 2008), linseed (Fenollar *et al.*, 2010) and broccoli (Audic *et al.*, 2014) can be used. However, their employment is facing the controversy of applying food based materials in the production of chemicals. Nevertheless, epoxidized castor oil from the castor oil plant, which is not cultivated as a food plant, can be applied as a plasticizer after epoxidation (Fu *et al.*, 2019). A further example of bio-based raw material is cardanol, a side product obtained from cashew nut production, which is not concurring with foods (Greco, Maffezzoli, 2016). Another bio-based example is citric acid produced fermentative in large scale, which is then further esterified to obtain different plasticizers. These citrate based products are regarded as safe and are in worldwide use (Jia *et al.*, 2018). Adipic acid can also be produced by fermentation on the basis of glucose using genetically modified yeast, yielding another building block for the synthesis of bio-based aliphatic plasticizers (Raj *et al.*, 2018).

Recently, the group of Hu *et al.* (Hu *et al.*, 2020) published a synthesis for a bio-based plasticizer conserving the cyclic structure of phthalates and cyclohexanoates with esters in 1,2-position. Their approach is similar to the one presented in this thesis and

consists of Diels-Alder reaction of fumarates and a diene, which is stabilized by subsequent hydrogenation established as a one pot reaction. The researchers investigated the toxicity, which revealed a possibly safe product. However, they did not check the plasticizing properties within their work.

1.2 Inline Analytics

1.2.1 Differentiation of in-, on-, at- and offline analytics

Different measurement methodologies can be classified according to the position where the measurement is performed within the process. A schematic overview is found in Figure 5 (Minnich *et al.*, 2016). Traditional sampling followed by workup (e.g. derivatization or dilution) and the analysis itself is called *offline* analytic. For example, gas chromatography (GC) or high performance liquid chromatograph (HPLC) is usually used offline. If the sampling unit is directly connected with the analytical device, this approach is called *atline*. The sample is processed automatically and transported to the measurement unit. Using a flow cell, analytic devices can be implemented in a bypass stream next to the reactor unit, which is then called *online*. Here, examples are flow-Nuclear Magnetic Resonance (NMR) (usually low field), ultraviolet/visible (*UV/VIS)* and Infrared (IR) spectroscopy.

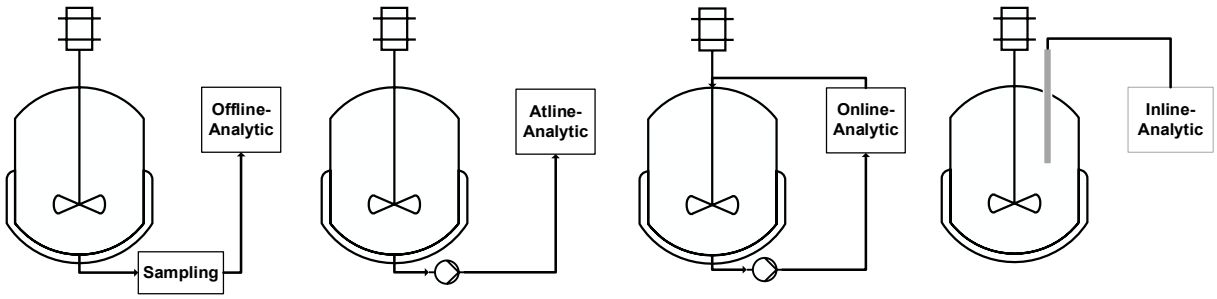

Figure 5: Differentiation of in-, on-, at- and offline measurements according to their position in the reactor setup.

Inline analytics are implemented directly inside of the reactor vessel applying a probe. The measurement is carried out automatically in distinct time intervals, which usually takes only some seconds. As the result, the signal can be evaluated directly, and, therefore also considered as control signal. A proven example of this methodology is a pH-probe, for example applied in fermentations, where the signal is directly coupled to a pump adding acid or base. More recently, probes for mid IR spectroscopy are available, with almost unlimited applications in organic synthesis (Hamminga *et al.*, 2004, Littler *et al.*, 2010, Roberge, Dubé, 2007).

1.2.2 Fourier-Transformed Infrared Spectroscopy

Within this work, Fourier-transformed Infrared (FTIR) Spectroscopy together with an Attenuated Total Reflection (ATR) probe is applied. In the following section the theoretical background of this measurement technique is introduced and the principle of ATR is explained.

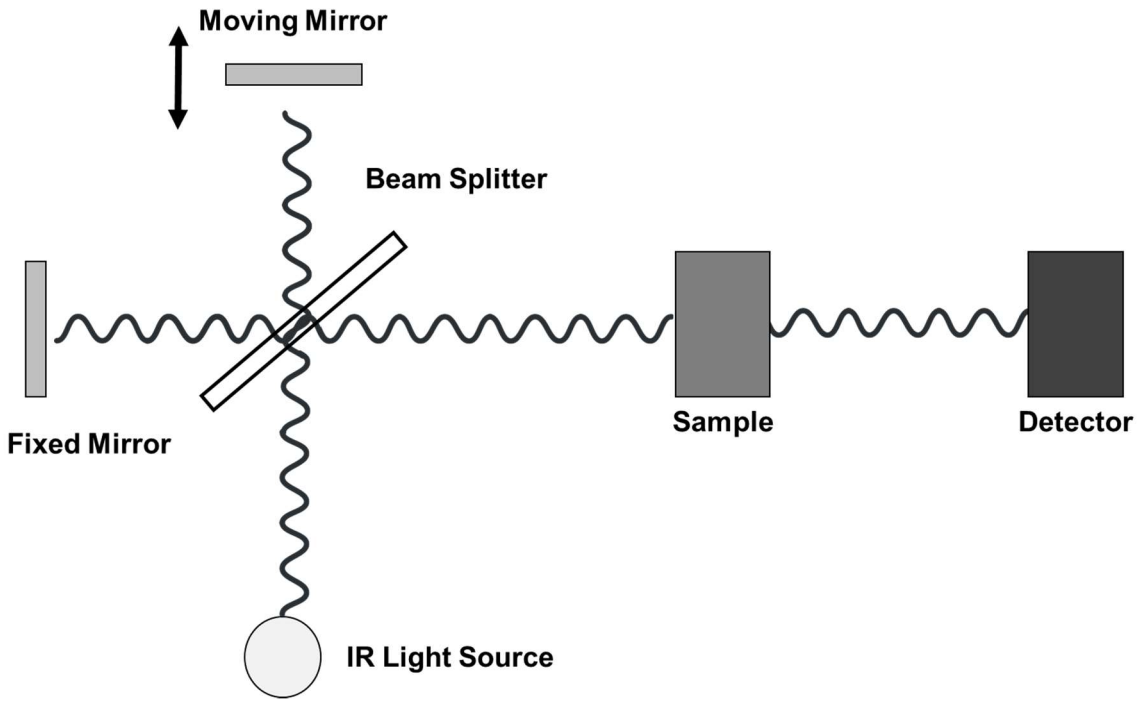

Figure 6: Schematic setup of a Michelson Interferometer. From a light source, a beam of Infrared light is impinging a beamsplitter. Half of the light beam is heading to a fixed mirror, the other half to movable mirror. Both light beams are then reflected and superimposed, passing the sample heading to the detector.

The central element of an FTIR spectrometer is the MICHELSON interferometer, which is shown in Figure 6. From a light source, an IR light beam is forwarded to a beamsplitter, where the light is split into two different beams. Half of the light is reflected to a fixed mirror, the other half to a movable mirror. Both beams are reflected backwards and are summed up again heading through the sample towards the detector. Depending on the interference of both light beams and the absorption of the IR light by the sample, an interferogram is obtained at the detector. By Fourier-transformation, from the interferogram, the absorbance at every wavenumber is obtained.

The analytical principle can be extended to applications according the ATR effect. In Figure 7, the ATR effect is shown schematically. An incoming light beam, transmitted

using optical fibers, is arriving at the tip of the ATR crystal with a critical angle Θ and is then reflected internally at the interface. While this internal reflection occurs, a part of the light is forming an evanescent wave, which is absorbed by the surrounding media. Beside the critical angle, also the refractive indices of both, the ATR crystal and the surrounding media influence the penetration depth, which is usually in the range of some micrometers. The penetration depth d_p can be calculated according to formula 1 (Averett *et al.*, 2008):

$$d_p = \frac{\lambda_0}{2\,\pi\, n_1 \sqrt{sin^2\,\theta - n_{21}}} \quad (1)$$

With λ_0 = wavelength in vacuum [m], n_1 = refractive index of the optically dense medium [-], n_{21} = ratio of n_1 and n_2 [-], θ angle of incidence [°].

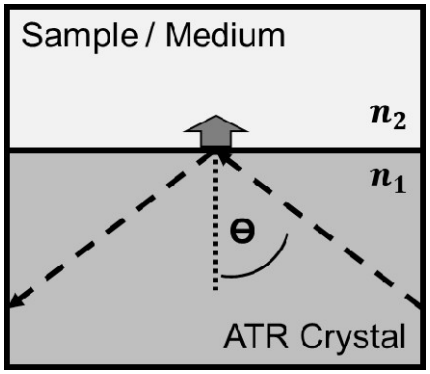

Figure 7: Principle of Attenuated Total Reflection (ATR).The incoming light beam is internally reflected for $\theta > \theta_{critical}$ and for $n_1 > n_2$. During internal reflection, an evanescent wave is formed penetrating into the media.

FTIR spectroscopy implemented with an ATR probe exhibits the advantage, that it is not affected by solids or bubbles, reliably measuring the liquid phase (Mueller *et al.*, 2011). Therefore, it is a highly suitable method for multiphasic reaction systems. The spectra obtained, especially in the fingerprint region are useful for discriminating between starting materials, intermediates and products formed. Here, organic systems show a lot of different, sharp absorbance patterns, which can be used for differentiation and quantification as well. Another advantage is the velocity of the measurements, which is usually in the range of some seconds.

There are spectrometers available, which can handle several ATR probes in parallel. By this approach, spatial profiles can be recorded over a reactor at different position giving a detailed insight into reactor characteristics (Sellin *et al.*, 2017). In the same manner, temporal profiles in a plug flow reactor are possible.

Downside of this measurement technology is the relative high price compared to long established methods like e.g. *UV/VIS*. The fibers needed for transmitting the IR light

from the spectrometer to the probe and back are made of silver halogenide, which is highly sensitive and results in fibers not as flexible as a glass fiber used for near infrared (NIR) spectroscopy probes.

1.2.3 Chemometric Modeling

IR spectroscopy is a relative measurement, therefore, a suitable calibration is required. Unlike to a dilution series performed for the calibration of a gas chromatography (GC) measurement, mostly a univariate peak integration is adequate. The FTIR absorption bands of components in chemical reactions often show overlaps making this classical approach of peak integration not applicable. Here, more sophisticated multivariate chemometric methods are applied. A large variety of different approaches is available. The most prominent example is the Partial Least Square (PLS) algorithm, which was already established in the 1980s. A more recent modeling approach is Indirect Hard Modeling, which is discussed in detail in this chapter.

For the quantification of offline measurements performed with for example a GC coupled with diode array detector, a simple calibration/dilution series is measured and the respective concentration is linked to the integrated peak area. This is called a *univariate* method. In contrast, for the analysis of the FTIR spectra a chemometric model is needed, which translates the spectral information into concentration data. The approach is called *multivariate*, because more than one variable is evaluated for the quantification. It can be further differentiated between soft and hard modeling approaches. Soft models are set up on a statistical basis, while hard models have a mechanistic background describing for example the spectra based on their shape.

The most common used multivariate, soft modeling method for the evaluation of spectroscopic data is probably the PLS algorithm that was presented by SVANTE WOLD (Wold *et al.*, 1983). In PLS, the data are projected to new coordinates, reducing the overall complexity of the system. The measured data are further correlated with one or more target values by a linear regression model. Along with the upcoming (NIR) spectroscopy, this technique was becoming the most applied standard chemometric method.

Today there are various applications of the PLS methods. For example, it was possible to use NIR spectra along with PLS modeling to determine the origin of olive oil samples

with high accuracy (Lin *et al.*, 2012). Beside such typical classification problems, PLS is also applied for the analysis of spectra recorded from reactive mixtures. KILLNER *et al*. were following the transesterification reaction of soy bean oil to biodiesel by means of NIR measurements. They trained their PLS model using additional NMR measurements and achieved low errors in the calibrated range (Killner *et al.*, 2011). In addition, PLS is also employed in different fields like for example genome analysis or in marketing (Kessler, 2008). However, complex reactive systems with a strong overlap in frequency positions and shifts of absorption bands are difficult to analyze using PLS models. Here, physically motivated hard models show an advantage over pure statistical black box models, due to the fact that band shifts and overlaps can be more easily integrated into the chemometric model.

An example for a mechanistic modeling approach is Indirect Hard Modeling (IHM), which was introduced in 2004 for the evaluation of especially MIR, Raman and NMR data (Alsmeyer *et al.*, 2004). In contrast to the statistical motivated soft models, for hard modeling a mathematical function is used for the description of the spectrum. In detail, the spectrum is modelled by superimposed VOIGT-profiles, which are a combination of GAUSS and LORENTZ peak shapes. Its mathematical representation is shown in equation 2:

$$V(\tilde{\nu}) = \beta\ \alpha\ exp\left[-\frac{4\ln(\tilde{\nu}-w^2)}{\gamma^2}\right] + (1-\beta)\ \alpha\frac{\gamma^2}{(\tilde{\nu}-w)^2+\gamma^2} \quad (2)$$

With $\tilde{\nu}$ = wavenumber [cm^{-1}], w = peak position [cm^{-1}], α = max intensity [a.u.], β = fractional [-] parameter, γ = half width at half height [cm^{-1}].

For every component present in the reaction mixture, a single pure component model is set up, based on the sum of the VOIGT-profiles describing the pure component spectra:

$$A\ (\tilde{\nu}, \theta) = \sum_{i=1}^{I} V_i\ (\tilde{\nu},\ \psi_i) \quad (3)$$

With model parameters $\psi_i = (w_i, \gamma_i, \alpha_i, \beta_i)$ and model parameter vector $\theta = (\psi_1^T, \dots, \psi_I^T)$.

These pure component models are further fitted into a mixture spectrum. Different degrees of freedom can be integrated in this step, allowing for example peaks and baseline shifts or shape changes. In the last step, the IHM is calibrated using suitable reference data. By fitting the IHM onto spectra with known compositions, weights for the single pure component models are determined. This yields the calibration of the chemometric model. The calibration in the IHM approach is, unlike to PLS, a univariate

regression: the determined weights of the hard model are directly correlated with the concentrations. The workflow of the modeling process is schematically summarized in Figure 8.

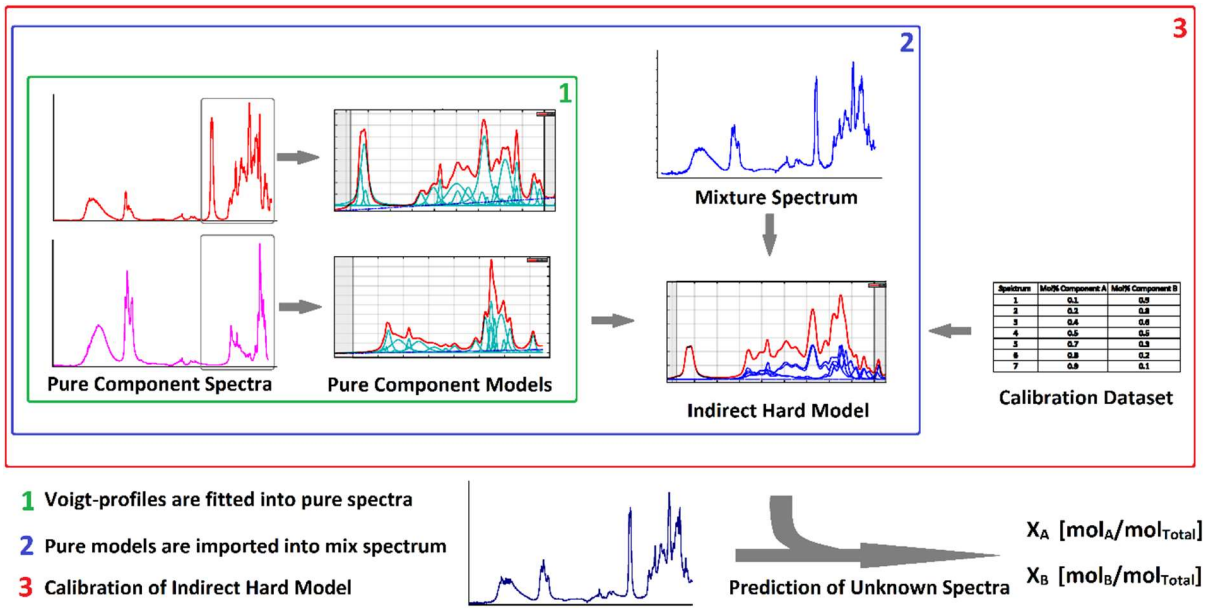

Figure 8: Workflow for setting up chemometric models using Indirect Hard Modeling (IHM) (Hiessl, 2016).

To set up the pure component, the respective compounds should be available in high purity. If in a mixture, one compound is unknown, the unknown spectrum can be deduced from the mixture as well as the known pure component spectrum using the IHM approach (Kriesten *et al.*, 2008). This modeling approach displays advantages compared to other chemometric methods: IHM is able to extrapolate from the calibrated range of the model. Additionally, a robust model can be created using only few calibration data. In comparison, for a PLS model describing the same reaction system, much more calibration data covering a broader range would be necessary to achieve the same preciseness and accuracy.

During the calibration, the error of the respective chemometric model is required to be determined. This is usually performed by cross validation. This means, one calibration measurement is excluded, the model is calibrated and in the next step the left-out measurement is predicted using the calibrated model. Now, the predicted value is compared to the known value, leading to the root mean square error of cross validation (RMSECV). The approach is repeated excluding other calibration data.

In literature, different examples of IHM applied in reactive systems are available. For example, the synthesis of microgels could be monitored inline using Raman

spectroscopy. The authors were able to reduce the RMSECV by a factor of two compared to a classical soft modeling approach (Meyer-Kirschner *et al.*, 2016). Using NMR, both low-field benchtop and a high-field instrument, it was possible to follow an esterification online. The NMR spectra have been analyzed with the IHM approach and the authors could show that the online signal derived from the benchtop device is in good accordance with the reference high-field NMR spectrometer (Zientek *et al.*, 2014).

Furthermore, it is useful to verify the robustness and accuracy of the chemometric model applying additional data sets, which are not part of the calibration. This is called external validation. The value determined by inline analytics is compared to a reference analysis. This chemometric model error is expressed as the root mean square error of prediction (RMSEP), which formula is shown below:

$$RMSEP = \sqrt{\frac{\sum_{i=1}^{j}(\hat{y}_i - y_i)^2}{j}} \quad (4)$$

With *i*: number of measurement [-], j: total number of measurements [-], $\hat{y}_i$: concentration of sample i measured with IR [mol L^{-1}], y_i: reference concentration of sample i (e.g. NMR, GC or gravimetric analysis) [mol L^{-1}].

Additionally, the bias can be calculated, which describes average distance of the measured values towards their references:

$$Bias = \hat{y}_i - y_i \quad (5)$$

With $\hat{y}_i$: concentration of sample i measured with IR [mol L^{-1}], y_i: reference concentration of sample i (e.g. NMR, GC or gravimetric analysis) [mol L^{-1}].

2 Aim of Thesis

This thesis is part of the "*Bio-Weichmacher*" (Bio-plasticizers) project, which was funded by the BMBF and carried out from 2016 to 2020. The project is a collaboration of the working group of Prof. Harald Gröger (Industrial Organic Chemistry and Biotechnology – University of Bielefeld), the BASF SE as industrial partner and the group of Prof. Andreas Liese (Institute of Technical Biocatalysis – Hamburg University of Technology).

Scope is the development of a process to produce alternative bio-based plasticizers for application in PVC. Traditionally, phthalates like DEHP are used for plasticized PVC. In recent years serious health concerns are associated with the use of these substances, resulting in an increasing demand for substitutes of DEHP that are less hazardous. There are various alternative plasticizers available, whose synthesis is based on renewable resources. However, their structures are highly different compared to traditionally applied phthalates. Some of the bio-based examples are produced from plant oils, leading to a competitive demand for these oils between food production and chemical feedstock.

In contrast, the planned structure of the new plasticizer is similar to phthalic acid based systems containing two ester bonds in 1,2-position. Already during the process development, inline analytics are to be applied to characterize all reaction steps in detail, which is depicted in Figure 9. By this approach, a high temporal data density is enabled without workup of samples.

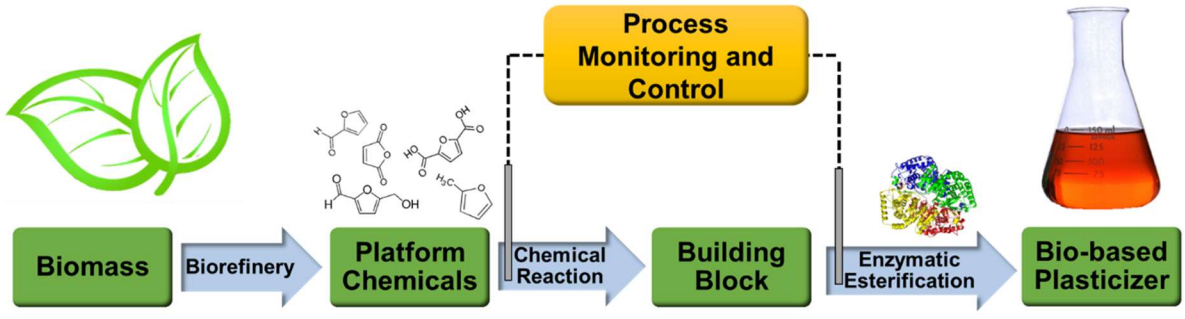

Figure 9: Scheme of the project "Bio-Weichmacher" (Bio-plasticizer) funded by the Federal Ministry of Education and Research (BMBF). Platform chemicals derived from ligno-cellulosic material in a biorefinery approach are used for the synthesis of plasticizer building blocks, which are further esterified with fatty alcohols preferably by application of a suitable lipase. The single reaction steps are monitored by means of inline analytics (Hiessl, Liese, 2020).

The reaction sequence is based on platform chemicals derived from ligno-cellulosic materials, which can be obtained in a bio-refinery. Starting from maleic acid anhydride and 2-methylfuran, a cyclic intermediate is formed within a Diels-Alder reaction. Since Diels-Alder reactions are reversible, this *retro*-Diels-Alder reaction needs to be avoided with respect to obtain a stable plasticizer. Thus, in a second reaction step, the intermediate is needed to be stabilized by hydrogenation. Furthermore, in an acid-catalyzed esterification step, alkyl chains are to be introduced, which are important for the plasticizing effect are added to the plasticizers building block. Moreover, the application of enzymes for the esterification step will be investigated, which allows a decrease of the reaction temperature. For this reason, a screening for suitable biocatalysts capable of converting cyclic substrates containing two acid/ester groups in 1,2-position is needed. In both approaches 2-ethylhexanol as alcohol moiety will be used, which is a common alcohol in the synthesis of a large variety of plasticizers. Therefore, the comparability in terms of application parameters of the newly developed plasticizer towards established ones is retained.

For the analysis of all process steps, ATR-FTIR spectroscopy will be applied as inline analytical method within the process development. This setup enables the non-destructive inline measurement of the composition in the liquid phase. For the analysis of the recorded spectra, a chemometric model is needed, which need to be designed for every reaction step. After calibration of the chemometric model, the inline measurement can be applied for reaction monitoring. The recorded inline data are to be used for characterizing the single steps. Additionally, kinetic models describing the reactions are to be set up using inline data and tested for simulation purposes.

In summary, for every reaction step…

- a chemometric model is developed for realizing an inline measurement.
- inline measured data are used for a detailed kinetic and thermodynamic characterization.
- the kinetic model is developed and applied in simulations.

The results obtained for every reaction step, are each presented in a separate chapter.

3 Material and Methods

3.1. Analytical Methods

3.1.1 GC

A GC method for the analysis of reaction sample from the esterification step was developed. DAPH, 2EH and DAPHE were available in sufficient purity and these were calibrated. The gas chromatograph used was a HP6890 (Agilent Technologies, Waldbronn, Germany) along with an Optima FFAPplus column (Machery-Nagel, Düren, Germany). The length of the column were 30 m with an inner diameter of 250 µm. The injection volume was 10 µL, with a split-ratio of 1:25. 2MeTHF was used as solvent and Helium as carrier gas. For quantification of the analytes, a FID detector was connected to the column. The initial temperature of the column oven was at 100 °C, which was hold for 2 min. A first temperature slope was applied, heating with 30 °C min^{-1}. 210 °C is hold for another 2 min, before second heating (30 °C min^{-1}) is carried out. The final temperature 240 °C was hold for 4 min, giving a total measurement time of the method of 13.2 min.

The retention times of DAPH, 2EH and DAPHE are summarized in Table 3.

Table 3: Retention time of the developed GC method for analyzing reaction samples from the esterification step.

Component	Retention time [min]
DAPH	7.6
2EH	2.7
DAPHE	11.8

For the listed components, a calibration was carried out by measuring a respective dilution series in the solvent 2MeTHF. The calibration was performed mass specific, relating the content of the sample to its weight and not the volume. By this approach, the pipetting error introduced by the high viscosity is avoided. Additionally, the exact dilution steps were determined by weighing. The obtained calibration curves are shown in Figure 10.

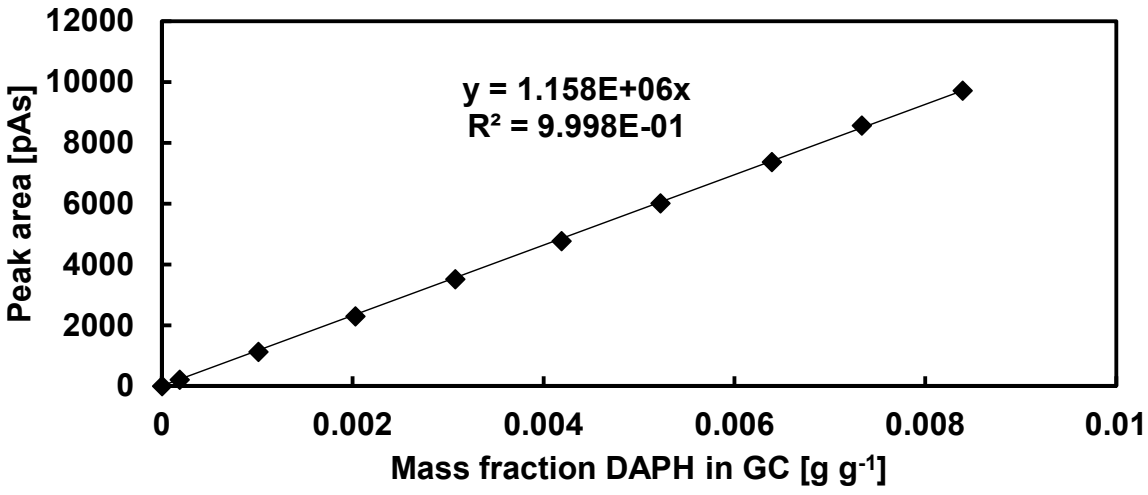

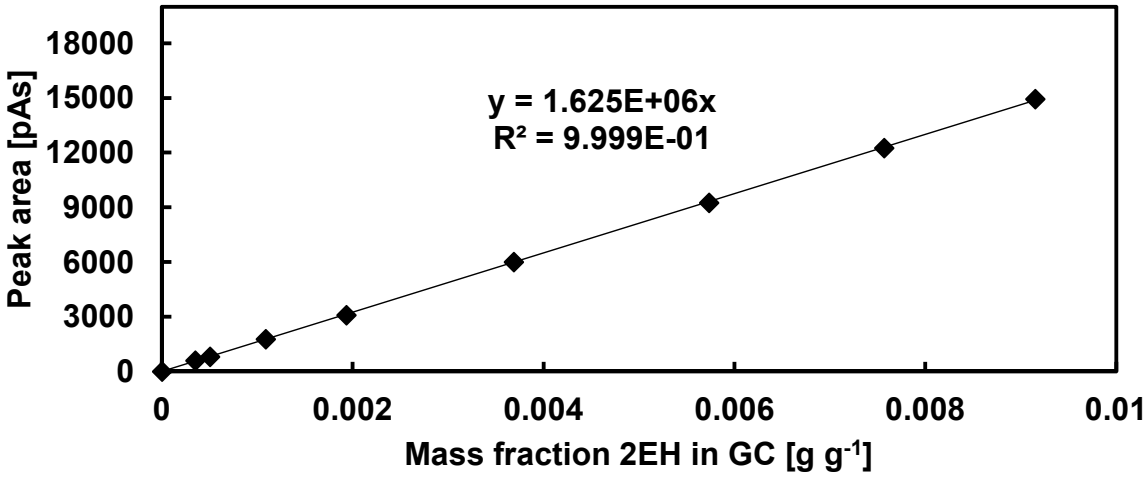

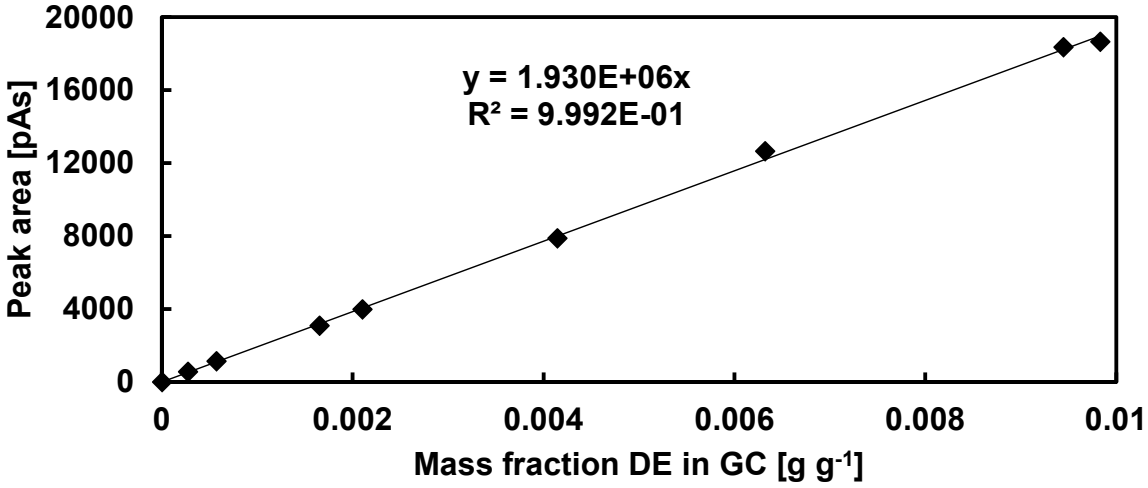

Figure 10: GC Calibration curve for DAP (top), 2EH (middle) and DAPHE (bottom).

3.1.2 ATR-FTIR

The IR measurements were performed with a Bruker Vertex70 spectrometer (Bruker Optics, Ettlingen, Germany) equipped with an IN-350T fiber optical probe (Bruker Optics, Ettlingen, Germany) according to the following procedure. The spectrometer itself is constantly purged with purge gas from a purge gas generator (PG-28L, cmc instruments GmbH, Eschborn, Germany) to avoid interference with water vapor and carbon dioxide. Before the measurements are started, the MCT (mercury cadmium tellurium) detector is cooled using liquid nitrogen. After the detector temperature and as well the amplitude are stable, the measurement can be started. First, before filling of the reactor is carried out, a background need to be recorded with the probe connected to the empty reaction vessel. The background spectrum (256 scans) contains the absorption of the spectrometer itself. After this spectrum is recorded and saved, the reactor can be filled and the regular measurements are started. Unless not stated otherwise, one spectrum per minute is recorded, which is an average of 128 scans each. The range of wavenumbers recorded is between 650 and 4000 cm^{-1}. After the experiment is finished, the probe is cleaned according to a fixed procedure: First the probe is rinsed with ethanol, then with water and finally with acetone, which is evaporating easily.

The procedure for the inline IR measurements within the hydrogen autoclave was similar. However, here another spectrometer, a ReactIR (Mettler-Toledo, Columbus, USA) is used. This spectrometer is not connected to the purge gas generator, therefore it needed to be flushed with nitrogen. The spectrometer was connected the previous day before an experiment is started and switched on to ensure the device is purged sufficiently and also the electric components reach a stable temperature. The position of the probe needs to be adjusted according to optimize the peak height measured, which is achieved according to the workflow given by the software (IcIR, Mettler-Toledo, Columbus, USA). When the intensity is within the specifications, the background is recorded with the empty reaction vessel, before the reaction and the measurement are started. For the background measurements 256 scans are averaged. The measured range is between 600 and 4000 cm^{-1}, one measurement is recorded every minute, which is an average of 128 scans each. After the experiment is finished, the cleaning is carried out in the same way like for the Bruker system, first rinsing the probe with water, then with ethanol and finally with acetone.

3.2 Synthesis Methods

3.2.1 Diels-Alder Product 4-methyl-3a,4,7,7a-tetrahydro-4,7-epoxyisobenzofuran-1,3-dione

Unless otherwise stated, DAP (4-methyl-3a,4,7,7a-tetrahydro-4,7-epoxyisobenzofuran-1,3-dione) was synthesized throughout this work according to this procedure. The solid MAA was grounded in a mortar until a fine powder is obtained. At room temperature, 1 equivalent of MAA (24.4983 g) was given into a plastic beaker containing a stirring bar placed on a magnetic stirrer. 1.2 equivalents of 2MF (27 mL) were added and the stirrer was started. The reaction mixture turned yellow and over the course of the reaction the viscosity is increasing until crystallization of DAP is occurring and the whole reaction mixture is solidifying. After complete solidification, the formed block is removed from the plastic beaker and grossly crushed, before the remaining 2MF was removed using a rotary evaporator (Büchi R-200). The temperature of the water bath was set to 40 °C, while the vacuum was set to 20 mbar. Finally the obtained product was grounded to a fine powder using a mortar. Since no analytical method for the determination of the purity is available, no yield could be calculated in this step. The obtained product is shown in Figure 11 (left).

Figure 11: DAP, DAPH and DAPHE synthesized (and partially purified) in this work.

3.2.2 Hydrogenated Diels-Alder 4-methylhexahydro-4,7-epoxyisobenzofuran-1,3-dione

The hydrogenation of DAP to DAPH (4-methylhexahydro-4,7-epoxyisobenzofuran-1,3-dione), was carried out according to this synthesis protocol, if not specified in detail. The finely ground DAP (13.512 g) from the previous reaction step is mixed with 2 wt% of Pd/C and solubilized in 150 mL of 2MeTHF yielding a concentration of DAP of

500 mM. After the autoclave was sealed, the hydrogen pressure was set to 2 bar and the connections to the reactor opened. The reactions are carried out at room temperature. Due to the exothermic nature of this hydrogenation, immediately after adding the hydrogen, an increase in the reactor temperature can be observed. After the temperature is decreasing again, the reaction is assumed to be finished and the hydrogen line is closed and the excess pressure is removed. A black reaction mixture is obtained, which need to be purified before further processing.

The reaction mixture containing DAPH and the side product BSA is filtrated to remove the Pd/C catalyst. Here, a filter with a pore size of 0.2 µm (Millipore GNWP, Merck, Darmstadt, Germany) in combination with a vacuum pump (PC 3001 vario, Vacuubrand; Wertheim, Germany) was used. The pressure was set to 700 mbar. After this filtration step, a yellow/brown liquid is obtained. The solvent 2MeTHF is partially removed at the rotary evaporator. Here the water bath is set to 60 °C and the vacuum applied to 300 mbar. After the reaction mixture is concentrated, it is stored on ice to provoke crystallization of the product DAPH, which is observed to occur selectively yielding white crystals and a dark yellow supernatant. After separation of the crystals and the supernatant, the crystals are dissolved in fresh 2MeTHF again and the procedure is repeated to increase the purity further (usually three times). After no coloration is observable anymore, the concentrated DAPH solution is given into crystallization bowls. Overnight, 2MeTHF is evaporating and the remaining crystals are crushed and stored. The resulting product DAPH is found in Figure 11 (middle).

3.2.3 Di-ester bis(2-ethylhexyl) 1-methyl-7-oxabicyclo[2.2.1]heptane-2,3-dicarboxylate

The Diester DAPHE (bis(2-ethylhexyl) 1-methyl-7-oxabicyclo[2.2.1]heptane-2,3-dicarboxylate) needed for the calibration of GC and for the measurement of the pure component spectrum was synthesized and purified in this work. The synthesis was performed according to the method developed by Plass (Plass, 2020). 5.27713 g of the anhydride DAPH was given into thermostatic stirred tank reactor and 2.2 equivalents of 2EH (10 mL) were added. Additionally, 1 mol% of sulfuric acid was supplemented as catalyst. The reaction mixture was continuously stirred (1500 rpm on a magnetic stirrer) and heated to 80 °C. After 21 h, molecular sieves (300 mg, 3 Å) were added to remove the reaction water. Afterwards, the reaction mixture was diluted

with 50 mL cyclohexane and filtered using Al_2O_3 (Brockmann activity 1) to remove the monoester fraction. Cyclohexane was separated from the filtrate in the rotary evaporator. The remaining alcohol 2EH was removed in a vacuum distillation step. (45 °C, $1.1 \cdot 10^{-2}$ mbar, 4.5 h and 120 °C, $2.4 \cdot 10^{-2}$ mbar, 7 h) The obtained DAPHE has a honey-like color and is highly viscous. Its purity was checked by ^{1}H-NMR and was determined to 97%. In total, 7.73 g of DAPHE were obtained, which is corresponding to a yield of 61%. In Figure 11 (right), the obtained plasticizer can be seen.

3.3 Reactor Setups

The reactor setup used for both, the Diels-Alder reaction as well as the esterification reaction, is shown in Figure 13. A double-jacked glass reactor with a total volume of 10 mL was attached to a thermostatic bath, which was controlled using a PT-100 temperature probe inserted into the reactor vessel. An IN-350T ATR probe (Bruker Optics, Ettlingen, Germany) was implemented in the reactor ensuring the diamond tip is within the liquid phase.

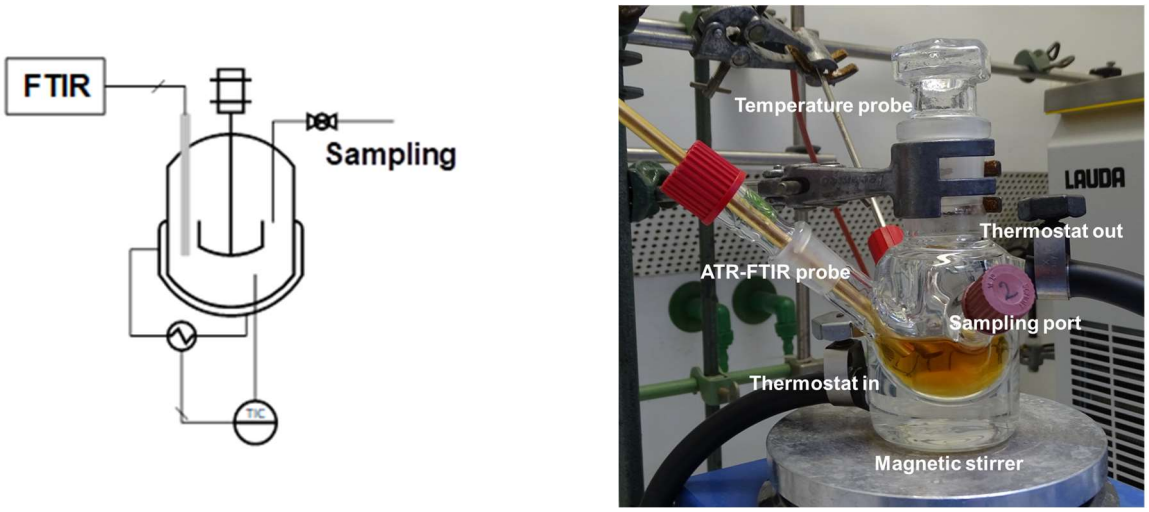

Figure 12: Stirred tank reactor used for the Diels-Alder reaction of 2MF and MAA leading to DAP. Same setup used for the Esterification of DAPH and 2EH to the diester DAPHE.

Before an experiment was started, the FTIR spectrometer was cooled down. After the detector of the system was reaching steady state in terms of the intensity measured at the MCT (Mercury Cadmium Tellurium) detector, the background spectrum for the experiment was measured. Thereafter, the starting materials were added. Now the stirrer as well as the FTIR measurement were started. From the sampling port, offline samples were withdrawn in case of the esterification reaction for further GC analysis.

For the hydrogenation reaction, a steel autoclave from Parr Instruments (Moline, USA) was used. The reactor had a total volume of 600 mL and was made from stainless steel. The reactor vessel had a special port for the application of a FTIR probe, which allowed inline measurements at pressures of up to 37 bar. Additionally, a PT-100 temperature probe as well as a pressure manometer were attached to the reactor, enabling a monitoring of these two parameters. The reactor setup is depicted in Figure 13.

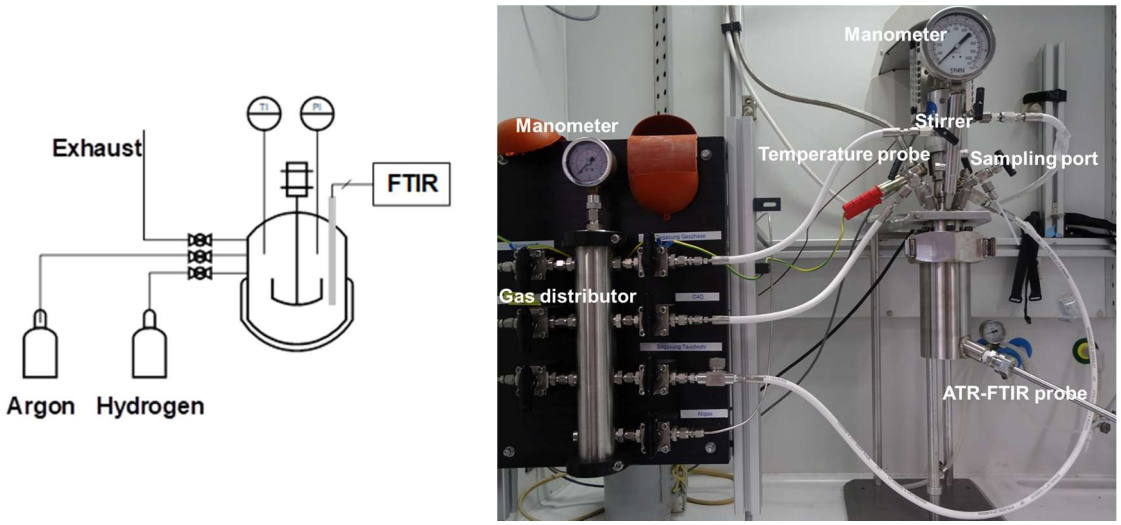

Figure 13: Parr hydrogen autoclave reactor setup used for the hydrogenation of DAP to DAPH.

The workflow for setting up the FTIR spectrometer in the experiments carried out in the hydrogen pressure autoclave were similar to these performed in the glass stirred tank reactor. After the FTIR spectrometer was in steady state, the ATR probe was mounted to the reactor and the background spectrum for the experiment recorded. Then the solid starting material DAP and the Pd/C catalyst were given into the reactor before the solvent 2MeTHF was added. The reactor was closed with the respective screws ensuring a tight setup. After the reactor was sealed, the stirrer and the inline measurement were started. Since hydrogen and oxygen are forming an explosive atmosphere, caution is needed during setup and operation of this experimental setup. Prior filling hydrogen into the reactor, the air inside the system has to be removed. The argon gas bottle and the connection line to the gas distributor were opened first. An argon pressure of about 10 bar was set at the gas distributor and thereafter the connection to the reactor was opened. The argon line and the respective valves were closed again and the pressure was released from the reactor. In the next step, the hydrogen bottle was opened and the desired hydrogen pressure was adjusted at the gas distributor station. After reaching the chosen hydrogen pressure, the connection

valve to the reaction vessel was opened, which was the start of the reaction. After the experiment was finished, the hydrogen line was closed again, and the exhaust line opened to release the excess pressure. Like during the startup, the reactor was flushed with argon to remove remaining hydrogen. After the reactor being flushed, the gas bottles have been closed and the remaining pressure of the gas distributor was released and the reactor was opened. The reaction medium was filtered to remove the Pd/C particles before the hydrogenated product was further purified.

3.4 Design of Experiments

To reduce the overall number of experiments necessary for the characterization of the esterification reaction, a Design of Experiments (DoE) (Design Expert 12, Stat-Ease, Minneapolis, USA) was used. More specific, the Response Surface Methodology (RSM) was applied. Besides decreasing the necessary amount of experimental data needed, DoE helps to identify coherence between different input variables. In addition, statistical tests are included to ensure significance of the obtained data.

In this work, two variables were chosen: the reaction temperature (Factor 1) and the ratio of the starting material 2EH and DAPH (Factor 2). A scheme of the DoE applied according to a central composite design is shown in Figure 14. The center point at 130 °C and a ratio of 3.5 is done as triplicate (black square). For factor one, the temperature, level -1 corresponds to 110 °C and level +1 to 150 °C. In parallel, for factor two, ratio of starting materials, as level -1, a ratio of 2 was chosen and as level +1, a ratio of 5. These four corner points (grey circle) are the points of factorial design. In addition, four axial points outside of the factorial design are used (white circle).

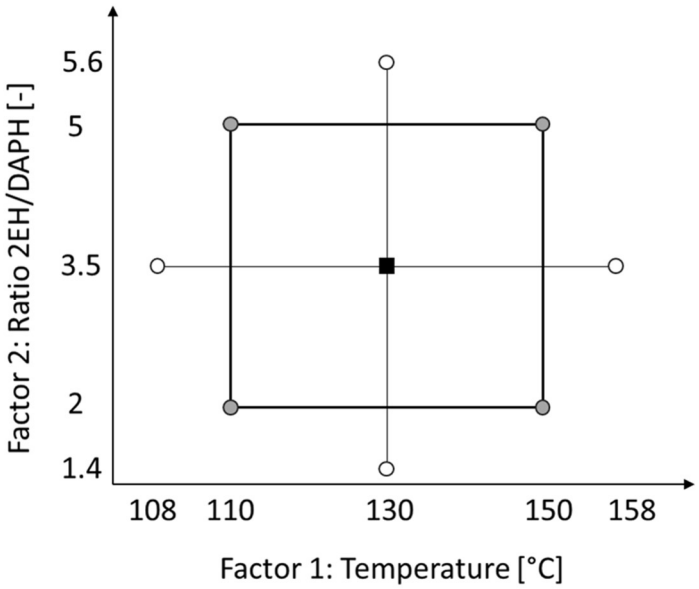

Figure 14: DoE Design applied with factor 1 temperature and factor 2 ratio of 2EH to DAPH.

In total, eleven experiments need to be carried out, to analyze the coherence of these both parameters. An overview of all experiments carried is listed in Table 4. For the evaluation of the DoE, a suitable response of the experiments is needed. Using here only the obtained concentration of the target component DAPHE, is not advisable. Excess amounts of alcohol are needed to shift the position of the equilibrium of the esterification reaction. Therefore, the conversion of the anhydride was chosen as response variable. To make the outcome of the experiment more significant, the conversions at 90 minutes and after 200 min were evaluated as target value.

Table 4: Experiments planned from DoE RSM Design with the corresponding temperature and ratio of starting materials.

DoE Run	Temperature [°C]	Ratio 2EH/DAPH [-]
1	130	3.5
2	150	2
3	110	5
4	130	5.6
5	130	3.5
6	158	3.5
7	150	5
8	110	2
9	102	3.5
10	130	1.4
11	130	3.5
Validation	142.5	3.3

3.5 Chemicals

In Table 1, the chemicals used in this work are listed including the vendor and the respective purity. All chemicals have been used without further purification.

Table 5: Chemicals purchased with their supplier and the corresponding purity.

Chemical	Supplier	Purity [%]
2-Methylfuran	Merck	≥99.0
Maleic acid anhydride	Merck	≥99.0
2-Methyltetrahydrofuran	Roth	≥99.0
Pd/C (10%)	TCI	-
***n*-Hexane**	Roth	≥99.0
Ethyl acetate	Roth	≥99.5
Succinic acid	Merck	≥98.0
2-Ethylhexanol	BASF	≥99.5
Sulfuric acid	Roth	96
Cyclohexane	Roth	≥99.9
Acetone	Roth	≥99.5
Hydrogen	Westfalen	≥99.999
Argon	Linde	≥99.999
Nitrogen	Linde	≥99.999
Helium	Linde	≥99.999

3.6 Devices

The devices used are summarized along with their manufacturer in Table 6.

Table 6: List of devices used with their corresponding manufacturer.

Device	Name	Manufacturer
FTIR spectrometer 1	ReactIR	Mettler Toledo, Columbus, USA
FTIR spectrometer 2	Matrix-MF	Bruker Optics GmbH, Ettlingen, Germany
FTIR spectrometer 3	Vertex70	Bruker Optics GmbH, Ettlingen, Germany
ATR Probe	IN-350T	Bruker Optics GmbH, Ettlingen, Germany
NMR spectrometer	Avance III HD 600 MHz	Bruker BioSpin GmbH, Rheinstetten, Germany
Gas chromatograph	HP 6890	Agilent Technologies, Waldbronn, Germany
Thermostat	RE1050 ECO Gold	Lauda Dr. R.Wobser GmbH, Lauda-Königshofen, Germany
Cryostat	Profi Cool UKT 303-1	National Lab GmbH, Mölln, Germany
Analytical scale 1	CP224S	Sartorius AG, Göttingen, Germany
Analytical scale 2	CPA224S-0CE	Sartorius AG, Göttingen, Germany
Purge gas generator	PG28-L	cmc Instruments GmbH, Eschborn, Germany
Rotary evaporator	R-200	Büchi Labortechnik GmbH, Essen, Germany
Hydrogen reactor	Reactor 4560, Controller 4848	Parr Instruments, Moline, USA
Magnetic stirrer	IKA Plate RCT Digital	IKA-Werke, Staufen im Breisgau, Germany
Vacuum pump	PC 3001 Vario	Vacuubrand GmbH, Wertheim am Main, Germany
Melting point apparatus	MFB595	Gallenkamp/Fison Instruments Ltd, Glasgow, Scotland

4 Diels-Alder Reaction of 2-Methylfuran and Maleic Acid Anhydride

4.1 Introduction: Diels-Alder Reaction

The Diels-Alder reaction is named after the chemists OTTO DIELS and KURT ALDER, who discovered this cycloaddition reaction in 1928 (Diels, Alder, 1928, 1929) and for which they were awarded the Nobel Prize in Chemistry in 1950. In this section, the mechanism of the reaction, some examples and applications are summarized.

For this type of reaction a conjugated diene and a dienophile (substituted alkene) are needed. Four electrons of the diene and two electrons of the dienophile are involved in the reaction mechanism. For this reason, the reaction is also named a [4+2] cycloaddition. The mechanism is shown for 2-methylfuran (2MF) and maleic acid anhydride (MAA) in Figure 15. The resulting Diels-Alder product 4-methyl-3a,4,7,7a-tetrahydro-4,7-epoxyisobenzofuran-1,3-dione is abbreviated as DAP in the following.

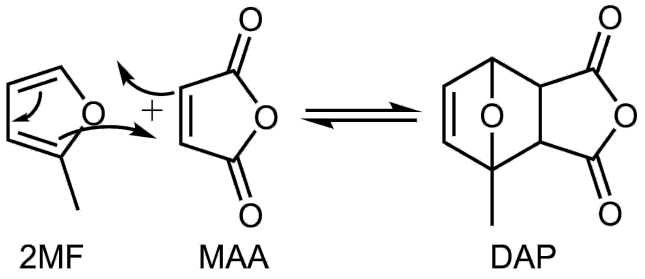

Figure 15: Mechanism of the Diels-Alder reaction of 2-methylfuran (2MF) and maleic acid anhydride (MAA) leading to 4-methyl-3a,4,7,7a-tetrahydro-4,7-epoxyisobenzofuran-1,3-dione (DAP).

During the reaction, the molecules' orbitals are overlapping and in the transition state two new σ-bonds as well as a π-bond are formed. The Diels-Alder reaction attracted a lot of interest, which can be attributed to the overall high atom efficiency and moreover to the stereoselectivity of the reaction. In principle, two different stereoisomers are possible, the thermodynamically favored *exo*-product and the kinetically favored *endo*-product (Eggelte *et al.*, 1973, Woodward, Baer, 1948). The *endo* isomer is suspected to isomerize to the *exo*-adduct, leading to a pure product at high conversions (Kamo *et al.*, 1974). The chemical structures of both, *endo*- and *exo*- 4-methyl-3a,4,7,7a-tetrahydro-4,7-epoxyisobenzofuran-1,3-dione are shown in Figure 16.

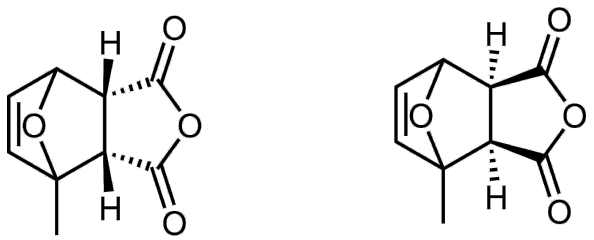

Figure 16: Endo and exo form of 1-Methyl-4,10-dioxatricyclo[5.2.1.02,6]dec-8-ene-3,5-dione (DAP).

In general, the reaction mechanism is reversible. At high temperatures, the so-called *retro*-Diels-Alder reaction occurs leading back to the starting materials (Froidevaux *et al.*, 2015). This behavior complicates the analysis operating traditional offline analytical devices like GC (Sparks, Poling, 1983). Besides, solubilization can lead to an (unwanted) *retro*-Diels-Alder reaction, which is disadvantageous for analyzing samples by HPLC. Interestingly, the rate for the *retro*-Diels-Alder reaction of anthracenedione was depending on the type of the solvents. In aqueous solution, the backwards reaction was accelerated while the reaction in organic solvents was slowed down (Wijnen, Engberts, 1997). To avoid this backwards reaction, the molecule needs to be stabilized prior to a further processing. For this reason, the remaining double bond can either be hydrogenated (Thiyagarajan *et al.*, 2015) or epoxidized (O'Brien, Gates, 1965). Alternatively, the Diel-Alder reaction product can be dehydrated leading to (substituted) aromatic compounds (Mahmoud *et al.*, 2014).

In literature, kinetic data for a variety of Diels-Alder reactions can be found. Due to the fact, that the reaction is reversible, an analysis using traditional offline analytical methods is not advisable. Therefore, the measurements are mostly performed using *UV/VIS* spectroscopy (Carneiro de Oliveira *et al.*, 2020, Gandini *et al.*, 2008, Liu *et al.*, 2013, Otto *et al.*, 1996). Besides using *UV/VIS* spectroscopy, also ^{1}H-NMR was applied to deduce the kinetics of these type of reaction (Gandini *et al.*, 2008, Liu *et al.*, 2013). In contrast to *UV/VIS*, higher concentrations could be applied (Carneiro de Oliveira *et al.*, 2020), which might be attributed to the relative small concentration range, in which the LAMBERT-BEER law is valid.

There are examples, where ATR-FTIR was applied to investigate the kinetics. While LIU *et al.* concluded that the accuracy of this analytical method is not sufficient (Liu *et al.*, 2013), Stirn and his coworkers demonstrated that the experimental data recorded with FTIR spectroscopy were in good accordance with the ^{1}H-NMR measurements (Stirn *et al.*, 2016).

However, all approaches were applying different solvents to investigate the respective kinetics. As early as in 1890, NIKOLAI ALEXANDROWITSCH MENSCHUTKIN showed that solvents have a significant effect on reaction rates (Menschutkin, 1890a, 1890b). Electrophilic solvents can enhance the reaction rate, while nucleophilic solvents are decreasing the rate of the reaction. The relative change in the reaction rate depends on their electrophilic or nucleophilic power (Desimoni *et al.*, 1994). In consequence, all the rate constants determined in the literature must not be transferred to other solvents or even neat (solvent-free) reaction conditions.

There are several fields of applications of the reaction, but especially in the synthesis of natural compounds, Diels-Alder reactions are of high interest. As one of the first applications, a synthesis for steroids involving a Diels-Alder cycloaddition was established in 1952 (Woodward *et al.*, 1952). The reaction is, in general, highly suitable for the synthesis of large molecules. Other examples were reported in the field of pharmaceuticals, flavors and also agrochemicals (Funel, Abele, 2013, Gregoritza, Brandl, 2015). The Diels-Alder reaction of 2MF and MAA was also investigated in terms of a possible energy storing system (Sparks, Poling, 1983).

In the recent context of the transition to a bio-based, circular economy, the Diels-Alder reaction gained new interest for the synthesis of intermediates and building moieties. Different cyclic compounds can be produced from so-called platform chemicals (e.g. furans) derived from lignocellulosic materials in a biorefinery (Kucherov *et al.*, 2017). For instance, a process for the synthesis of *p*-xylene based on a Diels-Alder reaction of dimethylfuran and ethylene was confirmed. Followed by dehydration, this leads to an aromatic product (Williams *et al.*, 2012). In a similar way, Mahmoud *et al*. showed a synthesis for phthalic anhydride based on a Diels-Alder reaction of furan and maleic acid anhydride. Here a subsequent dehydration step, with an overall high selectivity of 80%, is necessary (Mahmoud *et al.*, 2014). THIYAGARAJAN *et al*. were expanding this synthesis to substituted phthalic anhydrides, which were also tested during this work. They inserted a further reaction step into the sequence: after the Diels-Alder reaction, first a hydrogenation was performed, which then was again followed by dehydration. This approach has the advantage that the Diels-Alder intermediate is stabilized in a fast reaction step and is therefore not accessible for the *retro*-Diels-Alder reaction anymore (Thiyagarajan *et al.*, 2015). Also in the field of novel biopolymers, the Diels-Alder mechanism is of increasing interest. Different copolymers were applied in

a Diels-Alder reaction forming elastomers, the reversibility of this reaction is suspected to obtain more easily recyclable materials (Gandini *et al.*, 2008, Gheneim *et al.*, 2002).

4.2 Chemometric Model Development

For the analysis of the inline measured FTIR spectra, a suitable chemometric model is required to deduce the concentration profiles. In the following section, the development of such a chemometric model describing the Diels-Alder reaction of 2MF and MAA to the product DAP is presented.

Due to the reversible nature of the Diels-Alder reaction, respective reference data cannot be measured with HPLC or GC. In addition, the approach of artificial reactant mixtures is not applicable, since 2MF and MAA will immediately start to react after mixing. Therefore, the essential reference data for the chemometric model calibration are recorded in experiments performed in a high field NMR spectrometer (Bruker Avance III HD 600 MHz, Bruker Biospin; Rheinstetten, Germany) at Bielefeld University. These experiments were carried out together with Carmen Plass, who also worked in the Bio-Weichmacher project within the scope of her PhD thesis. Unlike to the publications summarized in the previous section, the Diels-Alder reaction of 2MF and MAA is performed in solvent-free condition and in contrast to usual NMR measurements there is no need to apply deuterated solvents. However, NMR spectrometers need to be shimmed and locked to the resonance of these deuterated solvents. For this reason, acetone-d_6 was used as external standard in these experiments. To avoid solvent effects on the reaction, the deuterated solvent was added in small glass capillary, which was closed by melting after filling. Since the absolute number of moles of the external standard is unknown, the NMR measurements is relative and not in an absolute manner. In these NMR experiments, MAA was finely ground and filled into the NMR tube before 2MF was added. The tube was sealed and the solid material solubilized by shaking. After a homogeneous liquid phase was obtained, the measurement in the NMR spectrometer was started, which temperature was thermostated to 10 °C. A typical result of one of these experiments is provided in Figure 17.

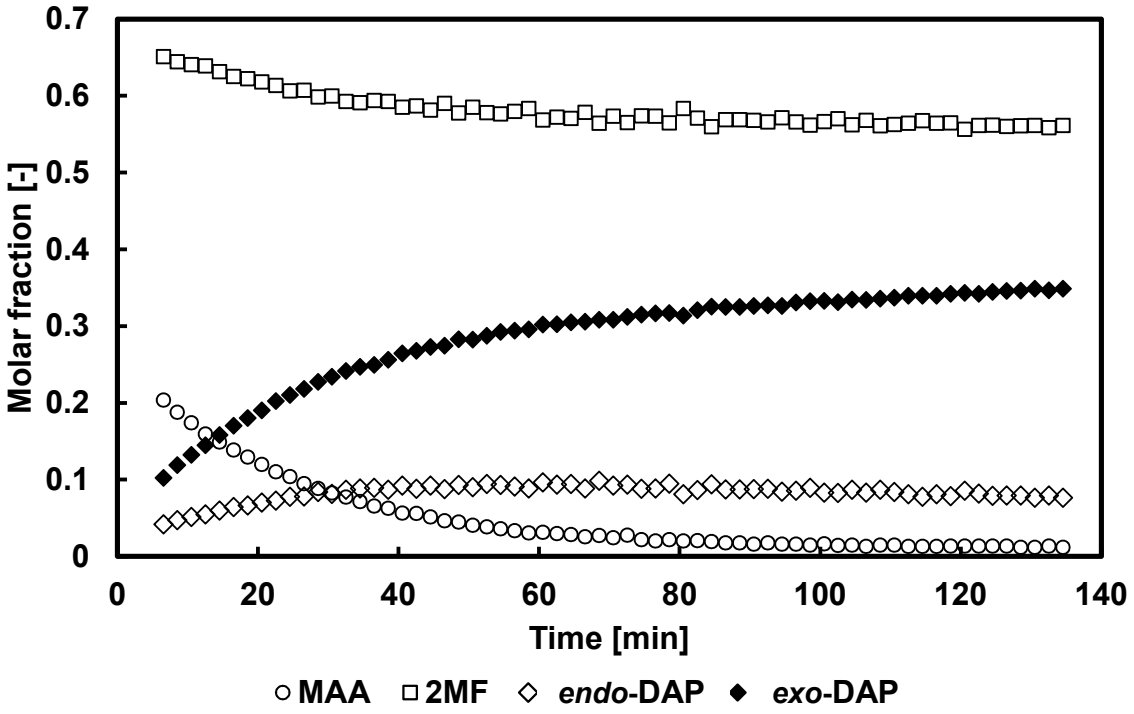

Figure 17: Diels-Alder reaction of 2-methylfuran and maleic acid anhydride. Experimental conditions: m_{MAA} = 0.1645 g, V_{2MF} = 0.301 mL, T = 10 °C, non-stirred, external standard: acetone-d_6. One ^{1}H-NMR spectrum measured every two minutes with Bruker Avance III 600 MHz, performed at Bielefeld University.

The molar fractions shown in Figure 17 are derived from ^{1}H-NMR spectra. Here not only the starting materials MAA and 2MF but also both forms of the product DAP are shown. NMR spectroscopy is able to distinguish between the *endo*- and the *exo*-form of the product DAP. From the graph it can be seen that in the beginning both products, *endo* and *exo*, are formed. After about 40 minutes, the *endo*-product starts isomerizing to the *exo*-product leading to a further increase of DAP, also after depletion of the starting material MAA. This behavior was also observed in a previous study using MAA and different furan derivatives (Kamo *et al.*, 1974). FTIR spectroscopy is not suitable for monitoring the difference between *endo* and *exo*. That is why both forms are summarized to one product for the rest of this work. The missing measurements in the beginning of the reaction are due to the setup and the general handling of this reaction: prior to measurement the solid starting material MAA needed to be solubilized in the liquid starting material 2MF within the NMR tube. Only after no solid particles were observed anymore, the NMR tube was inserted into the NMR spectrometer and the measurement was started with a measurement interval of two minutes.

A relative calibration, e.g. as mol% or molar fraction, is not suitable for the determination of kinetics describing a reaction with a changing absolute number of

molecules. Therefore, the obtained data from the NMR experiments are converted to an absolute measurement in mol L^{-1}. The procedure is described in the next section.

The weighed portions are used to calculate conversions of the substrate and the corresponding yield of the product depending on the reaction stoichiometry. The calculated conversion and yield values as a function of the molar fraction are fitted with a 3rd order polynomial equation. The results of this step are exemplarily summarized in Figure 18.

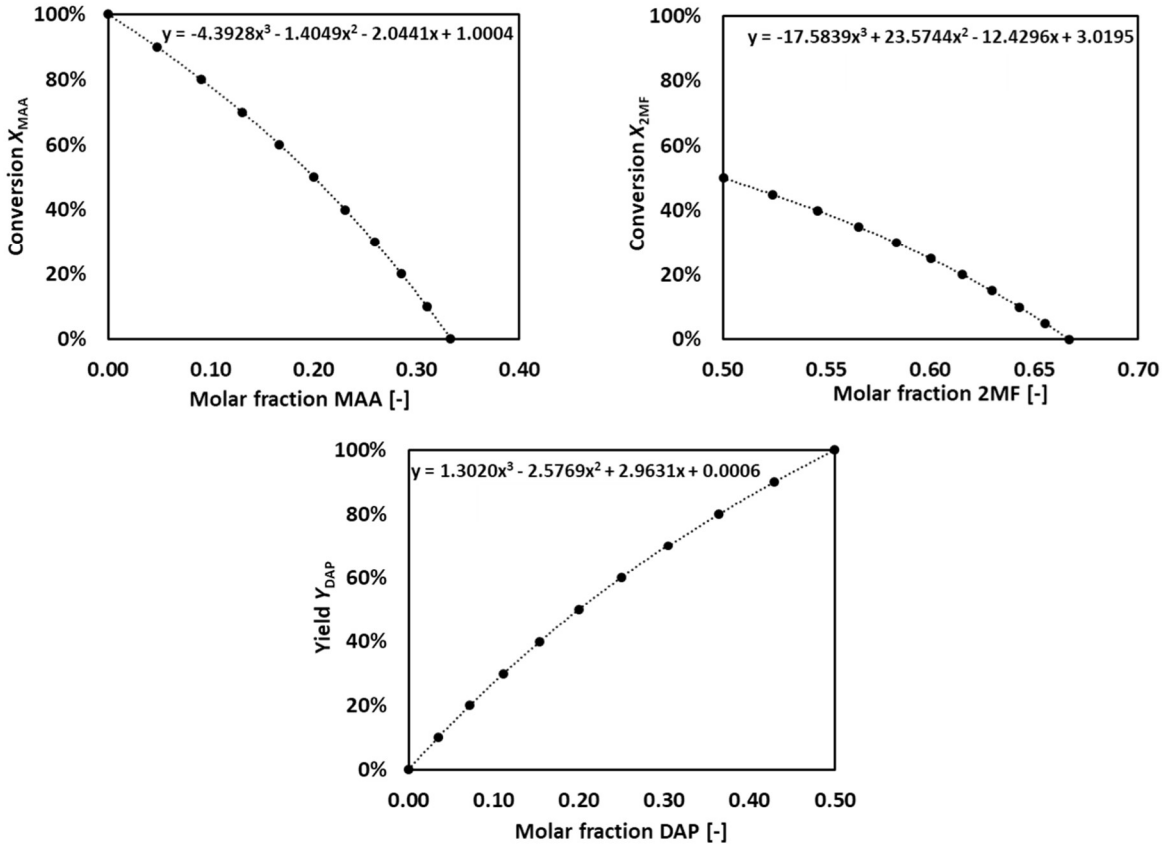

Figure 18: Stoichiometric conversion/yield vs molar fraction based on weigh-in portions with a 3rd order polynomial fit. Experimental conditions: m_{MAA} = 0.16395 g, V_{2MF} = 0.300 mL.

From the equations obtained in Figure 18, the actual conversions from the molar fractions measured in the NMR experiments are calculated. Along with the weighed portions of the respective experiments the actual number of moles at a certain point in time are obtained, which is shown for the NMR experiment with a ratio of MAA and 2MF of 1:2 in Figure 19.

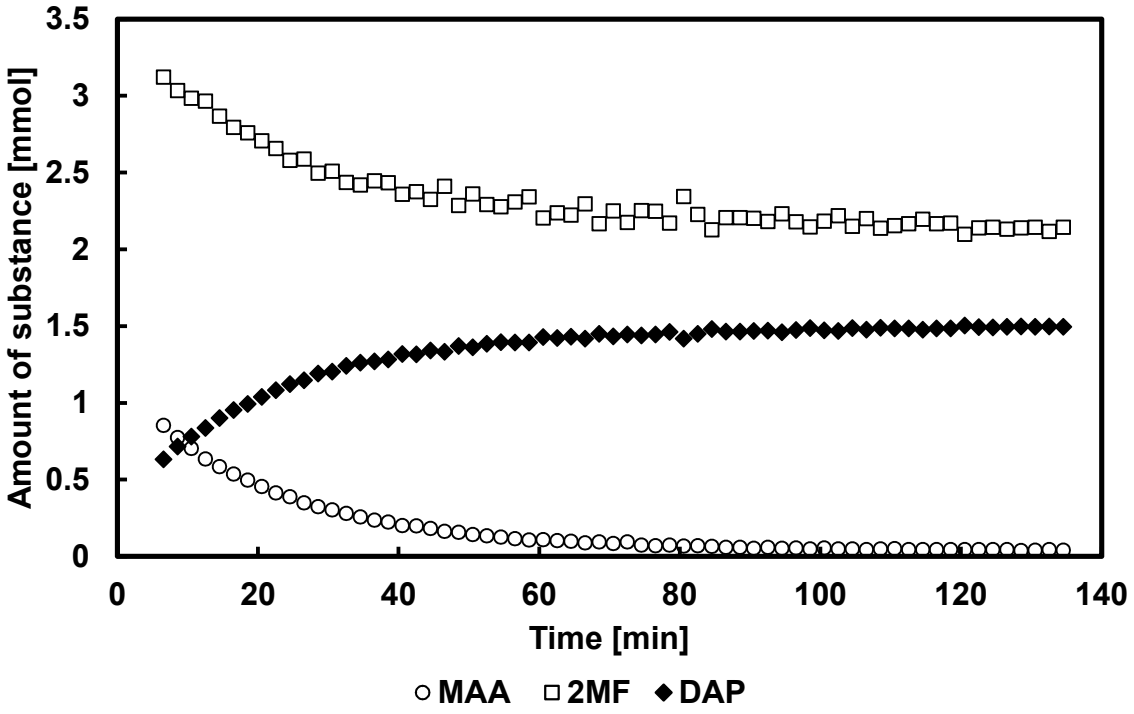

Figure 19: Diels-Alder reaction of 2-methylfuran and maleic acid anhydride. Amount of substance vs time plot. Experimental conditions: m_{MAA} = 0.16395 g, V_{2MF} = 0.300 mL, T = 10 °C, non-stirred, external standard: acetone-d_6. One ^{1}H-NMR spectrum measured every two minutes with Bruker Avance III 600 MHz, performed at Bielefeld University. Calculated using stoichiometric conversion/yield as a function of molar fraction.

In comparison to Figure 17, in this depiction of the experiment, the stoichiometry of the reaction becomes clear. To further generalize the calibration data into absolute concentrations, information on the density of the reaction mixture is necessary. A mixer unit operation at a constant temperature (10 °C) with different ratios of both starting materials, 2MF and MAA, was modelled using Aspen Plus 9.0 (Aspen Technology, Bedford, USA), which is shown in Figure 20.

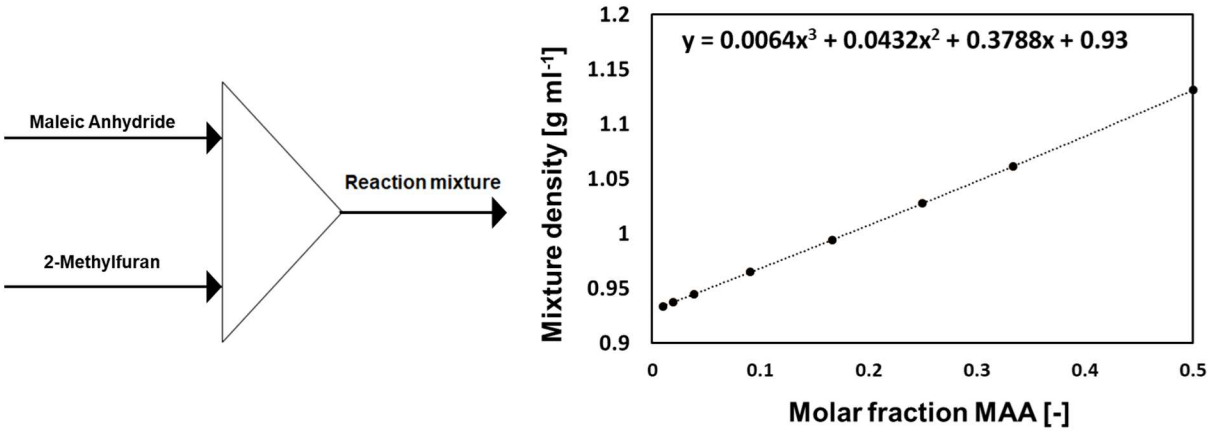

Figure 20: Mixer unit operation of 2MF and MAA modelled in Aspen Plus at 10 °C to correlate the reaction mixture density as a function of the molar fraction of MAA in the concentration range applied.

This calculation is based on the non-random two-liquid model (NRTL) which is an activity coefficient based modeling approach often used for the determination of phase equilibria or the composition of liquid phases (Renon, Prausnitz, 1968). The obtained mixture density data in the investigated concentration range are plotted versus the molar fraction of MAA and by fitting with a third degree polynomic equation.

Using the correlation obtained from the modelling in Aspen, a correlation of the reaction mixture density and the conversion of MAA is obtained. Here, the assumption that DAP shows similar solubility behavior as well as the same density compared to MAA is included. For conversions of 0 and 100% the mixture density is calculated and a linear correlation with the reaction progress is assumed. By this approach, at any conversion the mixture density can be calculated and in consequence the conversion from absolute moles to a concentration in mol L^{-1} is carried out. The result of the exemplary experiment performed with an initial ratio of MAA to 2MF of 1:2 is shown in Figure 21.

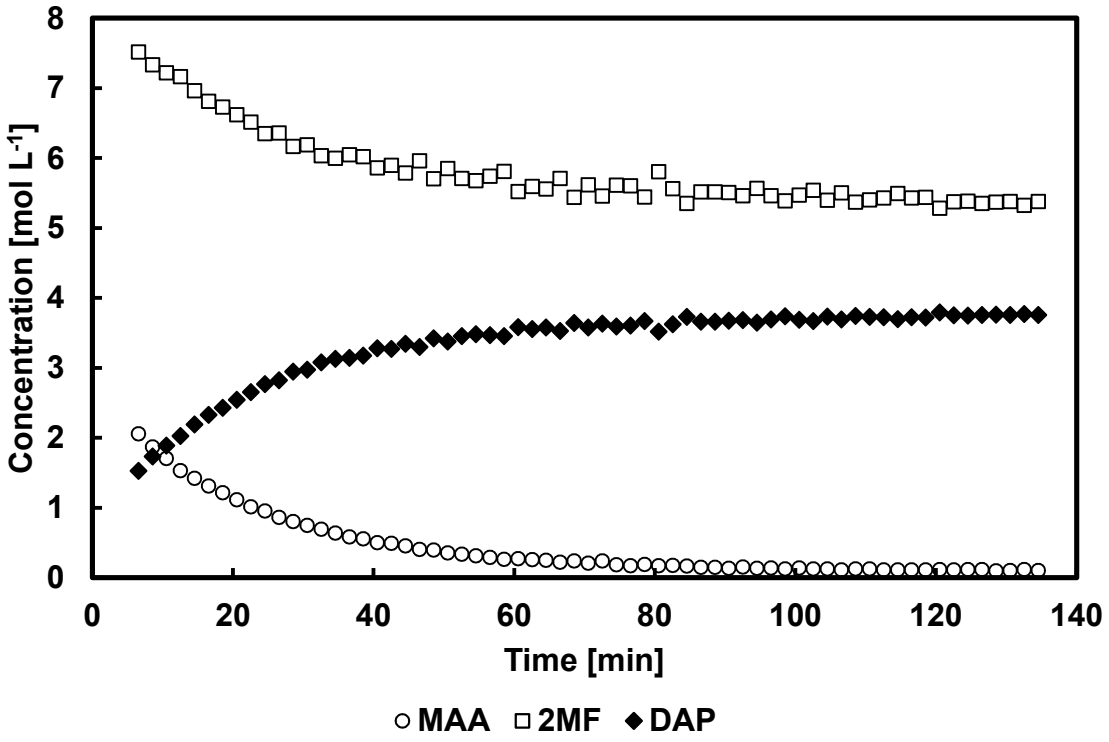

Figure 21: Diels-Alder reaction of 2-methylfuran and maleic acid anhydride calculated in mol L^{-1}. Experimental conditions: m_{MAA} = 0.16395 g, V_{2MF} = 0.300 mL, T = 10 °C, non-stirred, external standard: acetone-d_6. One ^{1}H-NMR spectrum measured every two minutes with Bruker Avance III 600 MHz, performed at Bielefeld University. Calculated based on stoichiometric conversion/yield as a function of molar fraction along with modeling the mixture density via Aspen.

At Bielefeld University, experiments with different ratios of starting materials were carried out. Starting from equimolar range of 2MF and MAA, the amount of 2MF was increased to two and five equivalents. The experiments were repeated for each

concentration three times to determine the repeatability. The runs performed at an equimolar ratio showed high deviations, which can be explained by the solubilizing step prior to the measurement in the NMR spectrometer. Therefore, only the data at a ratio of two and five equivalents were used for the development of the chemometric model.

For setting up the IHM, pure component FTIR spectra of both starting materials as well as the product were measured. Since MAA and DAP are both solids, however, the chemometric model is applied to liquid phase measurements, these had to be measured in solution as well. As solvent the structural similar 2-methyltetrahydrofuran (2MeTHF) was used. In contrast to 2MF, no double bonds are present, therefore no Diels-Alder reaction can occur. During the modeling, the spectral absorbance attributed to the solvent were excluded from the final IHM.

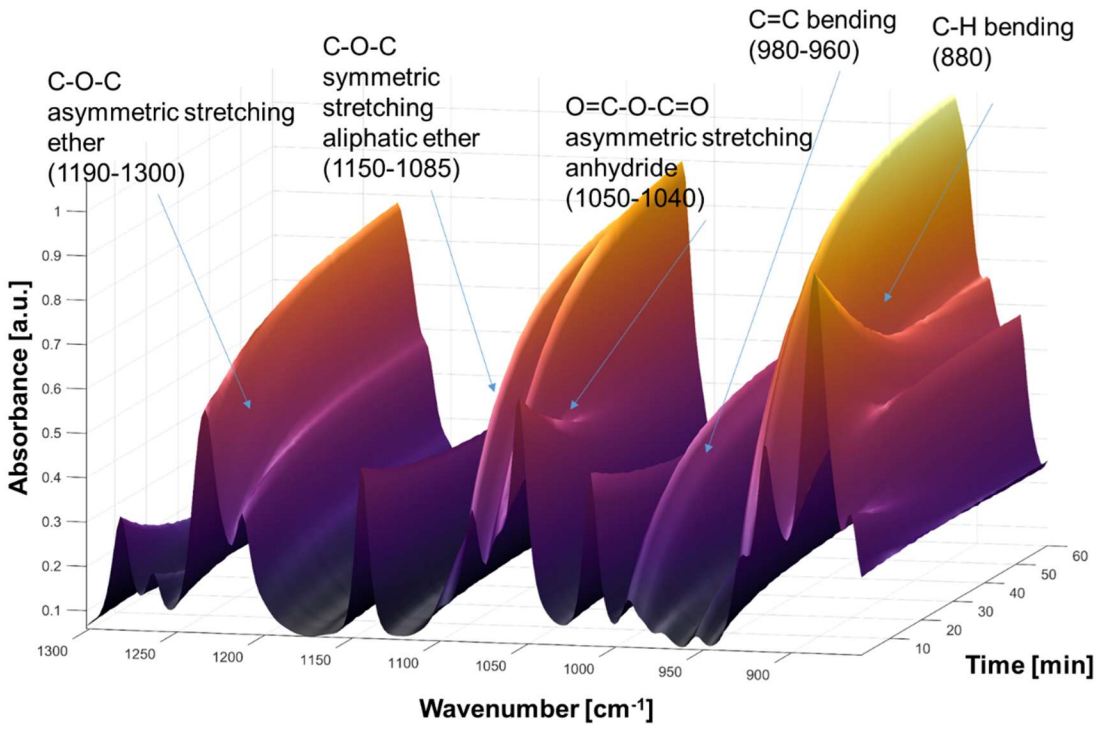

Figure 22: 3D-plot of the Diels-Alder reaction of 2-methylfuran and maleic acid anhydride. Experimental conditions: m_{MAA} = 2.4711 g, V_{2MF} = 4.5470 mL, T = 10 °C, non-stirred, One FTIR spectrum/min measured with Bruker Matrix-MF spectrometer equipped with Bruker IN-350T ATR probe.

To record calibration spectra, the reaction conditions were kept identical to those in in the experiments performed with NMR. In the NMR tube, no stirring was applied. Thus, the starting materials were mixed until all solid material was solubilized. Now, the mixture was funneled to the non-stirred glass vessel, in which the IR probe (IN-350T, Bruker Optics, Ettlingen; Germany) was inserted before. The temperature was kept

constantly at 10 °C using a thermostating bath. One IR spectrum per minute was recorded. The FTIR spectra are plotted versus time in Figure 22.

Since in a Diels-Alder reaction two molecules are fused, several shifts are present in the reaction spectra. The asymmetric stretching of the anhydride is shifted from 1040 cm^{-1} in MAA to 1050 cm^{-1} in DAP. A dominant absorption bands is found for the C=C bending vibration in DAP at 970 cm^{-1}.

From the recorded pure component FTIR spectra, the respective pure component models were set up. In the next step, these pure component models were combined into a mixture spectrum taken from the calibration experiment. The resulting IHM is shown in Figure 23. The pure component models are plotted in blue, while the IHM is depicted in red.

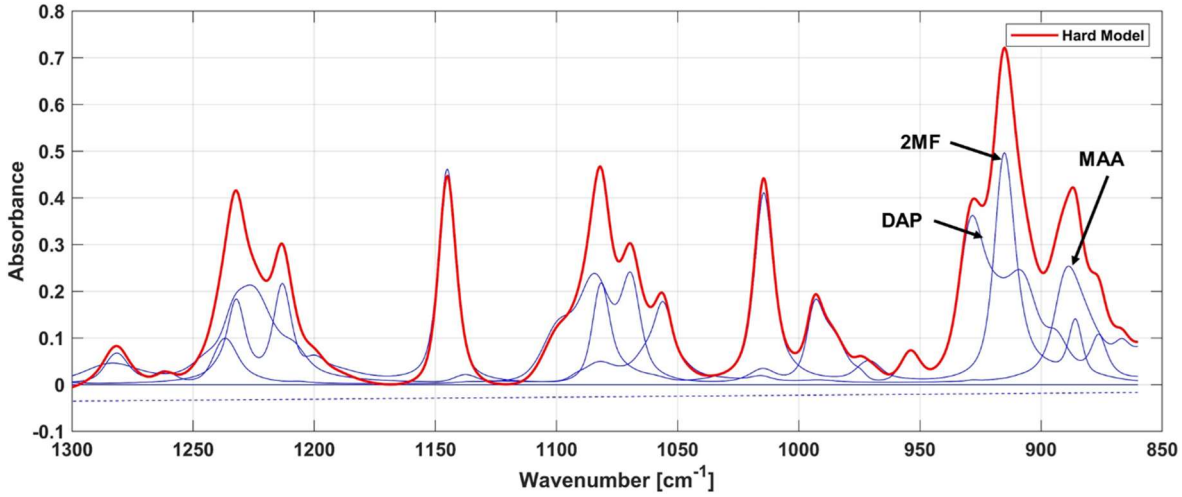

Figure 23: Indirect Hard Model for the Diels-Alder reaction of 2MF and MAA in the spectral range from 860 to 1300 cm^{-1}. Blue: pure component models, red: resulting IHM, plotted with PEAXACT 5.0 (S-Pact GmbH, Aachen Germany).

The resulting IHM was further calibrated with the converted NMR data obtained in the experiment carried out with two and five equivalents of 2MF. In the chapter *3.1. Analytical Methods*, the calibration curves are summarized. In Figure 24, the FTIR data are depicted as line (one spectrum/minute) and the respective calibration data points measured in the NMR spectrometer are shown as points. Both measurements are in accordance for all components. In the FTIR measurements, the dissolving process was faster compared to the ^{1}H-NMR experiments, hence, the measurement was started earlier. This behavior is attributed to the different sizes of the containers used for the mixing: The NMR tubes are of a very narrow diameter, which provide only a small void volume after filling with 2MF. In contrast, in the FTIR experiments, the mixing was

carried in falcon tubes, which were not completely filled, enabling a complete dissolution by shaking.

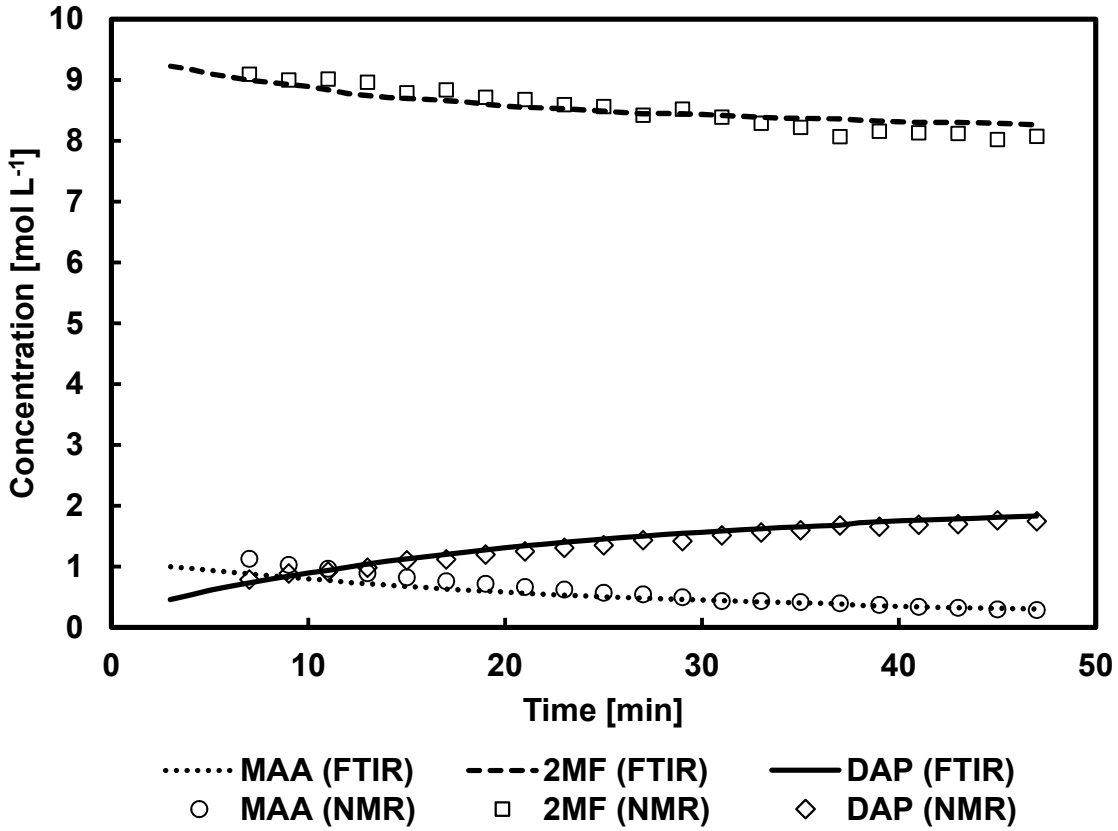

Figure 24: Concentration profiles derived from ^{1}H-NMR and FTIR measurements of the Diels-Alder reaction of MAA and 2MF at 10°C, non-stirred, five equivalents of 2MF. Experimental condition NMR: m_{MAA} = 0.09945 g, V_{2MF} = 0.455 mL, T = 10 °C, non-stirred, external standard: acetone-d_6. One ^{1}H-NMR spectrum measured every two minutes with Bruker Avance III 600 MHz conducted at Bielefeld University. NMR derived concentrations calculated based on stoichiometric conversion/yield as a function of molar fraction along with modeling the mixture density via Aspen Plus 9.0. Experimental conditions IR: m_{MAA} = 0.9136 g, V_{2MF} = 4.176 mL, T = 10 °C, non-stirred, one FTIR spectrum/min measured with Bruker Matrix-MF spectrometer equipped with Bruker IN-350T ATR probe.

To evaluate the accuracy of the chemometric model, the RMSEP is calculated according to equation 1 in section *1.2.3*. The RMSEP is calculated for every component of the reaction system at every point in time measured in the NMR calibration experiment. The results of these calculations are summarized in Table 7.

Table 7: RMSEP of the IHM model for the Diels-Alder reaction of 2MF and MAA.

Component	MAA	2MF	DAP
Ratio 1:2, RMSEP [mol L^{-1}]	0.201	0.072	0.154
Ratio 1:5, RMSEP [mol L^{-1}]	0.110	0.152	0.072

At higher contents of MAA, the error is higher too, which again can most likely attributed to the dissolving of the solid MAA in the liquid 2MF. The measurement of the product DAP shows a similar trend that can be explained by the increased product formation

rate caused by different solvation rates. Interestingly, the error of 2MF is increasing with higher liquid content. Here, a possibility is the error introduced from the conversion of relative to absolute amounts. Overall, in respect to the wide concentration range covered in the chemometric model, the errors between the two measurements seems to be acceptable. Subsequently, the model is applied for first reaction characterization and further for determining kinetics describing the reaction.

4.3 Reaction Characterization

In the previous section *4.2*, the workflow for the setup of the respective chemometric model is depicted. The experiments for the measurement of the calibration data were explained and the approach for converting the relative measurements into absolute concentrations presented. In the following, the application of the chemometric model is presented in terms of reaction characterization.

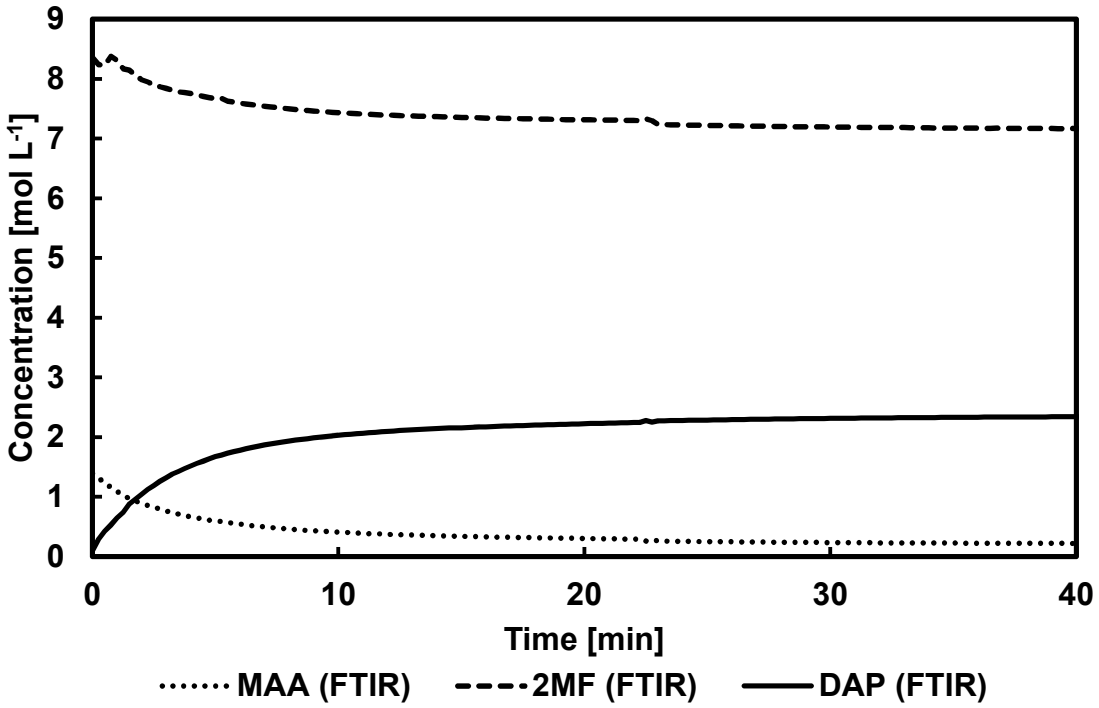

Figure 25: Concentration vs time plot of the Diels-Alder reaction of MAA and 2MF. Experimental conditions: m_{MAA} = 1.9619 g, V_{2MF} = 7.085 mL, T = 35°C, stirring rate: 550 rpm, four FTIR spectra per minute measured with Bruker Matrix-MF equipped with Bruker IN-350T ATR probe.

Unlike to the calibration experiments, in the following a magnetic stirrer was used to enhance the mass transfer and also to gain insights into the first minutes of the reaction. An exemplary run is plotted in Figure 25. In these runs, the solid MAA was

added to the thermostated double-jacked reaction vessel first, then 2MF was added and the FTIR measurement was started immediately.

The product formation starts immediately after both starting materials were mixed. The measurement of 2MF seems to be noisy in the beginning, which can be addressed to the dissolving process of MAA and 2MF. This becomes also clear, while looking at the concentration of DAP at the end of the reaction and comparing it to the concentration of MAA in the beginning. Since one molecule of MAA is transformed to one molecule of DAP, the concentration of MAA in the beginning should be approximately the same as the product has at the end of the experiment. Slight differences could be explained by changes in the reaction density. However, the difference observed in this case is more likely attributed to dissolving of MAA in 2MF. The solid MAA is dissolving and instantaneously available for the reaction. Since the solid MAA is not measured, this difference becomes obvious.

4.3.1 Influence of Temperature

In a series of experiments, the influence of temperature on the reaction rate was investigated in the range from 10 to 35 °C. All of these experiments were stirred using a magnetic stirrer to also monitor the reaction from the beginning onwards. First, the solid MAA was given to the reactor before the liquid 2MF was added. By stirring, the dissolving process was enabled starting the reaction. In Figure 26, for reasons of clarity only the DAP concentration is plotted, MAA and 2MF were also measured and recorded. The data depict a clear increase of the reaction rate with increasing temperature, while at the end of each individual experiment, the same concentration is reached independently of the temperature.

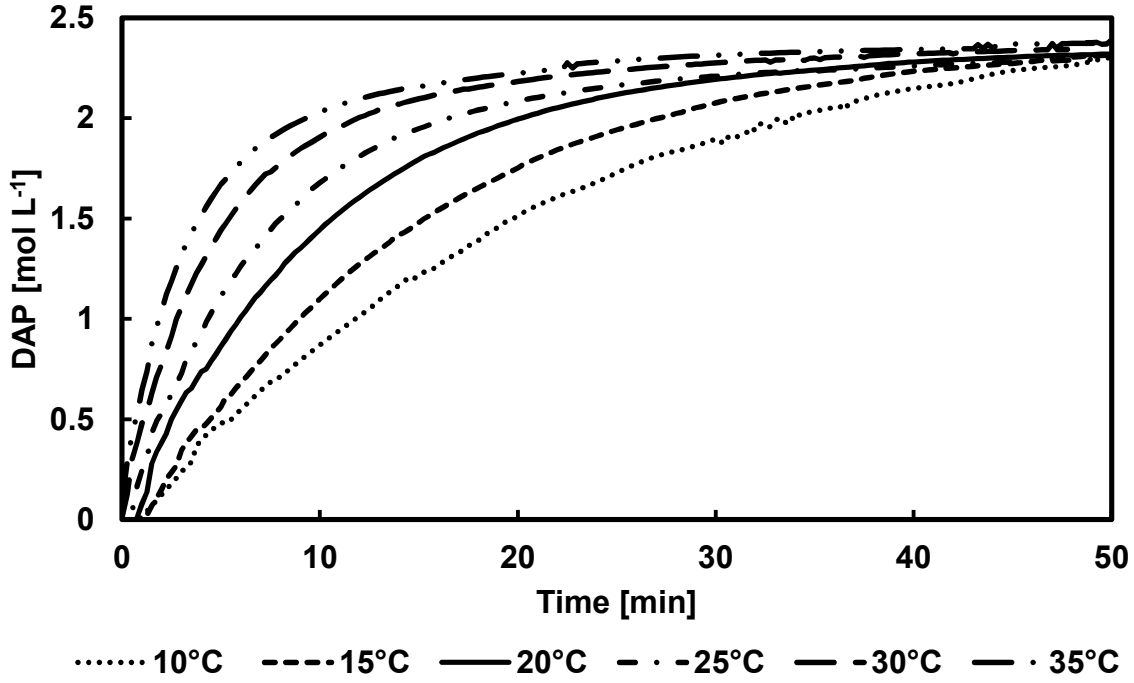

Figure 26: DAP formation vs time of the Diels-Alder reaction of 2MF and MAA in the temperature range of 10 °C to 35 °C, Experimental conditions: stirring rate: ratio 2MF:MAA = 4:1; four FTIR spectra per minute measured with Bruker Matrix-MF equipped with Bruker IN-350T ATR probe, stirring rate: 550 rpm; T = 10 °C: m_{MAA} = 1.9606 g, V_{2MF} = 7.085 mL; T = 15 °C: m_{MAA} = 1.9614 g, V_{2MF} = 7.085 mL; T = 20 °C: m_{MAA} = 1.9622 g, V_{2MF} = 7.085 mL; T = 25°C: m_{MAA} = 1.9614 g, V_{2MF} = 7.085 mL; T = 30 °C: m_{MAA} = 1.9614 g, V_{2MF} = 7.085 mL; T = 35 °C: m_{MAA} = 1.9619 g, V_{2MF} = 7.085 mL.

A further increase of the temperature was also tested, but these experiments resulted in the formation of a polymerization product precipitating at the reactor wall as well as on the stirrer. KAMO *et al*. were following Diels-Alder reactions of MAA with 2MF, furan and 2,5-dimethylfuran, also in terms of polymerization. For the reaction of furan with MAA they analyzed the polymerization product using NMR and IR, according to their analysis the polymer is a homopolymer formed from the *exo*-Diels-Alder product (Kamo *et al.*, 1974).

4.3.2 Influence of Starting Material Concentration

The influence of the ratio of the starting materials on the reaction rate was investigated. For this reason, a set of reactions was carried out in a thermostated stirred tank reactor analyzed with the established inline analytics. The temperature was set to 10 °C and one spectrum was measured every 30 seconds. The concentration of DAP as function of time is shown in Figure 27. The ratio of 2MF to MAA was successively increased throughout this experimental series, as indicated in the legend of the figure. With a higher ratio of 2MF, the overall concentration achieved in the experiments is

decreasing as expected. At equimolar, as well as low ratios of 2MF, the experiments were stopped when the crystallizing product was observed, since this affects the reaction rate obviously by influencing the equilibrium in terms of the law by LE CHATELIER.

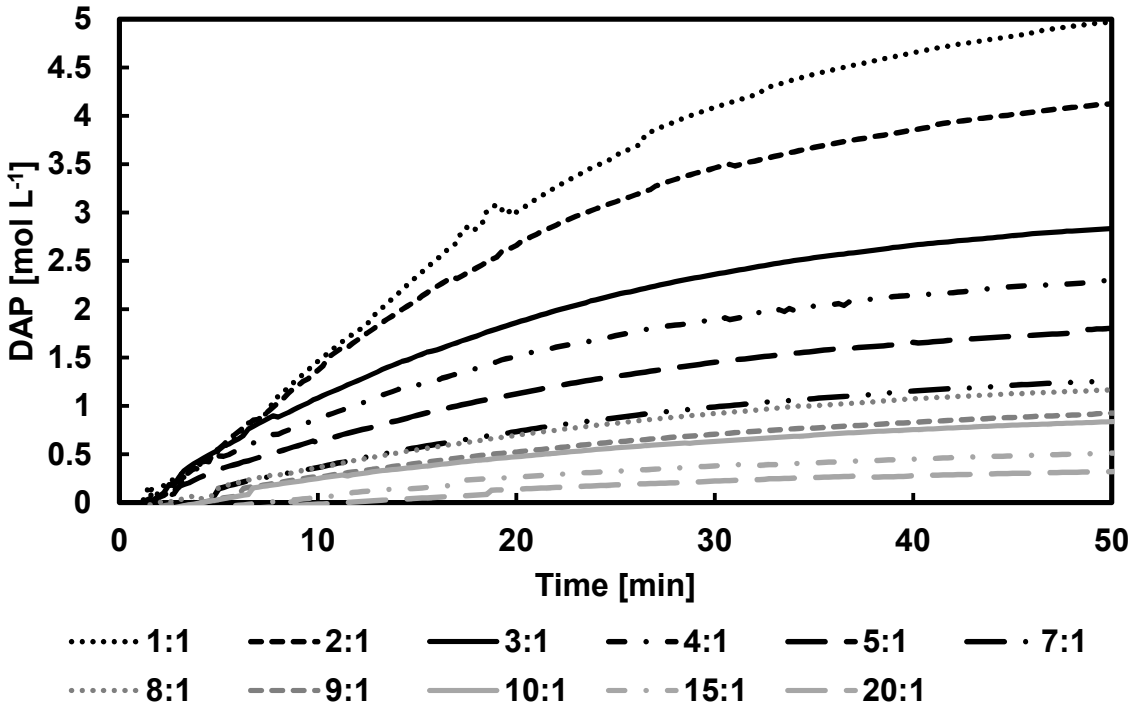

Figure 27: DAP concentration vs time of the Diels-Alder reaction of 2MF and MAA for different concentrations of starting material. Experimental conditions: four FTIR spectra per minute measured with Bruker Matrix-MF equipped with Bruker IN-350T ATR probe, T = 10 °C, stirring rate: 550 rpm, ratio MAA:2MF = 1:1: m_{MAA} = 5.8840 g, V_{2MF} = 5.314 mL; ratio 2:1: m_{MAA} = 3.9226 g, V_{2MF} = 7.085 mL; ratio 3:1: m_{MAA} = 1.9617 g, V_{2MF} = 5.314 mL; ratio 4:1: m_{MAA} = 1.9619 g, V_{2MF} = 7.085 mL; ratio 5:1: m_{MAA} = 1.4714 g, V_{2MF} = 6.642 mL; ratio 7:1: m_{MAA} = 1.0789 g, V_{2MF} = 6.8195 mL.; ratio 8:1: m_{MAA} = 0.9804 g, V_{2MF} = 7.085 mL.; ratio 9:1: m_{MAA} = 0.8825 g, V_{2MF} = 7.174 mL.; ratio 10:1: m_{MAA} = 0.7848 g, V_{2MF} = 7.085 mL.; ratio 15:1: m_{MAA} = 0.5397 g, V_{2MF} = 7.307 mL.; ratio 20:1: m_{MAA} = 0.3925 g, V_{2MF} = 7.085 mL.

In the beginning of all experiments carried out, a delay in product formation is observed. This delay is assigned to the solvation of the solid substrate MAA, which needs to occur before a reaction can take place. For higher ratios of 2MF to MAA, this delay is also visible. This behavior can also be explained by relatively low DAP concentrations that are in the range of the chemometric predictive error. In the equimolar run at 18 min, a deviation from the curve can be seen. This is probably due to moving of the ATR probe within the setup.

From the concentration time curves, the initial reaction rate can be calculated according to the initial rate method. Therefore, a linear increase of the product formation is assumed plausibly. This linear range is expected to be valid below conversion of 5% with acceptable errors in kinetic measurements (Casado *et al.*,

1986). The initial reaction rate is the slope of this linear trend line with moles per liter and minute. The results of these calculations are shown in dependence of the respective molar fraction in Figure 28.

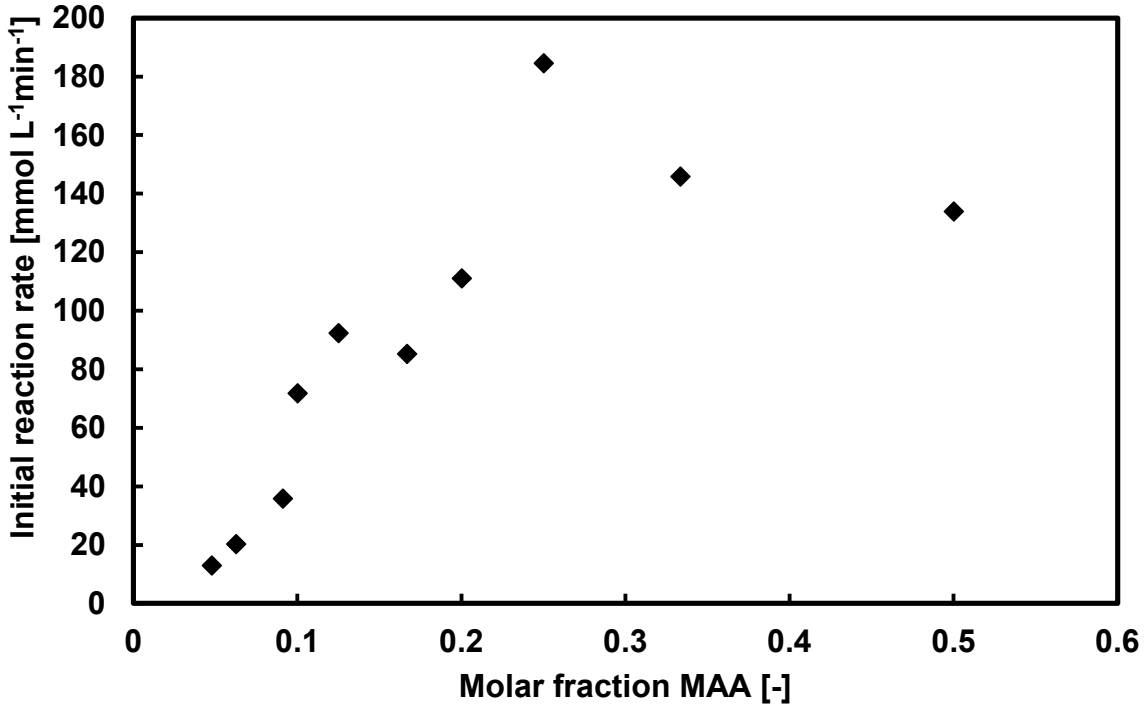

Figure 28: Initial reaction rate as function of the molar fraction of maleic acid anhydride. Experimental conditions: four FTIR spectra per minute measured with Bruker Matrix-MF equipped with Bruker IN-350T ATR probe, T = 10 °C, stirring rate: 550 rpm, ratio MAA:2MF = 1:1: m_{MAA} = 5.8840 g, V_{2MF} = 5.314 mL; ratio 2:1: m_{MAA} = 3.9226 g, V_{2MF} = 7.085 mL; ratio 3:1: m_{MAA} = 1.9617 g, V_{2MF} = 5.314 mL; ratio 4:1: m_{MAA} = 1.9619 g, V_{2MF} = 7.085 mL; ratio 5:1: m_{MAA} = 1.4714 g, V_{2MF} = 6.642 mL; ratio 7:1: m_{MAA} = 1.0789 g, V_{2MF} = 6.8195 mL.; ratio 8:1: m_{MAA} = 0.9804 g, V_{2MF} = 7.085 mL.; ratio 9:1: m_{MAA} = 0.8825 g, V_{2MF} = 7.174 mL.; ratio 10:1: m_{MAA} = 0.7848 g, V_{2MF} = 7.085 mL.; ratio 15:1: m_{MAA} = 0.5397 g, V_{2MF} = 7.307 mL.; ratio 20:1: m_{MAA} = 0.3925 g, V_{2MF} = 7.085 mL.

First an increase of the initial reaction rate with an increase of MAA can be observed, which seems to reach a maximum at a molar fraction of 0.25. At higher rations of MAA to 2MF, the measurement inaccuracy is increasing, which is explained by the increased solid fraction within the reactor. The dissolving process is affected and therefore, also the inline analytic, which only measures the liquid phase. The solution rate is depending on the particle size of the MAA, which was ground prior to the experiment. Since the grinding was carried out using a mortar, the same particle size could not always be achieved leading to these deviations. For a more detailed analysis of this dissolution process, deeper insights into the particle size distribution are necessary.

4.4 Kinetic Model

In this chapter, the inline data evaluated with the respective chemometric model are applied for the determination of the reaction kinetics. Since the Diels-Alder reaction is in principle reversible, especially at high temperatures, also the kinetic modeling is carried out assuming a backward reaction. However, in the investigated temperature range, a *retro*-Diels-Alder reaction is unlikely, therefore, also an irreversible approach is tested. Both approaches are shown in Figure 29. For the reversible as well as for the irreversible kinetic model, a second order reaction is assumed.

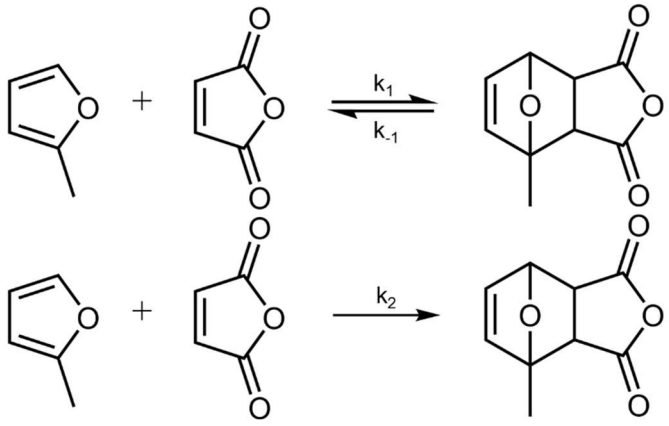

Figure 29: Reversible (top) and irreversible (bottom) kinetic approach for the reaction of 2MF and MAA.

Using Matlab (R2019a, Mathworks, Natick, USA), the inline data are fitted to both approaches with the method of progress curve analysis and the obtained data are evaluated in the following section. For the determination of these kinetic data, only experiments carried out at 10 °C with a range of one to 25 equivalents of 2MF in respect to MAA were taken into account. A further increase of the 2MF equivalents resulted in very low product concentrations, which are close to the error range of the IHM. The respective script used can be found in the *supplemental information 9.4.1* Matlab script Diels-Alder reaction of 2MF and MAA.

For the reversible approach, the rate equations 6, 8 and 7 are shown, which were given to the Matlab script performing the progress curve analysis:

$$\frac{dc_{MAA}}{dt} = -k_1\, c_{MAA}\, c_{2MF} + k_{-1}\, c_{DAP} \quad (6)$$

$$\frac{dc_{2M}}{dt} = -k_1\, c_{MAA}\, c_{2MF} + k_{-1}\, c_{DAP} \quad (7)$$

$$\frac{dc_{DAP}}{dt} = k_1\, c_{MAA}\, c_{2M} - k_{-1}\, c_{DAP} \quad (8)$$

With k_1: forward reaction constant [L mol^{-1} min^{-1}], k_{-1}: reverse reaction constant [min^{-1}] c_{MAA}: concentration MAA [mol L^{-1}], c_{2MF}: concentration 2MF [mol L^{-1}], c_{DAP}: concentration DAP [mol L^{-1}].

In case of an irreversible kinetic, the following rate equations (9, 10 and 11) were used to determine the respective reaction constant:

$$\frac{dc_{MAA}}{dt} = -k_2\, c_{MAA}\, c_{2MF} \quad (9)$$

$$\frac{dc_{2MF}}{dt} = -k_2\, c_{MAA}\, c_{2MF} \quad (10)$$

$$\frac{dc_{DAP}}{dt} = k_2\, c_{MAA}\, c_{2MF} \quad (11)$$

With k_2: reaction constant [L mol^{-1} min^{-1}], c_{MAA}: concentration MAA [mol L^{-1}], c_{2MF}: concentration 2MF [mol L^{-1}], c_{DAP}: concentration DAP [mol L^{-1}].

To evaluate, which of the kinetic models, the reversible or the irreversible, fits the experimental data more accurately, the inline data recorded were fitted each in a single progress curve analysis first. The results of the rate constants, both for the reversible as well as the irreversible kinetic, are summarized in Figure 30.

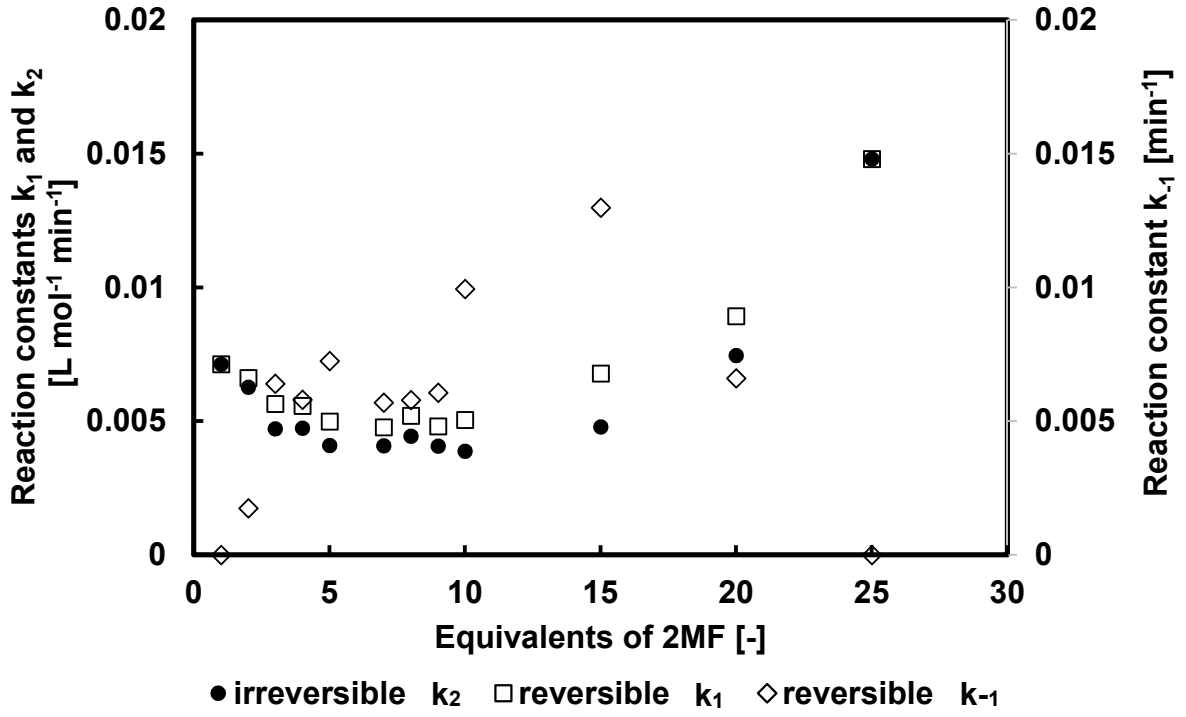

Figure 30: Kinetic constants determined from for the Diels-Alder reaction of 2MF and MAA. Inline data (four FTIR spectra recorded per minute) evaluated with the developed IHM, fitted by progress curve analysis. Reaction conditions: T = 10 °C, stirring rate: 550 rpm, ratio MAA:2MF = 1:1: m_{MAA} = 5.8840 g, V_{2MF} = 5.314 mL; ratio 2:1: m_{MAA} = 3.9226 g, V_{2MF} = 7.085 mL; ratio 3:1: m_{MAA} = 1.9617 g, V_{2MF} = 5.314 mL; ratio 4:1: m_{MAA} = 1.9619 g, V_{2MF} = 7.085 mL; ratio 5:1: m_{MAA} = 1.4714 g, V_{2MF} = 6.642 mL; ratio 7:1: m_{MAA} = 1.0789 g, V_{2MF} = 6.8195 mL.; ratio 8:1: m_{MAA} = 0.9804 g, V_{2MF} = 7.085 mL.; ratio 9:1: m_{MAA} = 0.8825 g, V_{2MF} = 7.174 mL.; ratio 10:1: m_{MAA} = 0.7848 g, V_{2MF} = 7.085 mL.; ratio 15:1: m_{MAA} = 0.5397 g, V_{2MF} = 7.307 mL.; ratio 20:1: m_{MAA} = 0.3925 g, V_{2MF} = 7.085 mL.

For the reversible modelling approach, the kinetic constant determined for the backward reaction is larger than the forward reaction for the experiments carried out with three to 15 equivalents of 2MF applied. This behavior is unrealistic, since no product formation could be observed.

A detailed look into the confidence intervals (Figure 31) reveals a large error for the backwards reaction constant, which may explain the product formation observed.

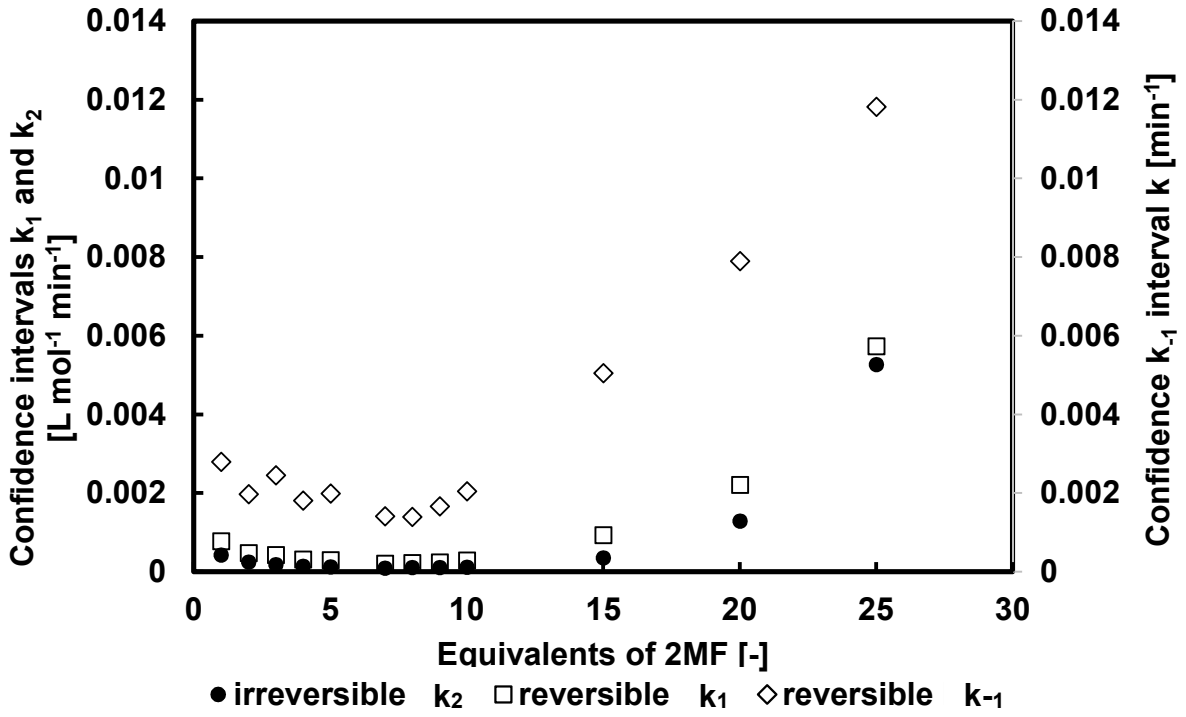

Figure 31: Confidence intervals of the kinetic parameters of the Diels-Alder reaction of 2MF and MAA. Inline data (four FTIR spectra recorded per minute) evaluated with the developed IHM, fitted by progress curve analysis. Reaction conditions: T = 10 °C, stirring rate: 550 rpm, ratio MAA:2MF = 1:1: m_{MAA} = 5.8840 g, V_{2MF} = 5.314 mL; ratio 2:1: m_{MAA} = 3.9226 g, V_{2MF} = 7.085 mL; ratio 3:1: m_{MAA} = 1.9617 g, V_{2MF} = 5.314 mL; ratio 4:1: m_{MAA} = 1.9619 g, V_{2MF} = 7.085 mL; ratio 5:1: m_{MAA} = 1.4714 g, V_{2MF} = 6.642 mL; ratio 7:1: m_{MAA} = 1.0789 g, V_{2MF} = 6.8195 mL.; ratio 8:1: m_{MAA} = 0.9804 g, V_{2MF} = 7.085 mL.; ratio 9:1: m_{MAA} = 0.8825 g, V_{2MF} = 7.174 mL.; ratio 10:1: m_{MAA} = 0.7848 g, V_{2MF} = 7.085 mL.; ratio 15:1: m_{MAA} = 0.5397 g, V_{2MF} = 7.307 mL.; ratio 20:1: m_{MAA} = 0.3925 g, V_{2MF} = 7.085 mL.

In the region of three to ten equivalents of 2MF, the determined kinetic constants assuming an irreversible reaction are constant at a value of about 0.004 to 0.005 L mol^{-1} min^{-1}. In addition, the confidence intervals determined in this region are close to zero, displaying that the kinetic equations are suitable to fit the inline measured data. For higher ratios of 2MF to MAA, the rate constant seems to increase, which may be attributed to increasing inaccuracies of the inline analytic and the respective chemometric model. Concluding, the reversible approach yields rate constant showing a high variation throughout the single experiments. In contrast, the reversible rate constants are in a similar range, especially in the experiments carried out with an

excess of 2MF between 3 and 15 equivalents. The variations of the rate constants are most likely attributed to the measurement and data treatment methods.

Since the intention of a kinetic model is to describe a reaction universally and independently from the applied concentration range, the kinetic in the following is determined using the experiments recorded in the region of five to ten equivalents assuming irreversible kinetics. For reasons of clarity, the respective rate constants for the reversible approach are also shown. The results of both are summarized in Table 8.

Table 8: Reaction rate constants for reversible and irreversible kinetic models and their confidence intervals determined from experimental inline data. Experimental conditions: ratio 5:1: m_{MAA} = 1.4714 g, V_{2MF} = 6.642 mL; ratio 7:1: m_{MAA} = 1.0789 g, V_{2MF} = 6.8195 mL.; ratio 8:1: m_{MAA} = 0.9804 g, V_{2MF} = 7.085 mL.; ratio 9:1: m_{MAA} = 0.8825 g, V_{2MF} = 7.174 mL.; ratio 10:1: m_{MAA} = 0.7848 g, V_{2MF} = 7.085 mL.

	Reaction rate constant	**Confidence interval**
$\mathbf{k_1}$ [$\cdot 10^{-3}$ L mol^{-1} min^{-1}]	4.959	0.115
$\mathbf{k_{-1}}$ [$\cdot 10^{-3}$ min^{-1}]	6.796	0.775
$\mathbf{k_2}$ [$\cdot 10^{-3}$ L mol^{-1} min^{-1}]	4.116	0.051

In Figure 32, the concentrations determined from the kinetic model as well as the inline measurements for a set ratio of 2MF to MAA of 7 are depicted. The course of the kinetic model fits the obtained data from the inline measurements with satisfying accuracy. In the beginning of the reaction, a deviation for both starting materials can be observed, which is caused by the dissolution process of MAA in the liquid phase 2MF. The concentration of DAP measured inline shows a slight delay in comparison to the kinetic model, which again can be attributed to the delay of the dissolution process. After the kinetic model was successfully validated, it can be applied for the simulation of experiments at different conditions to verify its correctness.

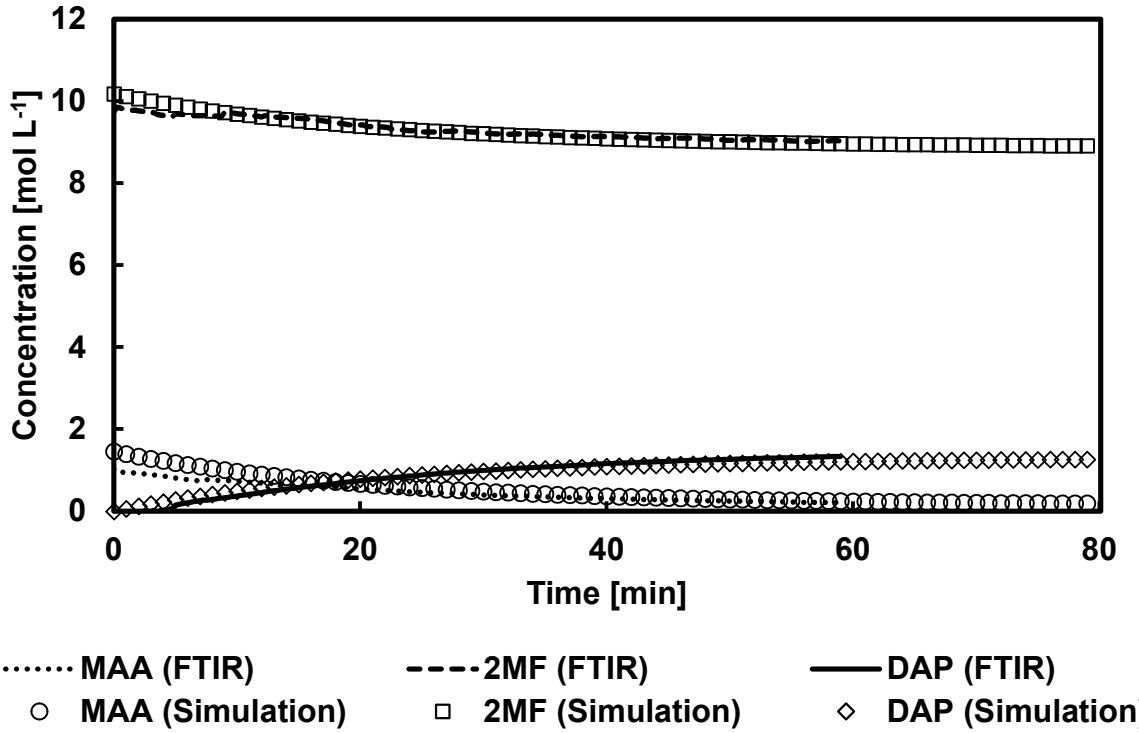

Figure 32: Inline data and the determined irreversible kinetic model for the Diels-Alder reaction. Inline data (four FTIR spectra recorded per minute) evaluated with the developed IHM, fitted by progress curve analysis. Reaction conditions: T = 10 °C, stirring rate: 550 rpm, ratio 7:1: m_{MAA} = 1.0789 g, V_{2MF} = 6.8195 mL.

The determined kinetics were shown to be correct and can be applied for simulations. In addition, the kinetic is tested in simulations outside of the experimental conditions used for the determination. Therefore, an experiment with four equivalents of 2MF is simulated and compared to the applied FTIR measurements. The results are shown in Figure 33. Again, in the beginning of the reaction, a deviation in the course of MAA is observed, caused by dissolving of the solid in the liquid phase. In the later course of the reaction, the inline measurement of DAP is higher than the values obtained by the kinetic model. The concentration of 2MF is also underestimated in respect to the inline measurements. A potential cause for the deviation of the kinetic model and the inline measurements is the quantification approach carried out with the calibration data collected in NMR experiments. For a further improvement of this analytical method, a direct quantification within the calibration experiments is needed. This can be achieved by quantifying the external standard (acetone-d_6) and relating the whole NMR spectrum to this external standard.

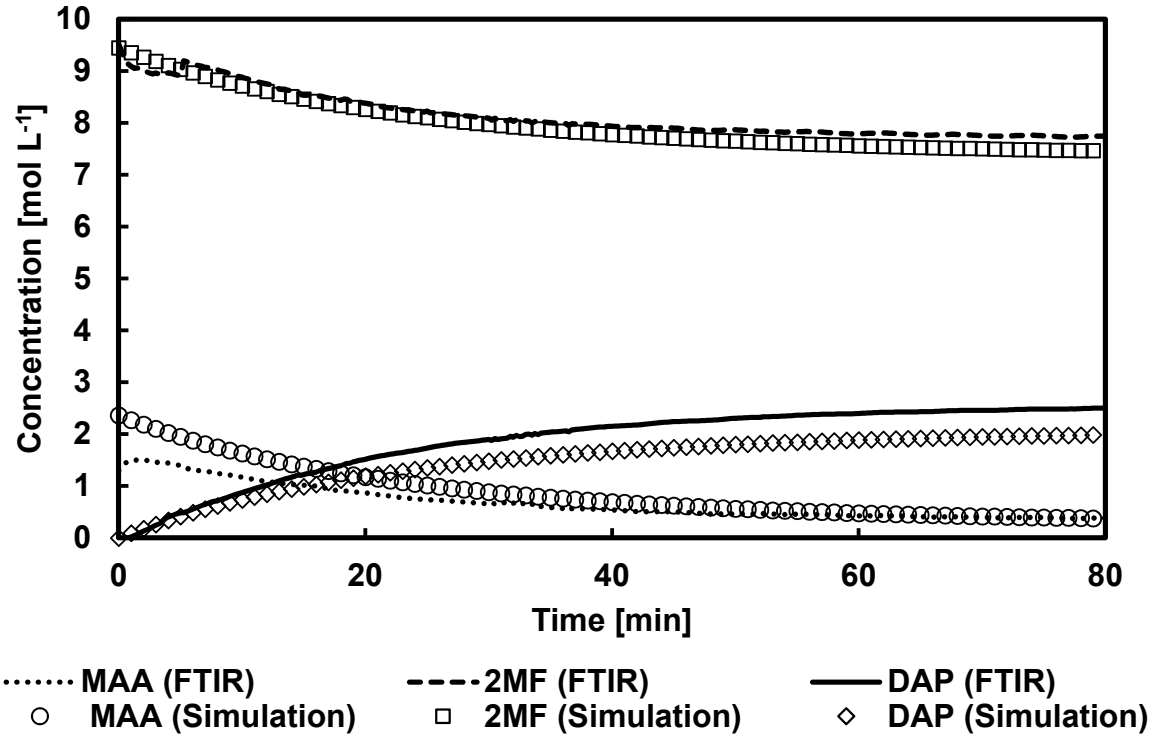

Figure 33: Inline data and simulation using the determined irreversible kinetic model for the Diels-Alder reaction. Inline data (four FTIR spectra recorded per minute) evaluated with the developed IHM, fitted by progress curve analysis. Reaction conditions: T = 10 °C, stirring rate: 550 rpm, ratio 4:1: m_{MAA} = 1.9619 g, V_{2MF} = 7.085 mL.

4.5 Determination of Activation Energy

Using the kinetic constants determined from the experimental series performed at different temperatures, the energy of activation is determined in the following. For the temperature range investigated, the position of the equilibrium is far on the product side and no significant *retro*-Diels-Alder reaction is expected, therefore, only the energy of activation for the forward reaction is determined.

In equation 12, the ARRHENIUS equation is shown:

$$k = A\, e^{\frac{-E_A}{R\,T}} \tag{12}$$

With k: reaction constant, E_A Energy of activation [kJ mol^{-1}], R: universal gas constant [J mol^{-1} K^{-1}] and T: temperature [K], A: pre-exponential factor.

The linearized ARRHENIUS equation is found in equation 13:

$$\ln k = \frac{E_A}{R\,T} + \ln A \tag{13}$$

With k: reaction constant, E_A Energy of activation [kJ mol^{-1}], R: universal gas constant [J mol^{-1} K^{-1}] and T: temperature [K], A: pre-exponential factor.

From the temperature experiment series, also an ARRHENIUS plot was obtained, which is shown in Figure 34. The kinetic constants determined by progress curve analysis from the inline measurements are plotted logarithmically versus the reciprocal temperature. As can be seen in the figure, a linear trend can be fitted. From the linear fit, the energy of activation as well as the pre-exponential factor are calculated.

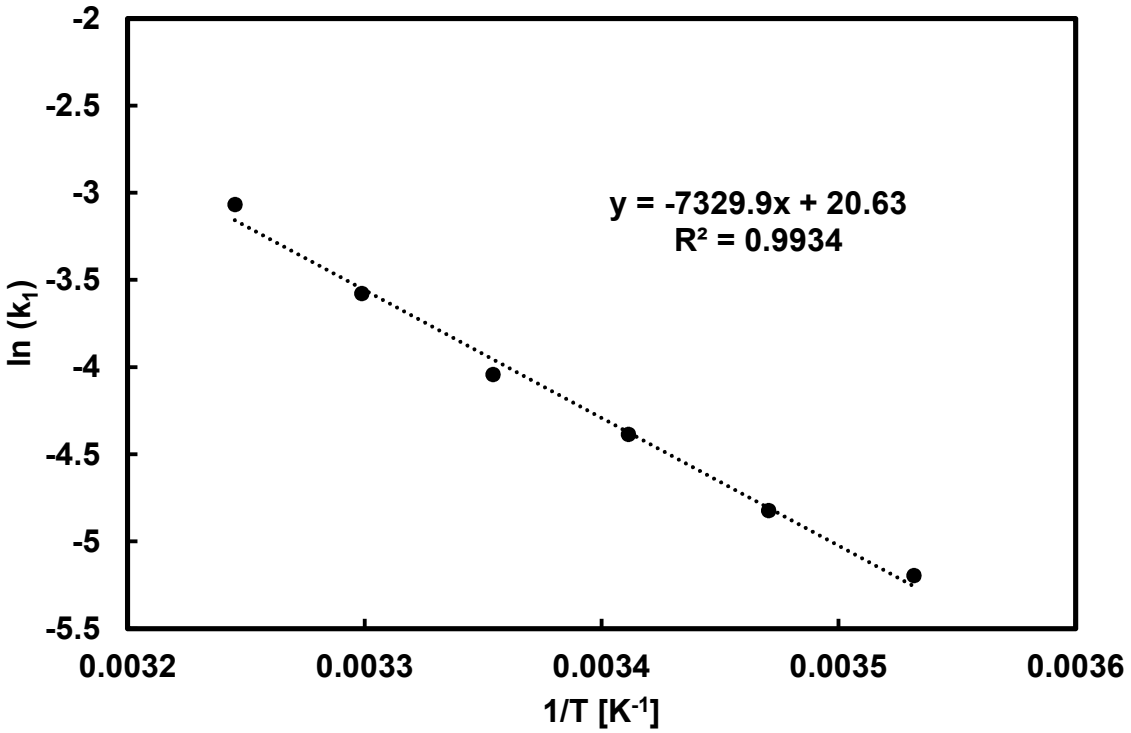

Figure 34: Arrhenius plot of the Diels-Alder reaction of 2MF and MAA in the range of 10 to 35 °C. Experimental conditions: ratio 2MF:MAA = 4:1; four FTIR spectra per minute measured with Bruker Matrix-MF equipped with Bruker IN-350T ATR probe, stirring rate: 550 rpm; T = 10 °C: m_{MAA} = 1.9606 g, V_{2MF} = 7.085 mL; T = 15 °C: m_{MAA} = 1.9614 g, V_{2MF} = 7.085 mL; T = 20 °C: m_{MAA} = 1.9622 g, V_{2MF} = 7.085 mL; T = 25°C: m_{MAA} = 1.9614 g, V_{2MF} = 7.085 mL; T = 30 °C: m_{MAA} = 1.9614 g, V_{2MF} = 7.085 mL; T = 35 °C: m_{MAA} = 1.9619 g, V_{2MF} = 7.085 mL.

From the gradient, the energy of activation is calculated to 61 kJ mol^{-1} and from the y-interception, the pre-exponential factor is determined to 9.11*10^{8}. The determined energy of activation is in reasonable range compared to other values reported for other Diels-Alder reactions. CARNEIRO DE OLIVEIRA *et al.* determined the energy of activation of the Diels-Alder reaction of furfuryl alcohol and *N*-hydroxymaleimide to 48 kJ mol^{-1} using ^{1}H-NMR measurements (Carneiro de Oliveira *et al.*, 2020). The experiments were carried out in deuterated dimethyl sulfoxide. Hence, the effect of a solvent on the reaction kinetics and thermodynamic behavior cannot be ruled out.

5 Hydrogenation of 4-methyl-3a,4,7,7a-tetrahydro-4,7-epoxyisobenzofuran-1,3-dione

5.1 Introduction: Heterogeneously Catalyzed Hydrogenation Reactions

About 200 years ago, the first example for a heterogeneously catalyzed hydrogenation reaction was reported: DÖBEREINER discovered that platinum can catalyze the reaction between hydrogen and oxygen at low temperatures. The first lighter was invented and commercialized as “Döbereiners lamp” (Wisniak, 2010). The hydrogenation reaction turned out to be a very useful tool in organic chemistry and in 1902 the first patent for a liquid phase hydrogenation was given to NORMANN (Normann, 1902). Soon in 1905, the Haber-Bosch process followed, being the first example for a large scale application (Jackson, 2018). Another important example of a hydrogenation reaction, is the Fischer-Tropsch reaction, which is used to produce liquid hydrocarbons from carbon monoxide and hydrogen (Fischer, Tropsch, 1923).

Hydrogenation reactions are exothermic in general, for alkenes the released heat varies in the range of 90 to 130 kJ mol^{-1} (Barnicki, 2012). These reactions can be applied in gas or liquid phase, not necessarily involving a solvent. For the catalysis either soluble, homogeneous or insoluble, heterogeneous catalysts can be used. In the latter case, metals from the platinum group elements are catalyzing the hydrogenation reaction. Mainly platinum (Pt), palladium (Pd), rhodium (Rh) and ruthenium (Ru) are applied, which show a high activity. Two different properties are important, the electronic and the geometric factor. The electronic factor determines the chemisorption of hydrogen on the metal surface and is influenced by the number of vacant *d*-orbitals. Furthermore, the geometric factor, the arrangement of the metal atoms defines the energy of the transition state, which should be at a minimum (Bond, 1957).

Heterogeneous catalysts bear the advantage of being easily recyclable, since these can be easily separated from a reaction mixture by filtration or application in a packed bed reactor. After washing and drying they can be reused for the next batch reaction. When metals are bound onto a suitable carrier, they can lose a part of their activity. However, this activity loss is only in the range of 2-5% for palladium and platinum, for ruthenium and rubidium the activity loss is higher, at about 10% (Jackson, 2018). In respect to the price of palladium of roughly 60000 € kg^{-1} (Gold.de, 2020), this activity loss is competed by the possibility of recycling the catalyst.

A possible reaction mechanism for the heterogeneously catalyzed hydrogenation of alkenes was proposed by HORIUTI and POLANYI in 1934. They assumed the reaction is taking place in three individual steps: First the C=C bond is adsorbed to the metal atoms on the surface of the catalyst particle, the π bond of the alkene is broken and two new carbon-metal bonds are formed (Bond, 1957). The molecular hydrogen is also adsorbed to the metal surface and is disassociating in this step. Next, a hydrogen atom is added to one of the alkenes carbons. The intermediate molecule can rotate, detach from the catalyst surface and a hydrogen atom can be released again. While the molecule is still adsorbed at the catalyst, a second hydrogen atom can be attached. This step is not reversible, therefore, determining the end of the reaction (Horiuti, Polanyi, 1934).

For heterogeneous hydrogenation reactions performed in a liquid phase using porous catalyst particles, gaseous hydrogen needs to be solubilized in the reaction media to be available for the reaction. As shown in Figure 35, the concentration of hydrogen is limited by three different mass transfer hindrances.

- First, from the gas phase, hydrogen is solubilized in the liquid phase. The concentration achieved in this liquid phase is determined by the Henry coefficient and the partial pressure of hydrogen as well as the respective solvent.
- Secondly, the hydrogen need to pass the boundary layer between the catalyst and the liquid phase. Moreover, its concentration is decreasing towards the particle. Here, the concentration of hydrogen is depending on the concentration in the liquid phase and the thickness of the boundary layer.
- Additionally, since palladium is also contained inside the pores of the catalyst, diffusion into the pores is also limiting the hydrogen transfer to the active sites.

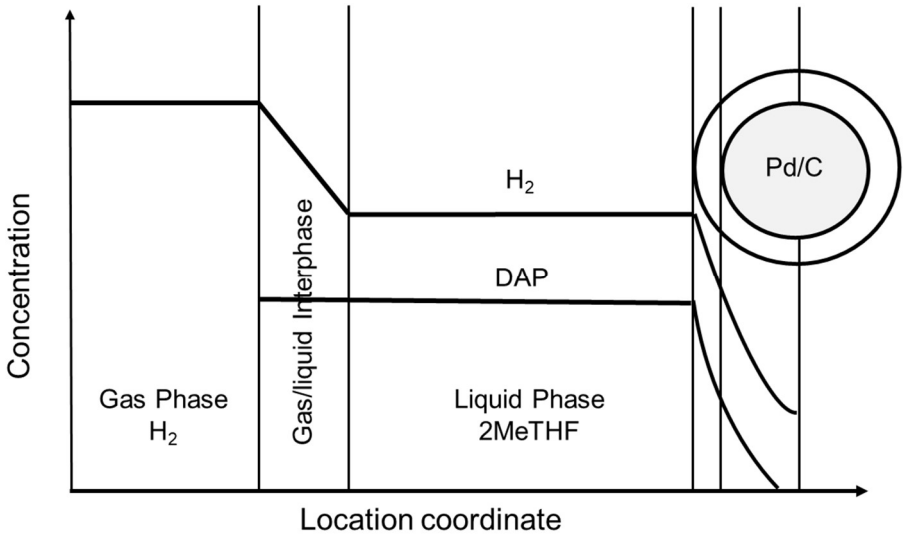

Figure 35: Mass transfer from the gas phase through the liquid 2MeTHF phase to the Pd/C catalyst particle during hydrogenation of DAP. Adapted from Machado (Machado, 2007).

Different applications of inline analytics in hydrogenation reactions are reported in literature. In a flow reactor, the hydrogenation of styrene was monitored using a high-field NMR equipped with a stripline NMR probe. By this approach, besides measuring the starting material and product concentration, the hydrogen solubility was determined (Tijssen *et al.*, 2019). Another experiment in a micro reactor flow system, RUEPING *et al*. applied a FTIR measurement to follow the conversion of the starting material to the product as a function of reactor temperature. By this approach, reaction parameters can be evaluated in a fast manner with reduced experimental effort (Rueping *et al.*, 2012). In batch reactors, additionally, different inline analytics were successfully established with higher hydrogen pressures. Here, traditional steel autoclaves are used with a probe inserted in a special port of the reactor. FISCHER *et al.* were following the hydrogenation of 1-octene with a Raman probe. They confirmed their measurements with GC samples analyzed. Their kinetic data are in agreement with the literature data, showing the preciseness of this approach (Fischer *et al.*, 2017). Also FTIR can be applied for measuring the concentration of hydrogenation reactions: the conversion of *y*-butyrolactone to 1,4-butanediol was followed with an ATR probe and additional offline GC measurements providing good accordance. By varying the ring size, information on the reaction mechanism were obtained (Hamminga *et al.*, 2004). Another group was applying Raman spectroscopy for the measurement of the conversion of different imines and in parallel, the product formation was analyzed with an ATR probe. They showed a high sensitivity also at low concentrations making these analytical methods highly suitable for real-time measurements (Knöpke *et al.*, 2010).

In the present work, the hydrogenation of the Diels-Alder intermediate (DAP) for obtaining a stable plasticizer building block is investigated. The reaction scheme is shown in Figure 36. In this reaction step, 2-methyltetrahydrofuran (2MeTHF) is employed as solvent. 2MeTHF is an example for a green solvent, which can be produced on the basis of renewable resources (Pace *et al.*, 2010). Beside hydrogenation towards the aimed molecule, side reactions based on the *retro*-Diels-Alder reaction are taken into account. The intermediate DAP can decay to MAA and 2MF, which are then also available for hydrogenation. 2MF, in the case of a full hydrogenation will form 2MeTHF (Kang *et al.*, 2017), which is at the same time applied as solvent in this process and therefore is neglected. However, hydrogenation of MAA is leading to succinic acid anhydride (BSA), which needs to be removed from the reaction mixture prior to the final esterification step. If this is not ensured, the BSA will consequently be esterified leading to bis-2-ethylhexyl succinate. Its removal from the plasticizer is more challenging, due to the high boiling point of the ester. For this reason, an inline measurement method for monitoring both products, 4-methylhexahydro-4,7-epoxyisobenzofuran-1,3-dione (DAPH) and BSA, was developed.

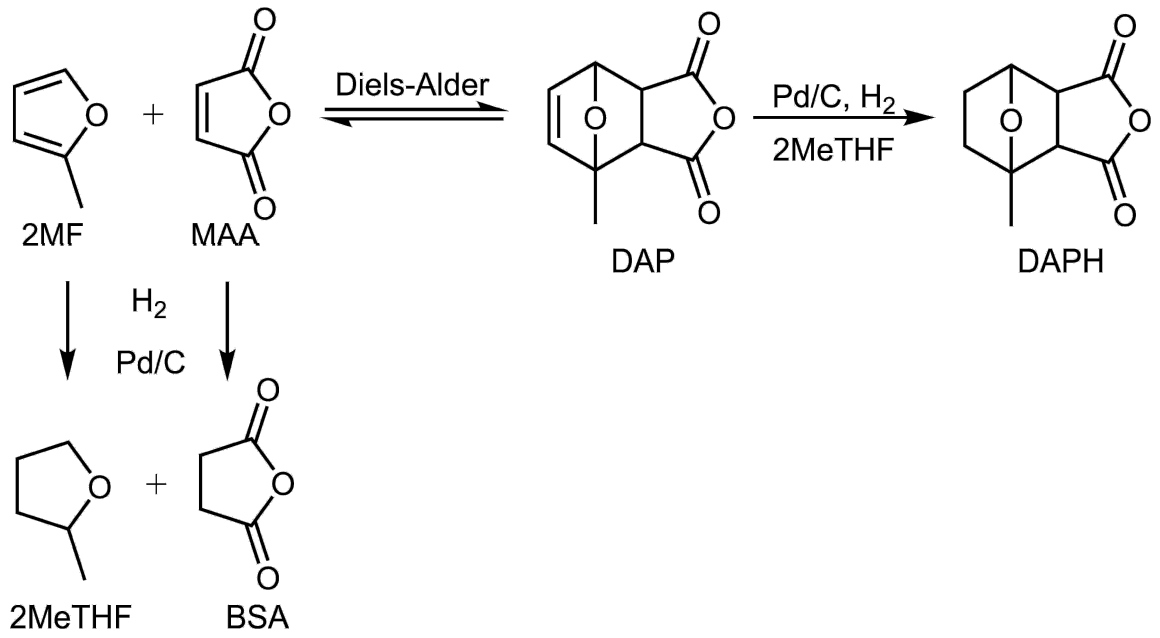

Figure 36: Hydrogenation of Diels-Alder product (DAP) to 4-methylhexahydro-4,7-epoxyisobenzofuran-1,3-dione (DAPH) shown with possible side product formation.

Besides recording inline FTIR spectra from the reaction, the pressure as well as the temperature in the reaction vessel is monitored. These measurements provide first

information about the reaction itself. In an exemplary experiment, these data were recorded and plotted in Figure 37.

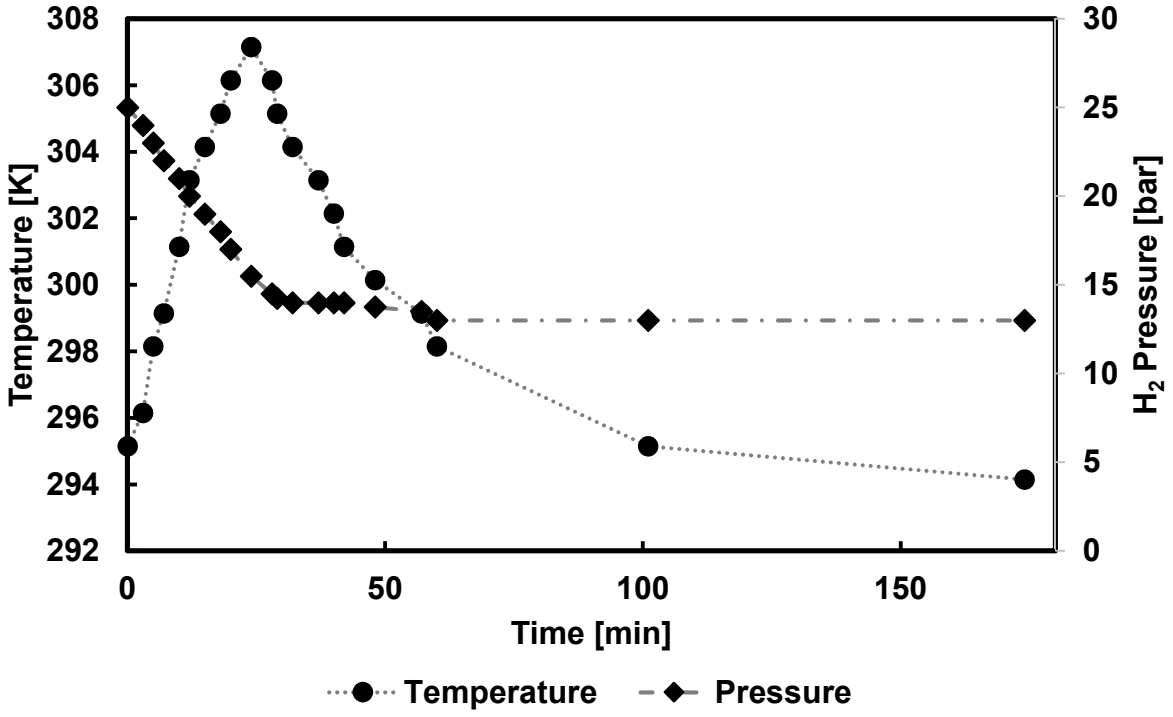

Figure 37: Temperature and pressure profiles recorded during the hydrogenation of DAP to DAPH. Reaction conditions: m_{DAP} = 25.0051 g; V_{2MeTHF} = 150 mL; $m_{Pd/C}$ = 1.0053 g, stirring rate: 400 rpm.

The pressure in the reactor is decreasing in a linear manner until a plateau is reached. In contrast, the temperature measured inside the reactor is increasing during the pressure decrease. The maximum temperature is reached, when the pressure reaches the final value. The linearity observed for the pressure decrease indicates either a first order reaction or else a present mass transfer limitation in the experimental setup. From the temperature measurement, an estimation for the heat of reaction can be drawn. For this estimation, different assumptions were made:

- The heat capacities of the starting material and of the product are neglected
- Ideal heat transfer between the reaction mixture and the reactor vessel is assumed
- The reactor vessel itself is adiabatic (no heat transfer to the environment)

With these assumptions made, the heat of the hydrogenation reaction is estimated to 139 kJ mol^{-1}, which is slightly above the range given by BARNICKI (Barnicki, 2012). However, it is clear that the assumption of an adiabatic reactor is not valid. Therefore, the heat of the reaction is overestimated since not the complete reactor is reaching the measured temperature. For a detailed determination, experiments in a calorimeter are

necessary. These measurement were outside the scope of this work, since for this first process development the estimation of the reaction heat is sufficient. Regarding a scale up of this hydrogenation step, the exact knowledge of the reaction heat is necessary. To quantify the heat removal from the reactor is crucial to ensure a stable process without a thermal runaway.

In the experiment shown in Figure 37, also inline FTIR spectra were recorded, which are shown as function of time in Figure 38. Here, the decrease of absorption of the C=C-H bending can be seen at 930 cm^{-1} over the course of the hydrogenation reaction. In the same time range, an increase in the absorption is present at 950 cm^{-1}, which is most probably attributed to the cyclohexane backbone of the product DAPH.

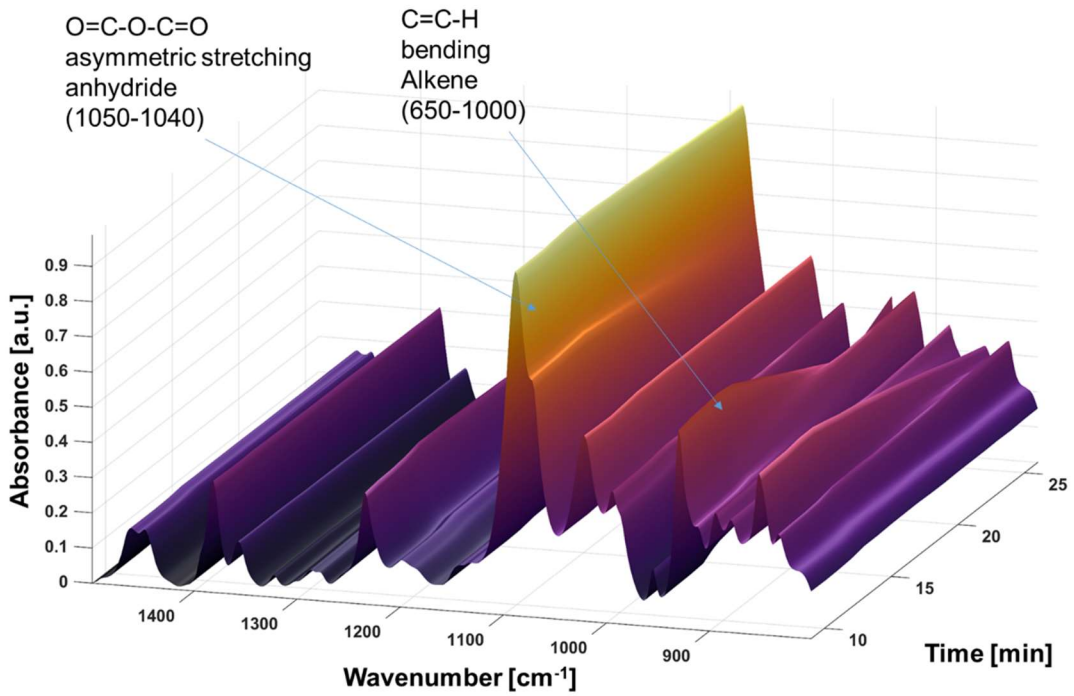

Figure 38: FTIR spectra recorded during hydrogenation of DAP to DAPH. Reaction conditions: H13: m_{DAP} = 25.0071 g; V_{2MeTHF} = 150 mL; $m_{Pd/C}$ = 1.5021 g, stirring rate: 400 rpm, $p_{H2(t=0)}$ = 30 bar. One FTIR spectrum per minute recorded.

The spectra recorded during a first reaction, already indicate the possibility for creating a chemometric model for the evaluation of concentration from the spectra data. Since the chemometric model should be able to differentiate between the two products DAPH and BSA, the pure component solutions of both are recorded for the chemometric model, which is presented in the next section.

5.2 Chemometric Model Development

In this section an inline analytical method for the final product DAPH and the side product BSA is developed. For the inline measurement applied, an ATR-FTIR probe is attached to the hydrogenation reactor. The spectra recorded need to be transferred into concentration data, therefore, a chemometric model is set up using IHM. To ensure the model can fully discriminate between BSA, DAP, DAPH and the solvent 2MeTHF, all of these components are included in the chemometric model.

The pure component spectra of DAP, DAPH and BSA are recorded as solution in 2MeTHF. Here, stock solutions with 750 mM of DAP and 300 mM of BSA were prepared. Within the modelling process, the spectrum of 2MeTHF is also modelled as pure component and consequently removed from the pure component models of BSA and DAPH.

Since the concentration of 2MF is expected to be low and in the case of its hydrogenation, it will turn into the solvent 2MeTHF, it is excluded from the chemometric model. DAP is included into the IHM. However, due to the *retro*-Diels-Alder reaction, quantification is not reliably possible due to dissolving effects. The solvent 2MeTHF is modelled as pure component, but it is also not calibrated as a component in the model. The amount of 2MeTHF is indirectly included, since the calibration of DAPH and BSA is achieved in mol L^{-1}. In Figure 39, the pure component models (blue) as well as the resulting IHM (red) are shown.

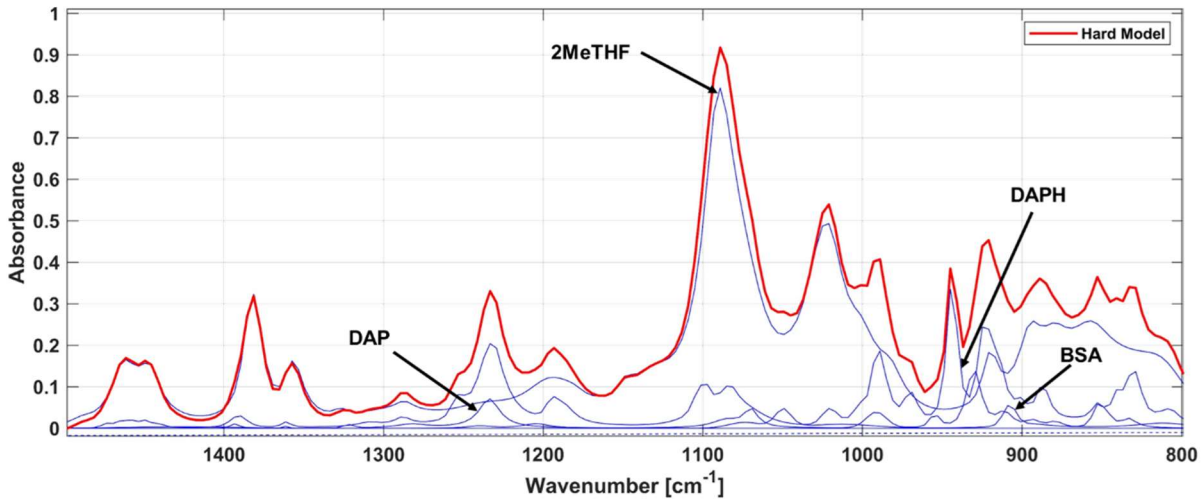

Figure 39: Indirect Hard Model of the hydrogenation of the Diels-Alder intermediate DAP to DAPH with side reaction product BSA.

To calibrate the respective chemometric model, reference data are necessary. For the IHM describing the formation of both products, the approach of artificial mixtures was selected (Dinç *et al.*, 2010). Here, mixtures of both components solubilized in 2MeTHF with known concentrations were prepared. These mixtures are then measured by ATR-FTIR, yielding the calibration data set. Both components, BSA and DAPH are included in a dilution series. To account for mixture effects and possibly overlapping absorption bands, mixtures of both were included in the calibration mixtures. The concentration range of DAPH is set between 0 and 750 mM. Higher concentrations are limited by the solubility in the respective solvent. The side product BSA is expected to be lower compared to the product. Here, the range is set between 0 and 300 mM. A table summarizing the concentrations measured for the calibration data set is shown in the appendix *Calibration of Chemometric Models*. The calibration curves show a linear trend (Figure 66), with small root mean errors of cross validation (RMSCEV) determined. The RMSECV is calculated similar to equation 4 (see *1.2.3 Chemometric Modeling*). The IHM is calibrated leaving one calibration point out, then the left out value is predicted and compared to the known one. This approach is repeated leaving other data points out. For DAPH this internal model error is calculated to 14 mM and for BSA to 6 mM. The errors are relatively low in respect to the calibrated to the calibrated range. An external validation was not carried out due to limited accessibility *via* suitable offline analytics.

5.3 Reaction Characterization

The established chemometric model for the analysis of both products of the reaction is applied for the inline analytical characterization of this process step. Different parameters like stirrer speed, concentrations of starting material and catalyst, as well as the influence of hydrogen pressure are investigated. The results of this characterization are presented in the following section.

5.3.1 Agitation Rate

The first parameter investigated is the stirring rate. The product DAP from the previous Diels-Alder reaction was finely ground and the excess 2MF was removed in the rotary

evaporator. The obtained intermediate is then put into the hydrogen autoclave for the hydrogenation of the remaining alkene bonding. The detailed description of the experimental workflow is summarized in *3.3 Reactor Setups*. In order to evaluate the mass transfer in the given reactor setup, a series of experiments with fixed experimental conditions (c_{DAP} = 250 mM; 2 wt% Pd/C; 2 bar H_2) was carried out. Here, only the stirring rate was varied. The results of these experiments are shown in Figure 40:

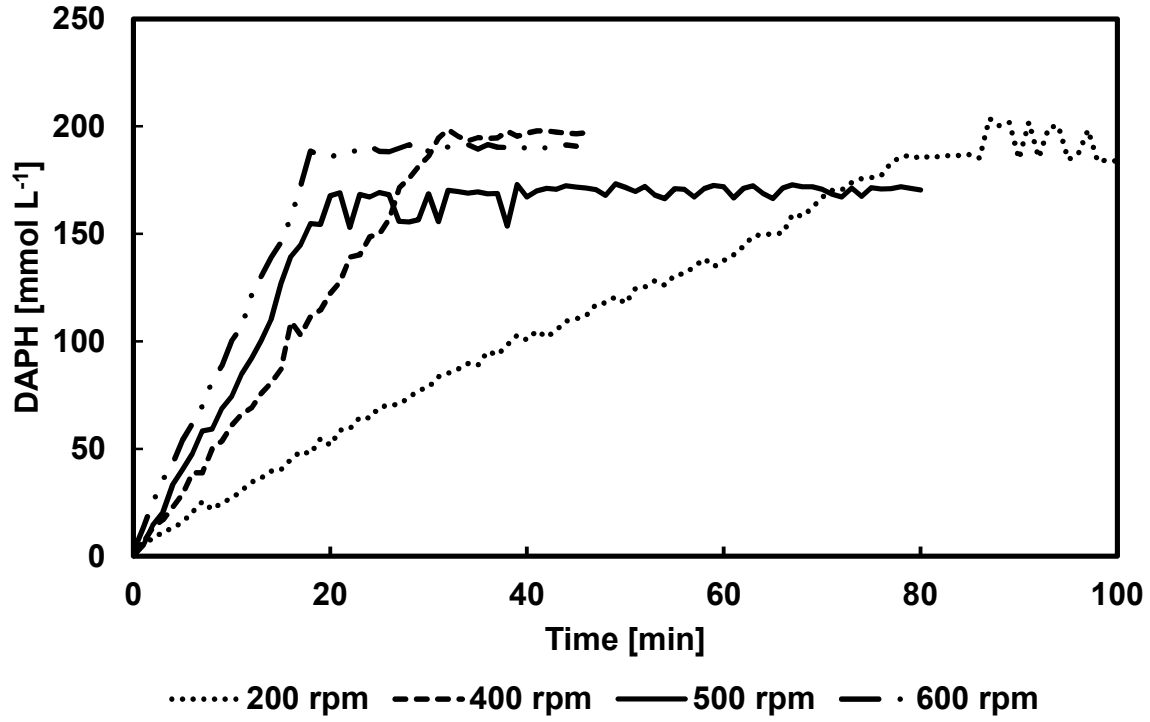

Figure 40: DAPH concentration determined from inline measured FTIR spectra (one spectrum per minute) in hydrogenation reactions of DAP. Reaction conditions: T = RT, c_{DAP} = 250 mM, 2 wt% Pd/C, 2 bar H_2; stirring rate 200 rpm: m_{DAP} = 6.7524 g; V_{2MeTHF} = 150 mL; $m_{Pd/C}$ = 0.1361 g; stirring rate 400 rpm: m_{DAP} = 6:7581 g; V_{2MeTHF} = 150 mL; $m_{Pd/C}$ = 0:1338 g; stirring rate 500 rpm: m_{DAP} = 6.7624 g; V_{2MeTHF} = 150 mL; $m_{Pd/C}$ = 0.1369 g; stirring rate 600 rpm: m_{DAP} = 6:7564 g; V_{2MeTHF} = 150 mL; $m_{Pd/C}$ = 0.1341 g.

For the runs performed with 200, 400 and 600 rpm, the starting material was derived from the same batch, leading to a similar product concentration in the end of the experiment. However, the experiment with 500 rpm was conducted using a previous batch of DAP yielding a final concentration of DAPH 170 mM. The difference is probably due to the crystallization during the Diels-Alder reaction of 2MF and MAA. This occurs spontaneously and is solidifying the reaction mixture, therefore, the reaction has stopped earlier. The deviations observed at the end of the run at 200 rpm are a measurement error in the error range of the chemometric model.

Within all batches the product formation follows a linear trend. For 200 rpm the slope is the lowest and it increases with an increasing stirring rate. The difference between the run at 500 and 600 rpm is relatively small. Nevertheless, the product formation rate in the experiment with 600 rpm is still linear until no starting material is left over, indicating a mass transfer limitation in terms of hydrogen availability. The reaction itself is quite fast, leading to instant depletion of the solubilized hydrogen as long as additional starting material is contained in the reaction solution. For the hydrogenation of aromatic compounds, also constant reaction rates have been observed. In this case, by numerical simulations, the mass transfer limitation was found to be at the diffusion into the catalyst particle (Toppinen *et al.*, 1997).

The stirrer used in the hydrogenation autoclave is a pitch-blade stirrer containing six blades fixed with an angle of 45°. The stirrer is operated in downwards direction, pushing the liquid phase in the direction of reactor bottom. Determination of kinetics in mass transfer limited systems is not useful and therefore not carried out in this work. The mass transfer limitation leads to a constant production rate throughout the reaction. This production rate can be determined from the slope of the DAPH concentration as a function of time, leading to the observed product formation rate P_{obs} in mmol L^{-1} min^{-1} (equation 14).

$$P_{obs} = \frac{dc}{dt} = \frac{(c_2 - c_1)}{(t_2 - t_1)} \quad (14)$$

With P_{obs}: observed product formation rate [mmol $L^{-1}min^{-1}$], c: concentration [mmol L^{-1}], time [min].

By correlating the observed product formation rate with the hydrogen pressure and the catalyst loading, the specific product formation P_{sp} is calculated. The approach is shown in equation 15.

$$P_{sp} = \frac{P_{obs}}{m_{Pd/C} * p_{H_2}} \quad (15)$$

With P_{sp}: specific product formation rate [mmol $L^{-1}min^{-1}$ $g_{Pd/C}$ bar_{H2}], P_{obs}: observed product formation rate [mmol $L^{-1}min^{-1}$], $m_{Pd/C}$: mass of Pd/C catalyst [g], p_{H2}: hydrogen pressure [bar].

By evaluating the specific product formation rate, the different experiments become comparable. Despite the mass transfer limitation, a characterization for the hydrogenation reaction step in the given reactor setup is possible. The results of the specific product formation rate are shown in Figure 41.

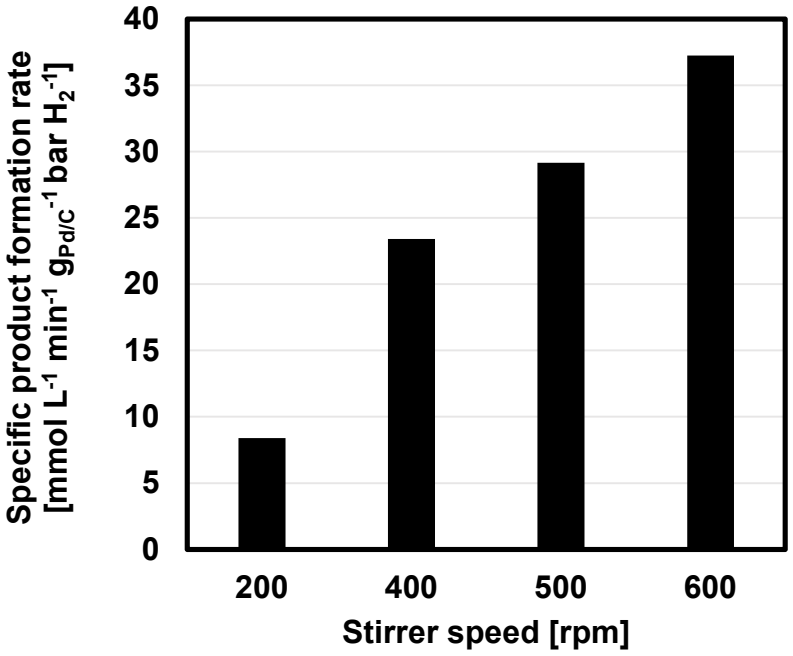

Figure 41: Specific DAPH product formation rate at different stirrer speeds. Calculated from concentration profiles determined from inline measured FTIR spectra (one spectrum per minute) in hydrogenation reactions of DAP. Reaction conditions: T = RT, c_{DAP} = 250 mM, 2 wt% Pd/C, 2 bar H_2; stirring rate 200 rpm: m_{DAP} = 6.7524 g; V_{2MeTHF} = 150 mL; $m_{Pd/C}$ = 0.1361 g; stirring rate 400 rpm: m_{DAP} = 6:7581 g; V_{2MeTHF} = 150 mL; $m_{Pd/C}$ = 0:1338 g; stirring rate 500 rpm: m_{DAP} = 6.7624 g; V_{2MeTHF} = 150 mL; $m_{Pd/C}$ = 0.1369 g; stirring rate 600 rpm: m_{DAP} = 6:7564 g; V_{2MeTHF} = 150 mL; $m_{Pd/C}$ = 0.1341 g.

Visualization of the specific product formation rate as function of the stirrer speed also underlines the given mass transfer limitation observed before. The specific DAPH formation rate is increasing with increasing stirring rate throughout the experimental series. Higher stirring rates could not be investigated, since the maximum velocity of the motor is between 600 and 700 rpm. Therefore, with the given reactor setup, the mass transfer limitation cannot be overcome.

5.3.2 Catalyst Loading

In the following section, the influence of the catalyst loading on the specific productivity is discussed. A series of experiments was performed with different Pd/C ratios from 0.5 wt% to 10 wt% in respect to the anhydride. Hydrogen pressure and the stirring rate have been kept constant throughout the experimental series. The DAPH concentration observed with inline analytics is plotted versus the time in Figure 42.

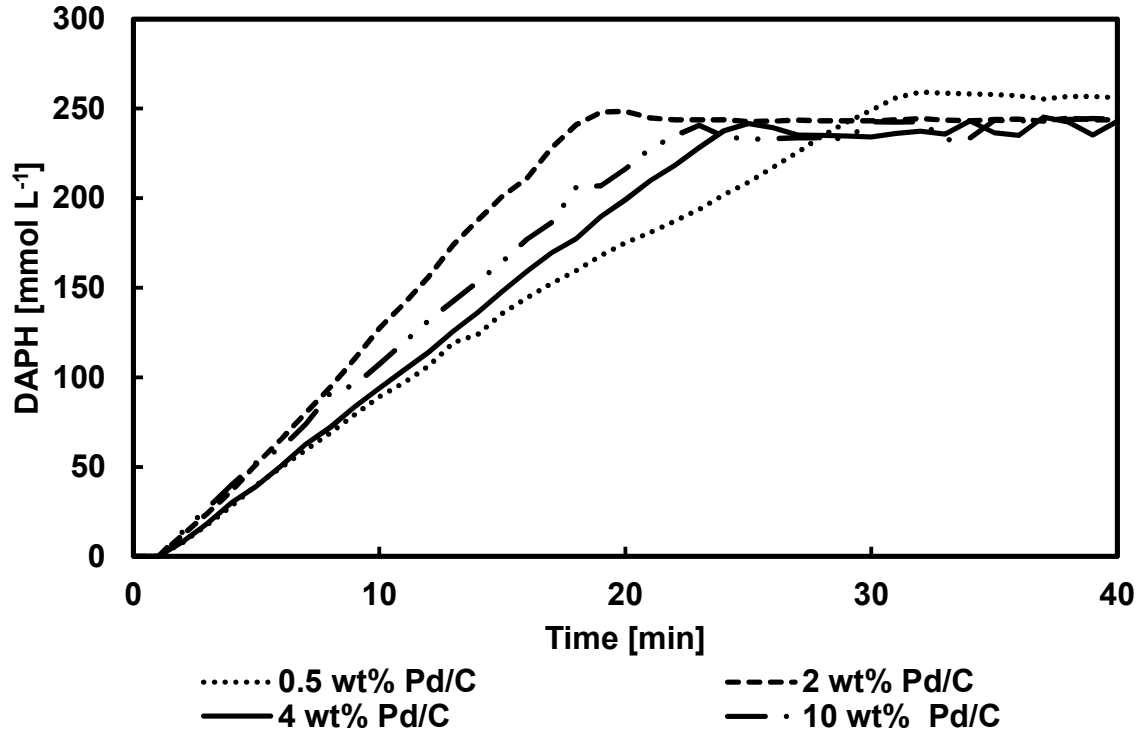

Figure 42: DAPH concentration determined from inline measured FTIR spectra (one spectrum per minute) in hydrogenation reactions of DAP. Reaction conditions: T = RT, c_{DAP} = 250 mM, 2 bar H_2; stirring speed: 500 rpm; 0.5 wt% Pd/C: m_{DAP} = 6.7586 g, V_{2MeTHF} = 150 mL, $m_{Pd/C}$ = 0.0336 g; 2 wt% Pd/C: m_{DAP} = 6.7589 g, V_{2MeTHF} = 150 mL, $m_{Pd/C}$ = 0.1373 g; 4 wt% Pd/C: m_{DAP} = 6.7535 g, V_{2MeTHF} = 150 mL, $m_{Pd/C}$ = 0.2695 g; 10 wt% Pd/C: m_{DAP} = 6.7573 g, V_{2MeTHF} = 150 mL, $m_{Pd/C}$ = 0.6724 g.

As observed in the experiments with varied stirring rates, also in the experiments with varied catalyst loading, a mass transfer limitation is present. For all runs, a clear linear increase in the DAPH concentration is perceived. For a 2 wt% loading of Pd/C, the fastest product formation was reached, while the lowest seems to be with 0.5 wt% loading. Between these two, the experiments conducted with 4 wt% and 10 wt% are found. From this distribution, no clear trend can be deduced. To further investigate the effect of catalyst loading on the performance of the reaction, again the specific productivity according to formula 9 is calculated. The results of these calculations are summarized in Figure 43.

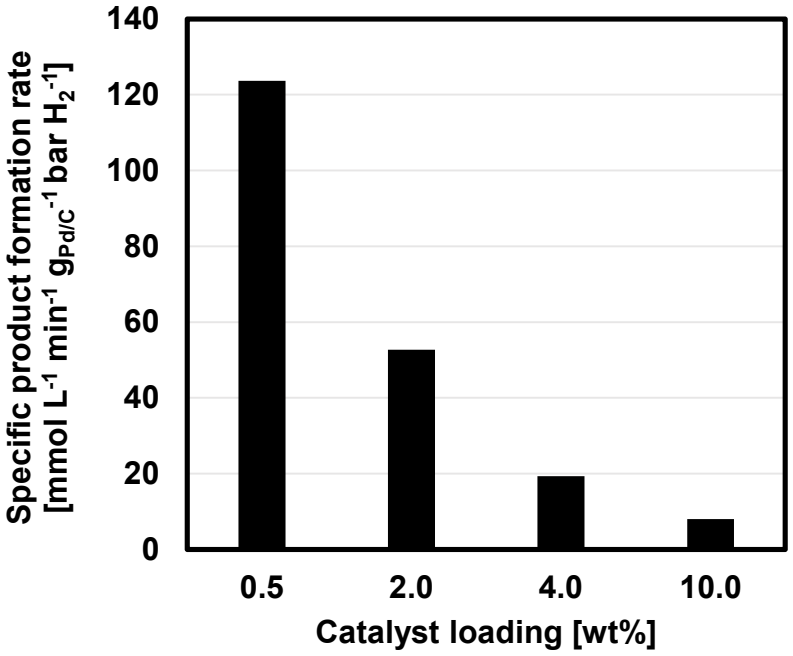

Figure 43: Specific product formation rate at different catalyst loadings. Calculated from concentration profiles determined from inline measured FTIR spectra (one spectrum per minute) in hydrogenation reactions of DAP. Reaction conditions: T = RT, c_{DAP} = 250 mM, 2 bar H_2; stirring speed: 500 rpm; 0.5 wt% Pd/C: m_{DAP} = 6.7586 g, V_{2MeTHF} = 150 mL, $m_{Pd/C}$ = 0.0336 g; 2 wt% Pd/C: m_{DAP} = 6.7589 g, V_{2MeTHF} = 150 mL, $m_{Pd/C}$ = 0.1373 g; 4 wt% Pd/C: m_{DAP} = 6.7535 g, V_{2MeTHF} = 150 mL, $m_{Pd/C}$ = 0.2695 g; 10 wt% Pd/C: m_{DAP} = 6.7573 g, V_{2MeTHF} = 150 mL, $m_{Pd/C}$ = 0.6724 g.

While the observed productivity P_{obs} (the slope of the product formation in Figure 42) shows a maximum for a catalyst loading of 2 wt%, the representation using the P_{sp} reveals a more detailed view here, also in terms of efficiency. The specific productivity takes into account the absolute amount of Pd/C catalyst. Unlike to the observed product formation rate, which are in a similar range for all experiments, in the specific productivity, a trend for increasing the catalyst loading is visible. With higher amounts of catalyst applied, the specific productivity is decreasing throughout the experimental series. The amount of hydrogen supplied from the gas phase is also in the same magnitude, still hydrogen is the limiting reactant. Applying more catalyst only leads to absorption of more anhydride, which, however, is not hydrogenated due to the lack of excess hydrogen molecules.

5.3.3 Hydrogen Pressure

Furthermore, to characterize this hydrogenation reaction, the influence of the hydrogen pressure is investigated. Again, a series of experiments was carried out, changing the hydrogen pressure as the only variable. Stirring rate, catalyst loading and the amount

of starting materials have been kept constant. All experiments have been conducted with the same starting material DAP obtained from one single batch. The resulting DAPH concentration as function of time is plotted in Figure 44.

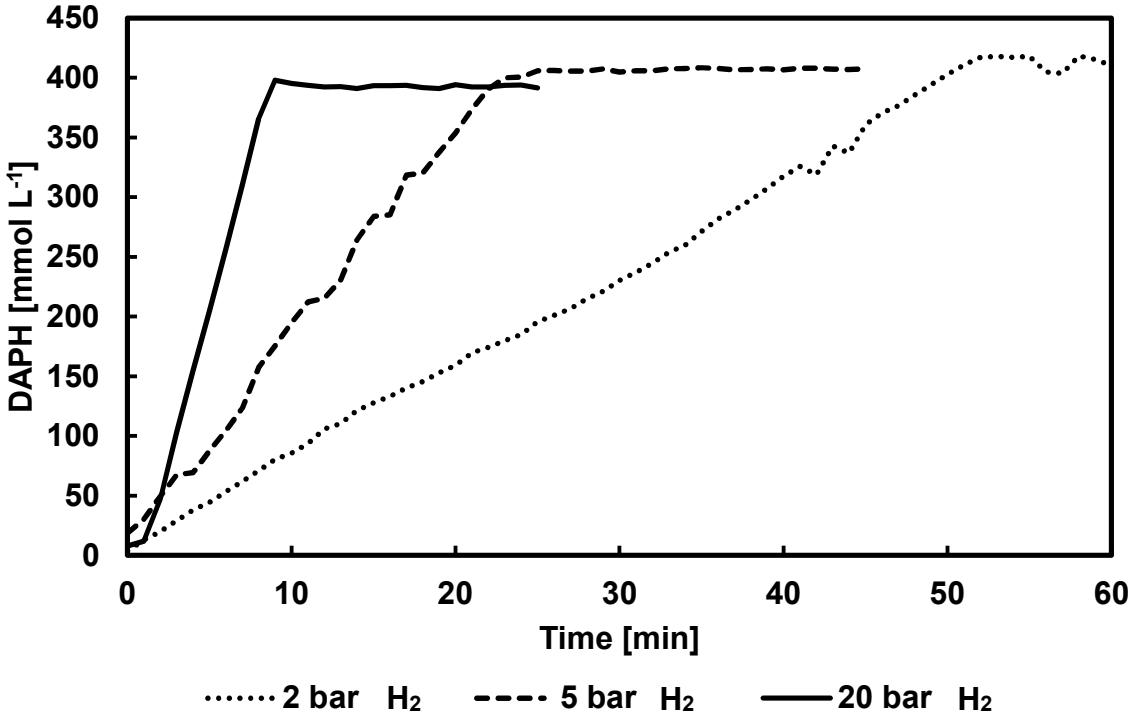

Figure 44: DAPH concentration determined from inline measured FTIR spectra (one spectrum per minute) in hydrogenation reactions of DAP. Reaction conditions: T = RT, cDAP = 500 mM, 2 wt% Pd/C, stirring speed: 500 rpm, 2 bar H_2: m_{DAP} = 13.5297 g, V_{2MeTHF} = 150 mL, $m_{Pd/C}$ = 0.2706 g; 5 bar H_2: m_{DAP} = 13.5245 g, V_{2MeTHF} = 150 mL, $m_{Pd/C}$ = 0.2730 g; 20 bar H_2: m_{DAP} = 13.5154 g, V_{2MeTHF} = 150 mL, $m_{Pd/C}$ = 0.2730 g.

Like already shown for the stirring rate as well as the catalyst loading, the concentration of DAPH is increasing linearly until the end of the reaction is reached. The slope of the product concentration, which is again the observed product formation rate, is increasing with increasing pressure. For the batch carried out at 20 bar, an increase in the slope can be seen after the first minute. Probably, this is a delay due to solubilizing of hydrogen in the solvent. However, using an excess of hydrogen is decreasing the hydrogen efficiency of this hydrogenation step, since no recycling of the excess hydrogen can be realized. Therefore, in this experimental series, the specific product formation rate is determined for a detailed analysis of the efficiency. The specific productivity determined for the different hydrogen pressures applied is shown in Figure 45.

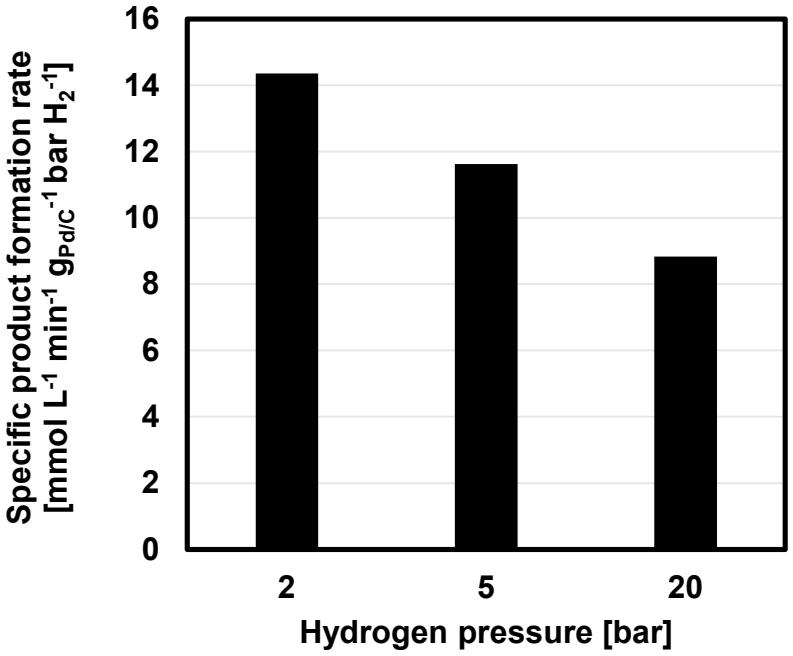

Figure 45: Specific product formation rate at different hydrogen pressures. Calculated from concentration profiles determined from inline measured FTIR spectra (one spectrum per minute) in hydrogenation reactions of DAP. Reaction conditions: T = RT, cDAP = 500 mM, 2 wt% Pd/C, stirring speed: 500 rpm, 2 bar H_2: m_{DAP} = 13.5297 g, V_{2MeTHF} = 150 mL, $m_{Pd/C}$ = 0.2706 g; 5 bar H_2: m_{DAP} = 13.5245 g, V_{2MeTHF} = 150 mL, $m_{Pd/C}$ = 0.2730 g; 20 bar H_2: m_{DAP} = 13.5154 g, V_{2MeTHF} = 150 mL, $m_{Pd/C}$ = 0.2730 g.

Taking the hydrogen pressure applied to the reactor into account, the specific product formation rate P_{sp} is decreasing with increasing pressure. At two bar, P_{sp} reaches the highest value in this series with about 14 mmol L^{-1} min^{-1} $g_{(Pd/C)}^{-1}$ bar_{H2}^{-1} and is decreasing to roughly 9 mmol L^{-1} min^{-1} $g_{(Pd/C)}^{-1}$ bar_{H2}^{-1}. Thus, it can be concluded that the excess pressure applied to this batch reactor, is increasing only the reaction rate, however decreasing the overall reaction efficiency. According to Henry's Law, the applied hydrogen pressure, the solubility of hydrogen in the organic solvent 2MeTHF is increased and also the mass transfer from the gas to the liquid is enhanced. However, the availability of hydrogen at 20 bar is not sufficient to overcome the mass transfer limitation observed in Figure 44.

5.4 Selectivity Control

In the last part, the inline analytics in combination with chemometrics is applied for analyzing the selectivity of the reaction. Both, the concentration of the main product DAPH, as well as the concentration of the side product BSA are determined with the chemometric model established in section *5.2.* A set of experiments was carried out, with successively increasing the content of MAA. Aim of this approach was to evaluate

the established inline analytics in terms of determining the selectivity of the reaction at every single point in time. The absolute number of moles was kept constant throughout the experiments. The stirrer speed, catalyst concentration and the applied hydrogen pressure also were constant. The concentrations of both products, determined by the chemometric model are shown as function of time in Figure 46:

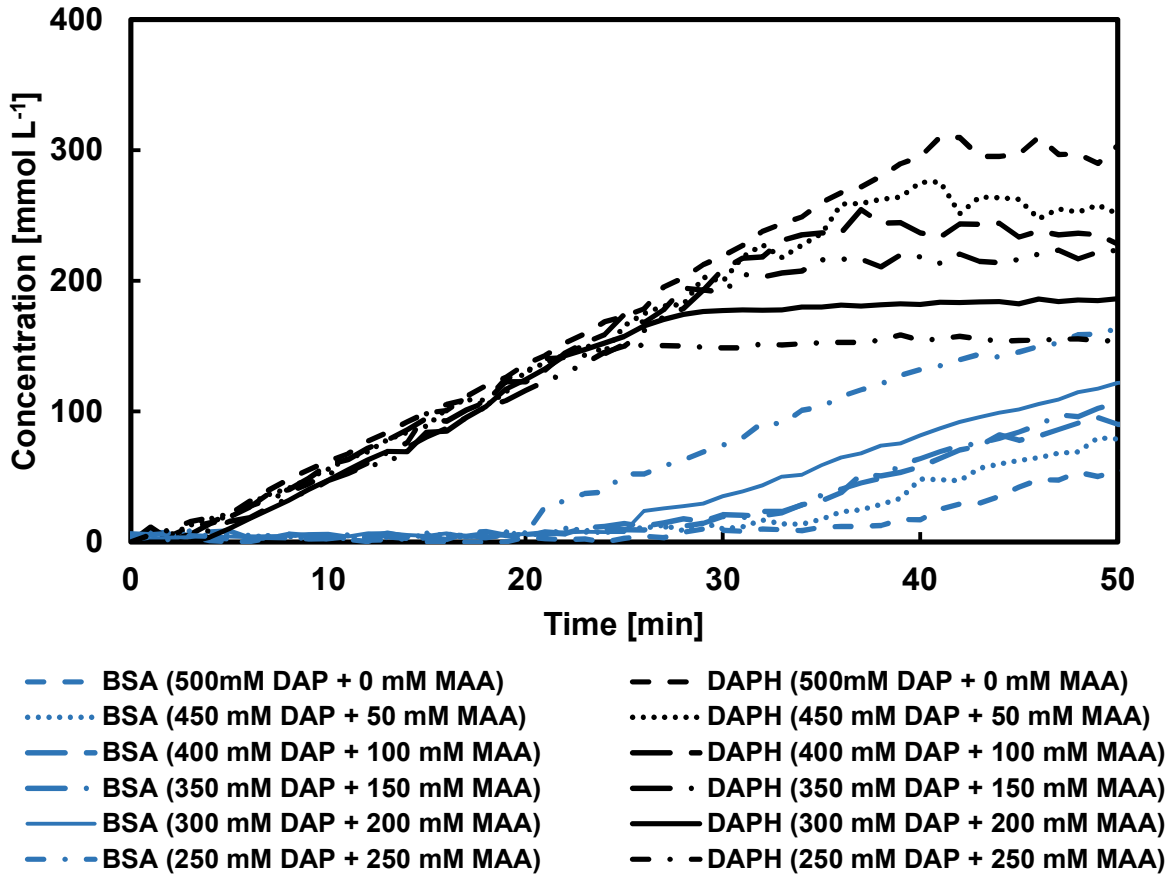

Figure 46: DAPH and BSA concentrations determined from inline measured FTIR spectra (one spectrum per minute) in hydrogenation reactions of DAP. Reaction conditions: T = RT, 2 wt% Pd/C in respect to the experiment conducted with 500 mM DAP, 2 bar H_2, stirring speed: 600 rpm. 500 mM DAP: m_{DAP} = 13.5139 g, V_{2MeTHF} = 150 mL, $m_{Pd/C}$ = 0.2711 g, 450 mM DAP: m_{DAP} = 12.1645 g, m_{MAA} = 0.7357g, V_{2MeTHF} = 150 mL, $m_{Pd/C}$ = 0.2712 g, 400 mM DAP: m_{DAP} = 10.8091 g, m_{MAA} = 1.3736 g, V_{2MeTHF} = 150 mL, $m_{Pd/C}$ = 0.2716 g, 350 mM DAP: m_{DAP} = 9.4589 g, m_{MAA} = 2.2070 g, V_{2MeTHF} = 150 mL, $m_{Pd/C}$ = 0.2700 g; 300 mM DAP: m_{DAP} = 8.1069 g, m_{MAA} = 2.9437 g, V_{2MeTHF} = 150 mL, $m_{Pd/C}$ = 0.2700 g, 250 mM DAP: m_{DAP} = 6.7579 g, m_{MAA} = 3.677 g, V_{2MeTHF} = 150 mL, $m_{Pd/C}$ = 0.2725 g.

The concentration of the main product DAPH is increasing again in a linear course until a plateau is reached. After most DAP is converted to DAPH, hydrogenation of MAA to BSA is starting to take place. In addition, this reaction seems to follow a linear behavior, however, the slope of the side product formation is lower compared to the main product. The amount of DAPH obtained in the end of the reaction is decreasing with increasing MAA concentration, while the concentration of BSA is increasing. For the last run with equimolar ratio of DAP and MAA, similar concentration for both products is achieved. The perceived sequential hydrogenation of product and side product might

be attributed to a difference in their adsorption on the catalyst particle. A similar behavior was observed for the hydrogenation of mixtures composed form different aromatic hydrocarbons. TOPPINEN suggests that this queue effect is based on the reactivity of the components but also on differences in their absorptivity (Toppinen *et al.*, 1997).

Striking for all experiments is the fact, that the mass balance cannot be closed using the inline analytical approach. In every experiment, a total concentration of 500 mM has been weighed in into the reactor. However, at the end of the experiment an average of only 340 mM was measured. There are several possible reasons explaining this behavior: First to mention is the predictive error introduced by the chemometric model, which is 6 mM for BSA and respectively 14 mM for DAPH. Secondly, substrates and products are likely available for crystallization, which can occur on colder parts of the reactor and was noticed after opening of the reactor. Beside the reactor wall, also the IR probe itself, the gassing pipe as well as the sampling tube act as a heat conductor. These metal parts are a direct connection to the environment and no temperature control is mounted. Therefore, crystallization of reaction components is possible on these relatively colder parts of the reactor setup. Thirdly, dead zones are possible in the reactor setup. In these zones, catalyst with adsorbed starting material or product can accumulate and consequently it is not available for the measurement and the reaction itself. This was observed in the IR-probe port of the reactor vessel. Finally, there is a possibility of a dilution effect: leftover 2MF from the previous Diels-Alder reaction is hydrogenated to 2MeTHF (Dong *et al.*, 2015), which is used as solvent in this step. This dilution effect for 50 mM of 2MF reacting to 2MeTHF results in a minor error of about 3 mM. However, in the case that the previous DAP reaction was not reaching full conversion, this potential source of error is becoming more important. Since product formation is always in a linear manner and both, side product BSA and product DAPH are affected, no influence is expected for the data evaluation.

Analyzing the reaction in terms of selectivity towards DAPH and BSA, in equation 16, the apparent selectivity is introduced:

$$S_{app}(t) = \frac{c_{DAPH}(t)}{c_{DAPH}(t) + c_{BSA}(t)} \tag{16}$$

With $S_{app}(t)$: apparent selectivity at point in time t [-], $c_{DAPH}(t)$: concentration of DAPH at pointin time t [mmol L^{-1}], $c_{BSA}(t)$: concentration of DAPH at point in time t [mmol L^{-1}].

To independently compare the different experiments with respect to the apparent selectivity, the data are related to the apparent conversion. Since the starting material DAP is not stable, it was not part of the artificial mixtures prepared for the calibration of the chemometric model. Thus, this component is not analyzed by the chemometric model, the conversion is calculated based on the absolute concentrations of DAPH and BSA at the end of the experiment. The formula is shown in equation 17:

$$X_{app}(t) = \frac{c_{DAPH}(t) + c_{BSA}(t)}{c_{DAPH}(\infty) + c_{BSA}(\infty)} \quad (17)$$

With $X_{app}(t)$: apparent conversion at point in time t [-], $c_{DAPH}(t)$: concentration of DAPH at point in time t [mmol L^{-1}], $c_{BSA}(t)$: concentration of DAPH at point in time t [mmol L^{-1}], $c_{DAPH}(\infty)$: concentration of DAPH at the end of the experiment [mmol L^{-1}], $c_{BSA}(\infty)$: concentration of DAPH at the end of the experiment [mmol L^{-1}].

Using the apparent conversion along with the apparent selectivity, the results of these selectivity experiments are plotted, which are shown in Figure 47.

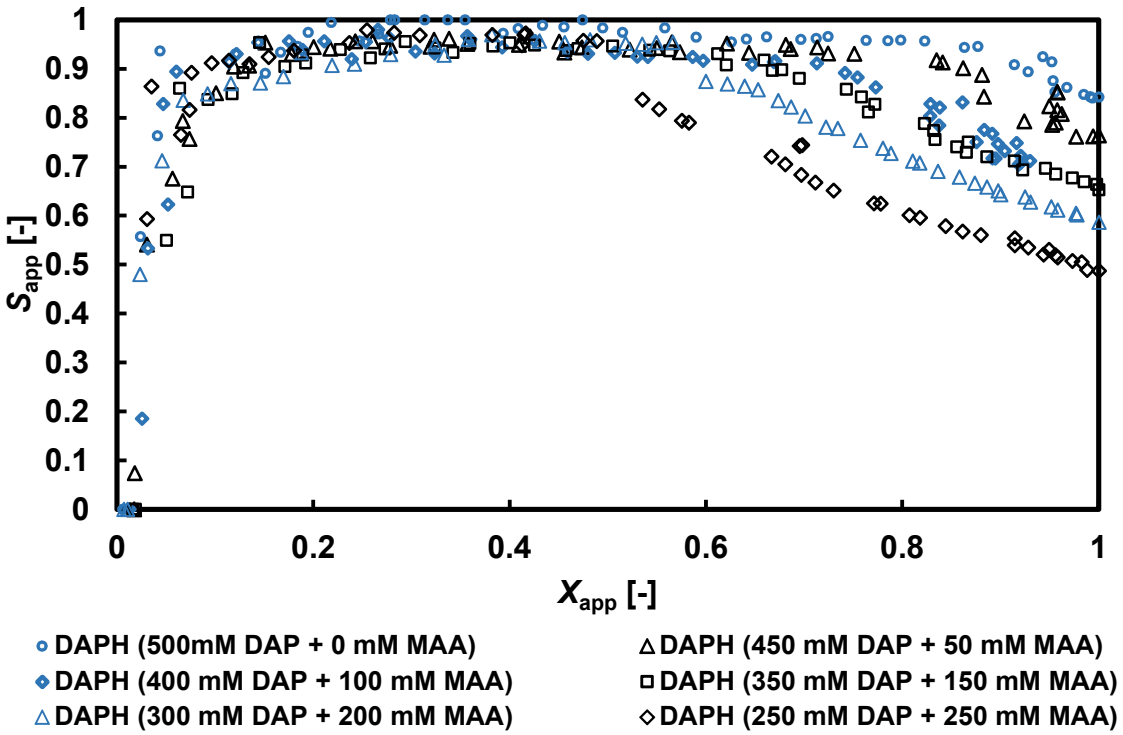

Figure 47: Apparent selectivity of DAPH as function of the apparent conversion. Calculated from DAPH and BSA concentrations determined from inline measured FTIR spectra (one spectrum per minute) in hydrogenation reactions of DAP. Reaction conditions: T = RT, 2 wt% Pd/C in respect to the experiment conducted with 500 mM DAP, 2 bar H_2, stirring speed: 600 rpm. 500 mM DAP: m_{DAP} = 13.5139 g, V_{2MeTHF} = 150 mL, $m_{Pd/C}$ = 0.2711 g, 450 mM DAP: m_{DAP} = 12.1645 g, m_{MAA} = 0.7357g, V_{2MeTHF} = 150 mL, $m_{Pd/C}$ = 0.2712 g, 400 mM DAP: m_{DAP} = 10.8091 g, m_{MAA} = 1.3736 g, V_{2MeTHF} = 150 mL, $m_{Pd/C}$ = 0.2716 g, 350 mM DAP: m_{DAP} = 9.4589 g, m_{MAA} = 2.2070 g, V_{2MeTHF} = 150 mL, $m_{Pd/C}$ = 0.2700 g; 300 mM DAP: m_{DAP} = 8.1069 g, m_{MAA} = 2.9437 g, V_{2MeTHF} = 150 mL, $m_{Pd/C}$ = 0.2700 g, 250 mM DAP: m_{DAP} = 6.7579 g, m_{MAA} = 3.677 g, V_{2MeTHF} = 150 mL, $m_{Pd/C}$ = 0.2725 g.

The selectivity is not starting at a value of one as expected, which is due to measurement inaccuracies in the beginning of a reaction. The chemometric model is calculating very small concentration of both, product and side product within the error range of the model. Along with equation 16, this is leading to this unusual behavior of the selectivity. The data reach a maximum for every measurement series at about 30% apparent conversion. From this point onwards, the influence of the predictive error of the chemometric model can be neglected and the apparent selectivity be interpreted. After the maximum, the apparent selectivity is decreasing again, which is then attributed to the upcoming side reaction of MAA to BSA. With increasing amount of MAA added to the reaction mixture, the decline of the apparent selectivity is enhanced. Additionally, the start of the side reaction is shifted to lower apparent conversions. Since the main reaction is completed earlier, also the beginning of the side reaction is shifted to earlier points in time or respectively apparent conversions. At equimolar ratio, only an apparent selectivity of 0.5 is reached in the end of the experiment. This value is expected since the same amounts of DAP and MAA were fed into the reactor. Hence, the difference between the concentration achieved and the expected one is similar for both products, BSA and DAPH. This underlines that the assumption of neglecting the measurement errors for this kind of data evaluation is acceptable. Within the process, the formation of BSA should be avoided, since this will lead to a stable side product in the reaction mixture. The FTIR inline analytics can support this approach by providing criteria for the batch reaction to be stopped at a defined conversion point. Here, two different criteria can be formulized:

1. A limit in apparent selectivity is defined (e.g. $S_{app} \geq 0.95$).
2. If the slope $\frac{dS_{app}}{dX_{app}}$ becomes negative.

By stopping the reaction, it is ensured that the MAA is not converted, respectively, converted only to a small degree. This approach enables the unreacted MAA to be separated from the reaction mixture by cooling crystallization and can be returned into the first reaction step, the Diels-Alder reaction, improving the overall efficiency of the whole process. Concluding, reaction conditions for the hydrogenation under the given setup can be concluded. The stirring rate should be kept at maximum to maximize the mass transfer from gas to liquid. Regarding the performance of this reaction step, the excess hydrogen pressure as well as the catalyst loading should be at a minimum, which is leading to the highest specific productivity.

6 Acid-catalyzed Esterification of 4-Methylhexahydro-4,7-epoxyisobenzofuran-1,3-dione

6.1 Introduction: Homogeneously Acid-catalyzed Esterification

A large variety of different valuable compounds can be produced *via* esterification processes. For example, in the field of pharmaceuticals and for the synthesis of flavor and fragrance components, esterification reactions are often applied. (Gomes Almeida *et al.*, 2017). Another important example are polyester polymers, which provide a wide range of applications, for example packaging foils (Siracusa *et al.*, 2012), clothing or plastic bottles (Andrady, Neal, 2009). Ester bonds are especially important in plasticizers, since these are crucial for the plasticizing properties: the ester bond acts as a cohesive block within the polymer by electrostatic interactions and hydrogen bonding (Bocqué *et al.*, 2016).

The esterification reaction was first described by EMIL FISCHER and ARTHUR SPEIER in 1895 (Fischer, Speier, 1895). In Figure 48, the reaction mechanism is shown. In the first step, a proton from an acidic catalyst is bound to the carbonyl oxygen of the carboxylic acid, leading to an increased electrophilicity of the carbonyl carbon. Now the oxygen of the alcohol is bound to the carbonyl carbon by nucleophilic attack forming an oxonium ion. The proton of the formed oxonium ion is removed in the next step. Further, the oxygen of an alcohol group is protonated, leading to another oxonium ion. This oxonium ion now is a suitable leaving group and a water molecule is detached from this intermediate complex. At the end, the molecule is deprotonated leading to the final ester (Li, 2014). The reaction rate of esterification reactions is highly depending on the electrophilic strength of the carbonyl carbon as well as the nucleophilic strength of the alcohol. In principle, all primary and secondary alcohols can be used.

As catalysts, Brønsted acids like for example sulfuric or methane sulfonic acid can be employed. In addition, Lewis acids are applied for catalyzing esterification reactions. Here, different examples like e.g. tin compounds (Casas *et al.*, 2013), triflates (Ho A Kwie *et al.*, 2010) or zeolites (Omar *et al.*, 2018) are used. Depending on the phase state of the catalyst, it can be differentiated between homogeneous and heterogeneous catalysis. Heterogeneous catalysts bear the advantage to be easily removable from the reaction mixture by, for example, filtration once the reaction is finished.

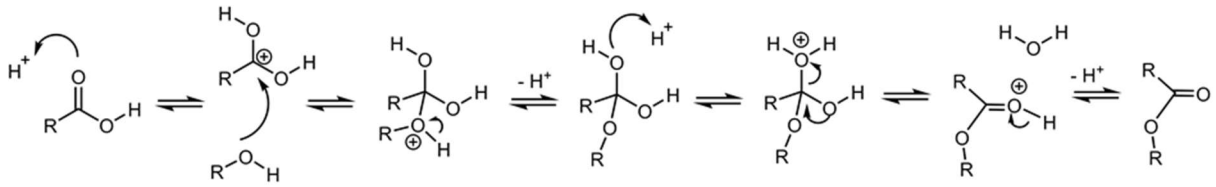

Figure 48: Reaction mechanism of acid-catalyzed (Fischer-) esterification.

The conversion in these reaction is limited by the equilibrium, since esterification reactions are reversible in principle. Therefore, also the hydrolysis of the ester appears, leading to a certain equilibrium of the reaction. To overcome this equilibrium, the alcohol can be applied in excess to the reaction mixture. Alternatively, water can be removed *in situ* from the reaction continuously. This can be achieved either by water scavengers like mole sieves in small scale, or predominantly vacuum distillation applied in large scale synthesis processes. A further option for water removal is gas stripping. When removing water by distillation, it is important to consider possible azeotropes formed by water and the respective alcohol. Additionally, the ester product can be removed to achieve this shift on the equilibrium.

In the following chapter, the esterification of the hydrogenated intermediate DAPH with 2-ethylhexanol (2EH) leading to bis(2-ethylhexyl) 1-methyl-7-oxabicyclo[2.2.1]-heptane-2,3-dicarboxylate (DAPHE) is investigated. 2EH is industrially applied as a solvent and it is also a standard alcohol in the production of various plasticizers, like DEHP, the use of which was recently restricted. However, 2EH alcohol is not only found in phthalates, it is also applied in aliphatic plasticizers like for example adipates. The alcohol 2EH is derived in an *oxo*-synthesis process (Roelen, 1938) in large scale with about 2.5 million tons annually based on butanal derived by hydroformylation of propylene. Recently, it was possible to show that 2EH can also be produced based on renewable resources (Menne, 2015). The reaction scheme of this two-step esterification process is shown in Figure 49. In a first alcoholysis step, the anhydride is opened and two different mono-esters are obtained (in Figure 49 only one isomer of the monoester is shown). This reaction step is taking place without the need of a catalyst. Secondly, the remaining free acid functions of the two regioisomers are esterified with a further alcohol unit by application of an acidic catalyst. In this work, sulfuric acid was chosen as catalyst.

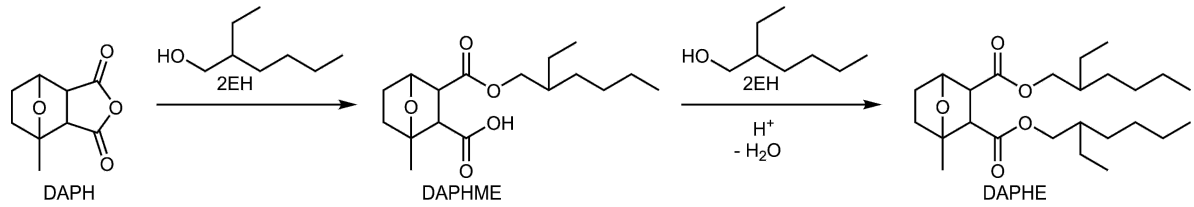

Figure 49: Alcoholysis of the cyclic precursor DAPH with 2EH to a mixture of monoesters (DAPHME) and subsequent second, acid-catalyzed esterification leading to the target plasticizer DAPHE. For reasons of clarity, only one regioisomer of both monoesters is shown.

Throughout this project, suitable enzymes for the biocatalytic esterification of DAPH were screened. Besides commercial available lipases and hydrolases, also enzymes derived from extremophiles were tested. Since no active enzymes were identified being capable of catalyzing the esterification reaction, the experiments have been carried out using sulfuric acid as catalyst. The results of these screening approaches are briefly summarized in the overall discussion found in the chapter *7.5 Biocatalytic Esterification.*

6.2 Chemometric Model Development

The results presented in the following sections are produced by BUESCHLER within the scope of a master thesis (Bueschler, 2020). Like in the previous chapters, the characterization of this esterification reaction is analyzed using inline FTIR measurements evaluated with a chemometric model. As well as in the previous experiments, IHM is chosen for model creation. The pure component spectra of all components are necessary. The anhydride DAPH was synthesized and purified according to *3.2 Synthesis Methods*. As a result, DAPH was obtained with high purity of >99% (see Figure 68 in *Supplemental Information*). The alcohol 2EH was purchased and used without further purification (≥99.5%). The corresponding diester DAPHE also was synthesized prior to the characterization according to the synthesis described in *3.2 Synthesis Methods*. The purification was employed using vacuum distillation and filtration on an aluminum oxide filter. By ^{1}H-NMR analysis the purity of DAPHE was determined to 97% (see Figure 68 in *Supplemental Information*).

Additionally, for a detailed analysis of the two-step esterification reaction, monitoring of the intermediate monoesters is necessary. However, in synthesis experiments only low amounts of monoesters were detected. Separating the monoesters from anhydride, alcohol and diester was not possible. In consequence, no sufficiently pure

monoester was obtained, which is needed to set up a reference analysis and the pure component model as well. Most probably, the monoester formation is the rate limiting step. This was also confirmed in other experiments performed by the project partner PLASS at the University of Bielefeld (Plass, 2020). Additionally, the monoester is suspected to catalyze its own esterification to DAPHE, leading to these low concentrations observed. In addition, the approach of determining the pure component spectrum of the monoesters from a mixture spectra by means of IHM (Kriesten *et al.*, 2008) was not successful. Therefore, this two step-esterification reaction analyzed is formally reduced to only one reaction step in terms of anhydride and alcohol depletion as well as diester formation.

An exemplary reaction was monitored using ATR-FTIR. After 70 min, the acidic catalyst was added. Prior to the addition of the sulfuric acid, the system seemed to run into an equilibrium. After the catalyst was added, a further increase of absorbance at different wavenumbers is observed. In Figure 50, the FTIR spectra of a typical course of a batch reaction are shown.

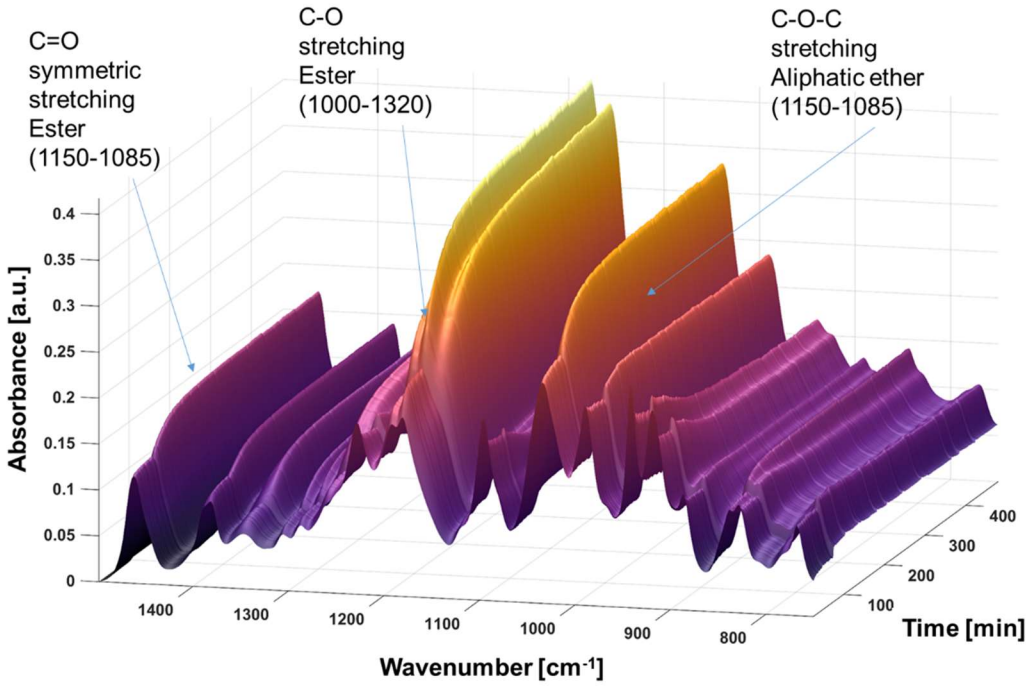

Figure 50: FTIR Spectra recorded over the course of an esterification reaction of DAPH and 2EH. Reaction conditions: T = 130 °C, m_{DAPH} = 2.709 g, m_{2EH} = 5.810 g, 1 mol% H_2SO_4, one FTIR spectrum measured per minute.

In the spectra, a clear increase of the absorbance of both the C=O symmetric stretching, as well as the C-O stretching of the ester can be seen. The increase of the

C-O-C stretching is assumed to be based on a change of the tension in the cyclic backbone, allowing the ether to stretch further compared to the anhydride system.

For both starting materials, as well as DAPHE, the pure component spectra were recorded. Prior, the melting point of the anhydride was determined to 102.9 °C ± 0.2 °C using a melting point apparatus MFB595 (Gallenkamp/Fison Instruments Ltd., Glasgow, Scotland). The pure spectra were measured at 130 °C to ensure the anhydride to be liquid. From these spectra, the respective hard models were built and combined into mixture spectra obtained from an esterification reaction. Here, it is important to mention, that first, the model was adjusted to an early point in time of the reaction, where almost only DAPH and 2EH were present. By this approach, the differentiation between these two compounds is enforced. Secondly, the model was fitted to a spectrum, which was recorded with a sufficient high DAPHE content to ensure a reliable differentiation of DAPH and DAPHE. The obtained model is found in Figure 51, in blue the single pure components and in red the resulting IHM is shown.

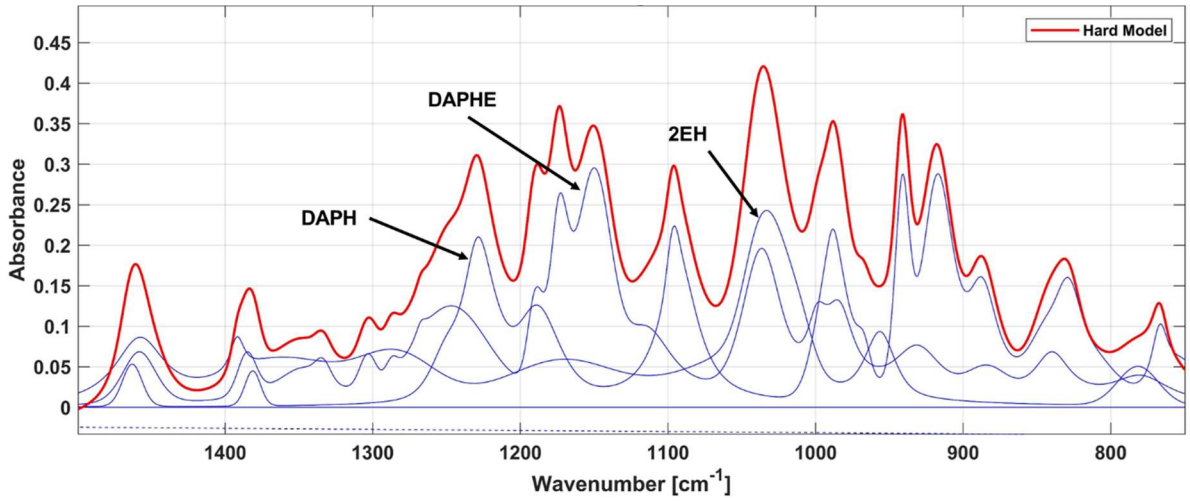

Figure 51: IHM Modell of the esterification of DAPH with 2EH leading to the diester DAPHE.

The obtained IHM need to be calibrated with suitable reference data. Unlike to the reference data applied in the chapters before (NMR and artificial mixtures), in this reaction step an offline analytic by GC analysis was chosen. For this reason, dilution series were carried out with DAPH, 2EH and the purified DAPHE and measured with GC. From these dilution series, the respective calibrations were obtained. Withdrawing a sample from the hot reactor will instantaneously lead to crystallization of the anhydride. Furthermore, the high viscosity of the reaction mixtures introduces large errors on the effective sampling volume. Thus, the calibrations of the GC analytic were employed with respect to the weight of the sample. Details of the sampling and GC

method, as well the obtained calibration curves can be found in *3.1.1 GC*. Hereafter, the IHM model was calibrated using the analyzed offline data along with the FTIR spectra recorded at the point in time of the sampling. The samples of the first calibration experiment were used and in addition several samples conducted at different temperatures and mass fractions of the starting materials were added. This increased the models accuracy towards changes of the reaction temperature and concentration changes. All samples and spectra used for the calibration can be found in Table 12 in *Supplemental Information*. The mass fractions determined from the inline analytical measurements, along with the offline samples from the calibration experiment are summarized in Figure 52:

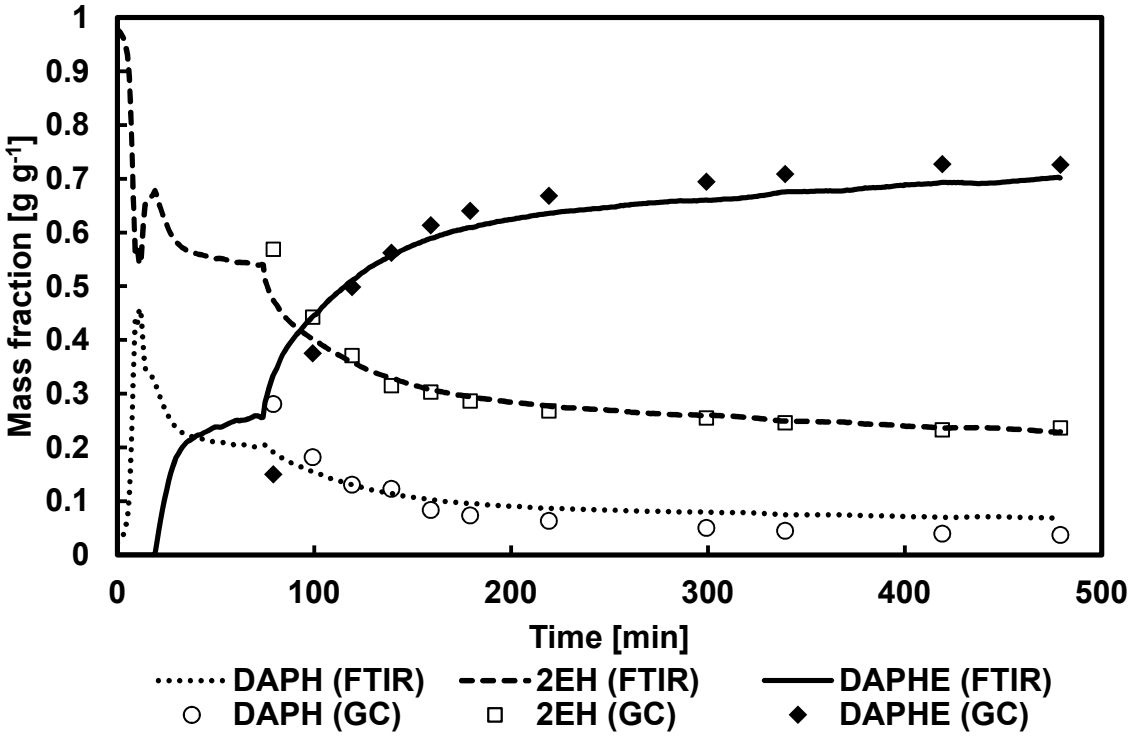

Figure 52: Mass fractions derived from Inline FTIR measurement and GC offline analysis. Reaction conditions: T = 130 °C, stirring rate: 1500 rpm, molar ratio 2EH:DAPH = 3, m_{DAPH} = 2.709 g, m_{2EH} = 5.810 g. 1 mol% H_2SO_4 (added after 75 min), One FTIR spectrum per minute recorded.

According to the inline measurement only 2EH is observed at the beginning of the experiment. Here, still some noise in the data can be seen, which is most likely attributed to the presence of two phases within the reactor. At a sufficient high temperature, all anhydride is molten and one uniformly mixed liquid phase is formed (after about 14 min). As a consequence, the formation of DAPHE starts, with initial high product formation rate, which is declining first. After 74 min, sulfuric acid was added as catalyst, leading again to an increased product formation. Offline samples were drawn after the substrates were present in only one phase to ensure a reliable measurement.

The trend of offline and inline measurements are in good accordance, only for the first sample, removed directly after acid addition, some deviation can be observed. Here, the DAPHE concentration is relatively lower compared to the value determined inline. For the alcohol 2EH, the behavior is *vice versa*.

Interestingly, even without the addition of the acidic catalyst, DAPHE formation occurs according to the inline analytic. This can be attributed to two different reasons. Firstly, the chemometric model does not differentiate between mono and diester, and therefore, potentially accounts initial monoester formation as DAPHE formation. Secondly, the monoester is directly converted to the final diester, already without the addition of catalyst. The monoester, an acid itself, may catalyze the esterification. With decreasing monoester content, the amount of free acid available for the catalysis is decreasing and therefore explaining this first equilibrium. In literature, this autocatalytic approach is described for the esterification of phthalic acid, therefore, also the autocatalysis is most probably responsible for the formation of DAPHE (Suter, 1969).

To check the accuracy of the developed inline analytical method, an external validation is carried out. The samples drawn in experiments, which are not part of the chemometric model calibrations, are analyzed by GC and thereafter compared to the predicted mass fraction obtained by the IHM. The results of this validation are plotted in Figure 53.

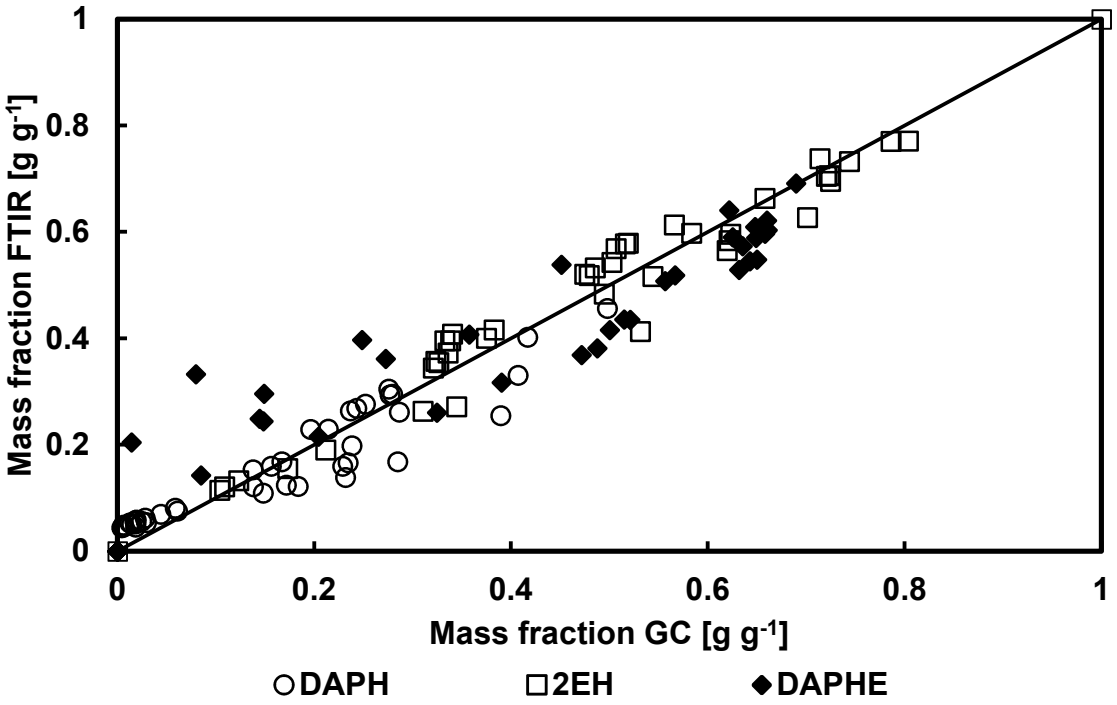

Figure 53: External validation with 40 samples taken from various experiments analyzed with GC and the corresponding predicted value from the FTIR measurement at the given point in time of the sample.

Both substrates, the anhydride DAPH and the alcohol 2EH, are relatively close on the identity line. For the product DAPHE, the largest deviations are found especially at low mass fraction. Here, the value obtained by the chemometric model is higher than the amount measured by GC. At higher DAPHE mass fractions, this error decreases. Both, GC and FTIR, derive the same value. To quantify the error introduced by the chemometric model, the RMSEP is calculated for the experimental data points shown in Figure 53 according to equation 4 in chapter *1.2.3 Chemometric Modeling.* In addition, the bias is calculated. The results are summarized in Table 9.

Table 9: RMSEP and Bias for DAPH, 2EH, DAPHE determined for external validation samples.

Component	RMSEP [g/g]	Bias [g/g]
DAPH	0.0473	-0.0035
2EH	0.0437	0.0056
DAPHE	0.0854	-0.0022

The RMSEP for the alcohol, as well as the anhydride, are lower than 5%. The anhydride determination leads to a negative bias, meaning that the inline analytic tends to underestimate this component. In contrast, the alcohol is overestimated, exhibiting a positive bias. The error of the inline measurement of the diester DAPHE is at about 8.5% and therefore higher as compared to the substrates. The bias for the product is

negative, which means the inline analytics on average is underestimating the mass fraction. Only for the samples at low diester content, this behavior is changed. Here, the inline analytic is overestimating the DAPHE mass fractions. This could be possibly attributed to a potential misallocation of monoesters as diester. Overall, the errors determined are in an acceptable range and the developed inline analytical method based on FTIR is further applied for the characterization of the reaction system.

6.3 Reaction Characterization by Design of Experiments

In this section, the esterification reaction of DAPH and 2EH is characterized using the previously developed inline analytics. The focus of this characterization is on the influence of reaction temperature and the ratio of the starting materials. To get insights into the combined effects of both, a Design of Experiments (DoE) by response surface design (RSM) is carried out. The plan of the DoE with all experiments and the conditions applied is summarized in Table 4.

The temperature range was chosen from 110 to 150 °C, while the molar ratio was specified between 2 and 5 equivalents of 2EH with respect to the anhydride DAPH. The levels of variables are summarized in Table 10.

Table 10: Levels of variables chosen for the DoE-RSM set up for the characterization of the esterification reaction of DAPH and 2EH.

	Levels		
Variable	-1	0	+1
Temperature [°C]	110	130	150
Molar ratio [-]	2	3.5	5

All experiments were conducted like described in *3.3 Reactor Setups*. The experiments were always carried out in a closed reactor system. This means, the reaction was always limited by the equilibrium, because no water was removed from the system.

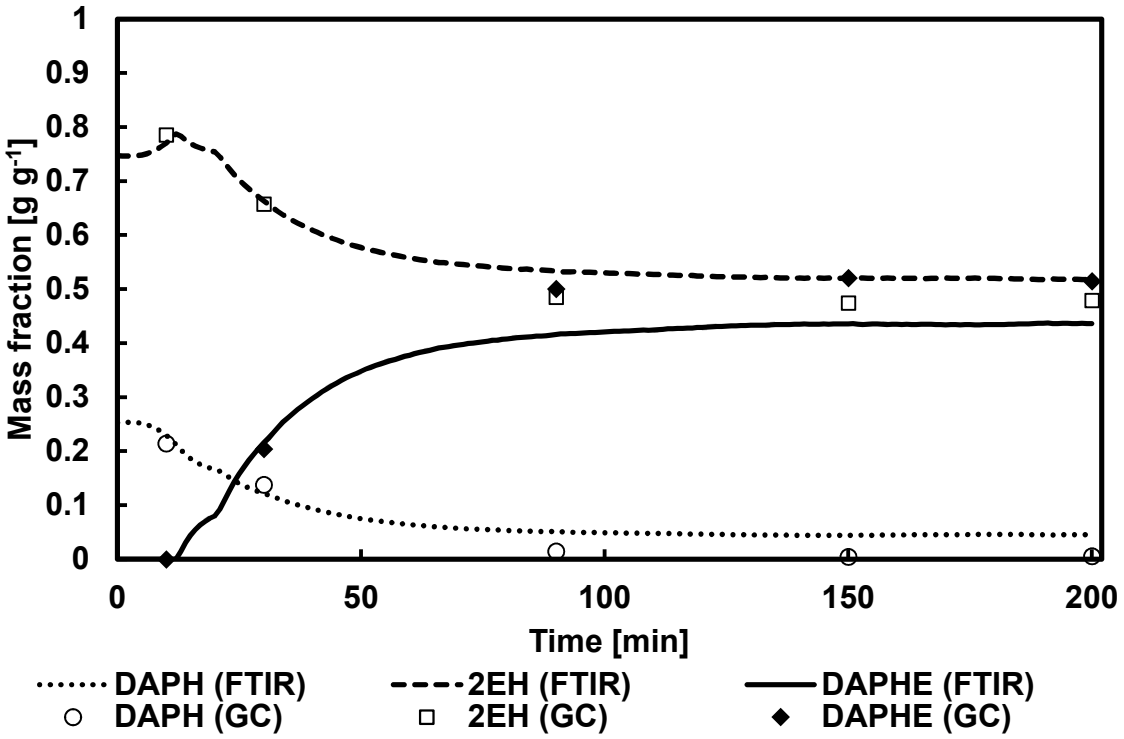

Figure 54: Mass fractions derived from Inline FTIR measurement and GC offline analysis. Reaction conditions: T = 150 °C, stirring rate: 1500 rpm, molar ratio 2EH:DAPH = 5, m_{DAPH} = 1.7415 g, m_{2EH} = 6.225 g. 1 mol% H_2SO_4 (added after 20 min), One FTIR spectrum per minute recorded.

The target value to be optimized during the DoE, is the conversion of DAPH determined by the inline spectroscopy. The reason for not choosing the mass fraction of DAPHE as target value, is that dilution effects by higher alcohol ratios would be included. The relative conversion of the starting material is unaffected by such dilution effects. Since the inline measurement yields one measurement per minute, in principle, every point in time of the conversion can be selected as a target value. The DoE experimental series was carried out with a total reaction time of 200 min. The acid was added in these experiments at 20 min. As target value, the conversion of DAPH at 90 min was chosen, since at this point of time, the reaction did not reach the equilibrium. As second target value, the conversion at 200 min was considered to include the effects of the molar ratio on the equilibrium. In Figure 54, one exemplary experiment of the DoE series is shown.

Already before acid catalyst addition, to some extent DAPHE formation is observed. After acid addition (t = 20 min), a further increase in product formation can be seen. The offline samples taken during this experiment and the measured inline data show some deviations, especially at higher conversion. While the offline analytic was not measuring any DAPH content, the inline analytic measures low mass fractions of

DAPH at the same time. At t = 90 min and t = 200 min, the conversion of DAPH is determined from the inline measurement according to equation 18:

$$X(t) = \frac{x_{DAPH}(t_0) - x_{DAPH}(t)}{x_{DAPH}(t_0)} * 100\% \quad (18)$$

With X(t): conversion at point in time t [-], $x_{DAPH}(t)$: mass fraction of DAPH at point in time t [g g^{-1}], $x_{DAPH}(t_0)$: mass fraction of DAPH at point in time zero [g g^{-1}].

All DoE-experiments were evaluated in respect to the target values. The results of this calculations for the conversion after 90 min are summarized in the DoE software Design Expert to obtain the corresponding surface plot, which is presented in Figure 55.

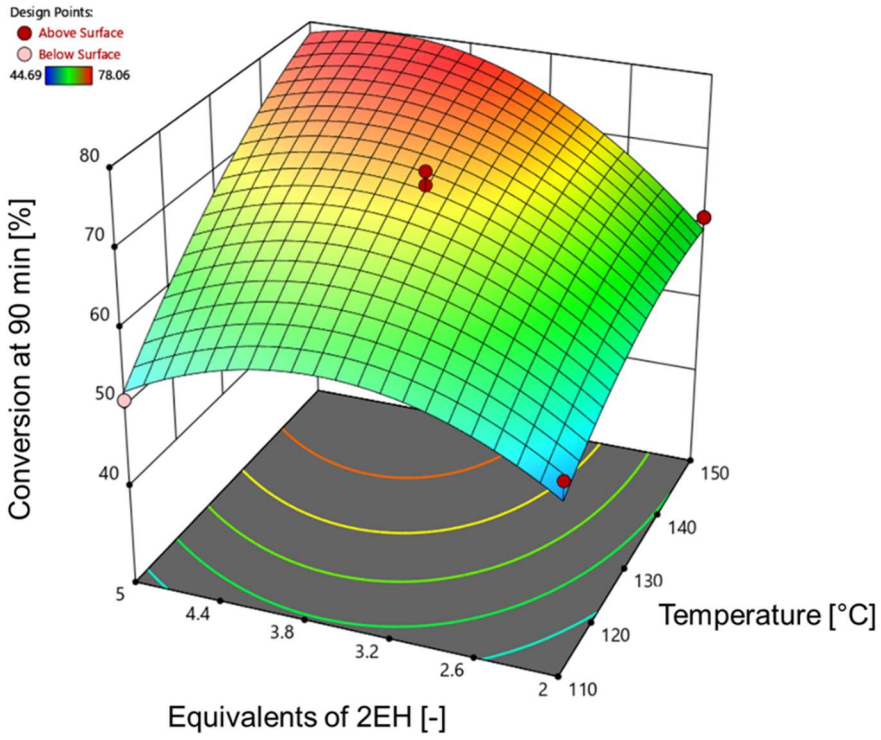

Figure 55: 3D surface plot of the Design of Experiment experiments in the range of 110 to 150 °C and molar ratios from 2 to 5 equivalents of 2EH in respect to DAPH shown with the target value conversion at 90 min.

For the influence of the temperature on the conversion of DAPH, a clear trend in the result of the DoE is found. With elevated temperatures, an increase of the conversion at 90 min is noticeable at all ratios of 2EH and DAPH. This trend is expected, since according to ARRHENIUS, a higher temperature results in a faster reaction rate. For the second parameter investigated, the molar ratio, the conversion shows according to the surface plot two minima, one at the lowest and one at the highest ratio of 2EH to DAPH. In between a maximum is determined by the DoE. This maximum is found for the

lowest temperature at a ratio of about 3.5 and is shifting to some extent to higher ratios at higher temperatures.

The resulting surface plot need to be validated in a further experiment. From the DoE, optimized reaction conditions are proposed, which are then experimentally verified. Conditions for this optimization were chosen as followed: while the conversions at 90 min and 200 min are maximized, the reaction temperature is minimized avoiding high rates of by-product formation. Additionally, the ratio of starting materials was minimized, which is advantageous in terms of a later downstream processing. At lower ratios, less alcohol has to be separated, which decreases the amount of energy for the following purification steps.

These optimized conditions are proposed by the DoE at a temperature 142.5 °C and a ratio of 2EH to DAPH of 3.3. An experiment was carried out with these conditions, which is shown in Figure 56. The model calculated a conversion after 90 min of 74.3% and 82.1% after 200 min.

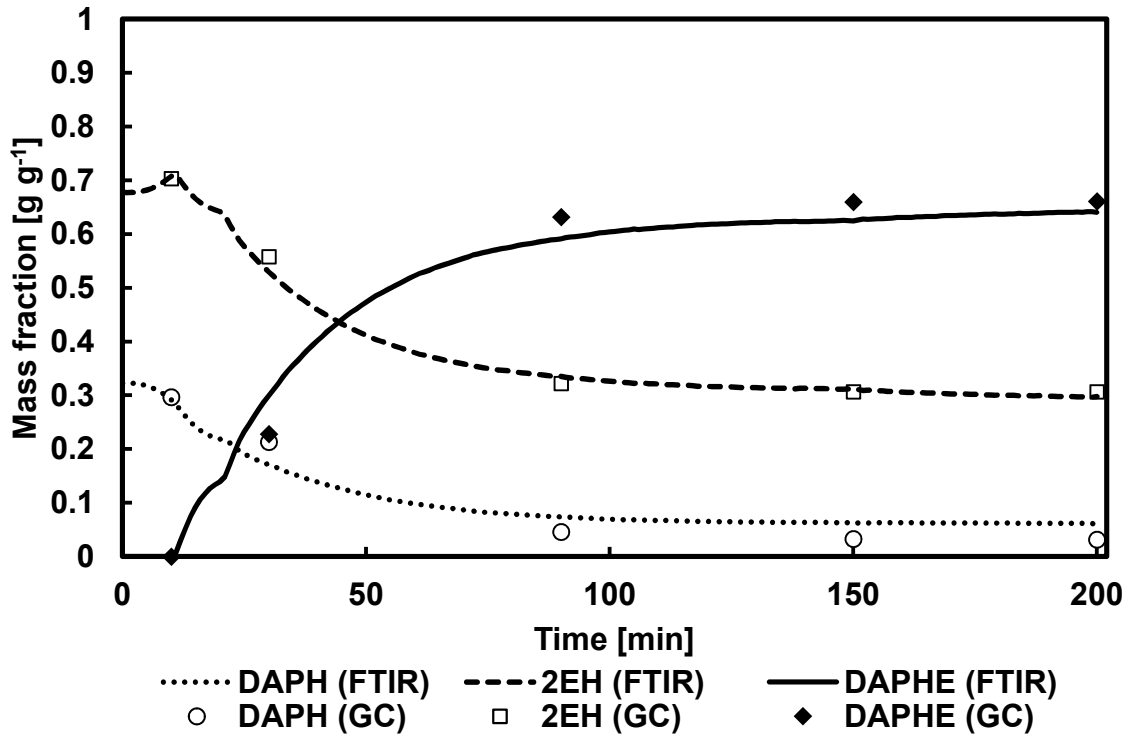

Figure 56: Mass fractions derived from Inline FTIR measurement and GC offline analysis of DoE-Validation. Reaction conditions: T = 142.5°C, stirring rate: 1500 rpm, molar ratio 2EH:DAPH = 3.3, m_{DAPH} = 2.4349 g, m_{2EH} = 5.7270 g. 1 mol% H_2SO_4 (added after 20 min), One FTIR spectrum per minute recorded.

The mass fraction profiles obtained for this DoE validation run are similar to the experiments carried out before. Already prior to the acid addition, DAPHE formation is

present, which is accelerated after acid addition. Furthermore, inline and offline data are in good accordance. In Figure 57, the 2D surface plot obtained from the DoE for the conversion after 90 min is shown along with the validation experiment. In the validation experiment, a conversion of 75.3% was reached. Compared to the predicted conversion of 74.3%, the relative deviation of the model is only about 1.3%. The deviation of the conversion at 200 min is slightly higher. Here, the DoE predicts a conversion of 82.1%, while the experimental validation yield a conversion of 79.3%. The optimization approach of the DoE was successful and was validated by an additional experiment.

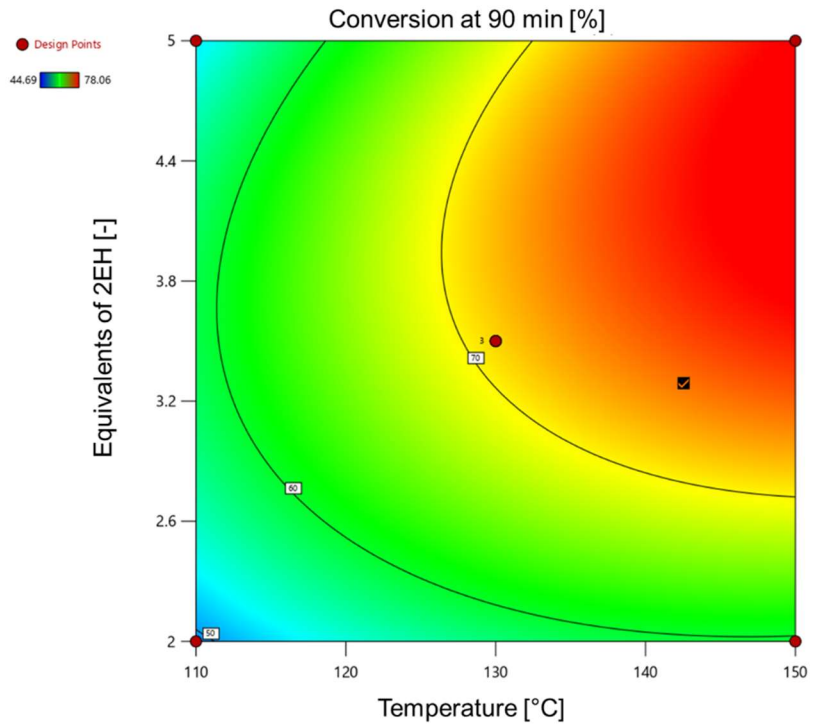

Figure 57: 2D surface plot of the DoE showing conversions of DAPH after 90 min of reactions in the investigated temperature range from 110 °C to 150 °C and molar ratios from two to five equivalents of 2EH. Validation experiment at optimized conditions indicated by a tick at 142.5 °C and 3.3 equivalents of 2EH.

6.4 Kinetic Model

Additional to the reaction characterization obtained by using a DoE, the inline measurements are employed to determine a kinetic model describing the reaction in a general manner. The reaction system is a two-step esterification, however, since the monoesters cannot be detected, the system was reduced to a one step reaction, which can formally be written as:

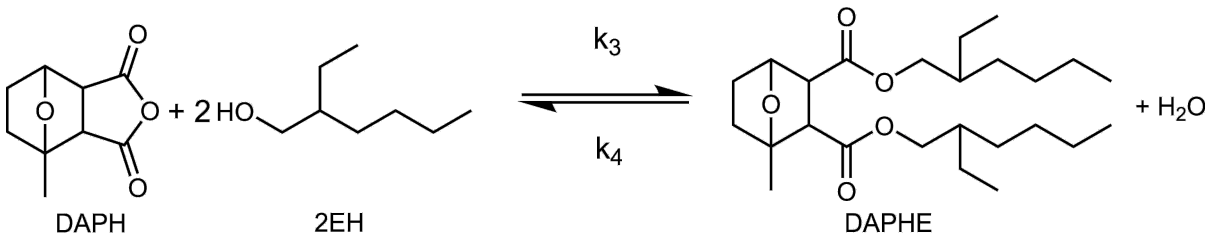

Figure 58: Kinetic model of the esterification of DAPH and 2EH to DAPHE. Reduced to only one reaction step leading to a pseudo-third order reaction kinetic.

For the kinetic approach, a fully reversible reaction mechanism was chosen, since esterification reactions are reversible in general and no water or product removal was carried out to shift the equilibrium to the product side. The mass fraction of monoesters was low throughout the reactions carried out. The two-step esterification was assumed to be concluded into only one step leading from the anhydride to DAPHE. The plasticizer is highly hydrophobic, so the water produced during the reaction is forming a second phase and is not available for a potential hydrolysis reaction. Thus, the side product water is excluded from the kinetic approach.

The kinetic equations (19, 20 and 21) were set up according to the assumptions made and follows the approach of a pseudo-third order kinetic system:

$$\frac{dc_{DAPH}}{dt} = -k_3\, c_{DAPH}\, {c_{2EH}}^2 + k_4\, c_{DAPHE} \tag{19}$$

$$\frac{dc_{2EH}}{dt} = -2\, k_3 c_{DAPH}\, {c_{2EH}}^2 + 2\, k_4\, c_{DAPHE} \tag{20}$$

$$\frac{dc_{DAPHE}}{dt} = k_3\, c_{DAPH}\, {c_{2E}}^2 - k_4\, c_{DAPHE} \tag{21}$$

With k_3: forward reaction constant [g² mmol^{-2} min^{-1}], k_4: reverse reaction constant [min^{-1}] c_{DAPH}: concentration DAPH [mmol g^{-1}], c_{2EH}: concentration 2EH [mmol g^{-1}], c_{DAPHE}: concentration DAPHE [mmol g^{-1}].

Since for the reaction of one molecule of DAPH to one molecule DAPHE, two molecules of alcohol are used, the kinetic equation of 2EH is multiplied by two in respect to both other equations. For the determination of the reaction kinetics, the inline analytical measurements were converted from mass per mass to moles per mass. This bears the advantage, that the reaction stoichiometry can be easily checked for plausibility. This is achieved by multiplying every compounds measured value with the molecular weight. The kinetic equations are fitted to the inline measurements by progress curve analysis implemented in Matlab (*9.4.2 Matlab script Esterification of*

DAPH and 2EH). Both, the inline measurement as well as the concentration profile obtained by the fitted kinetic are shown in Figure 59.

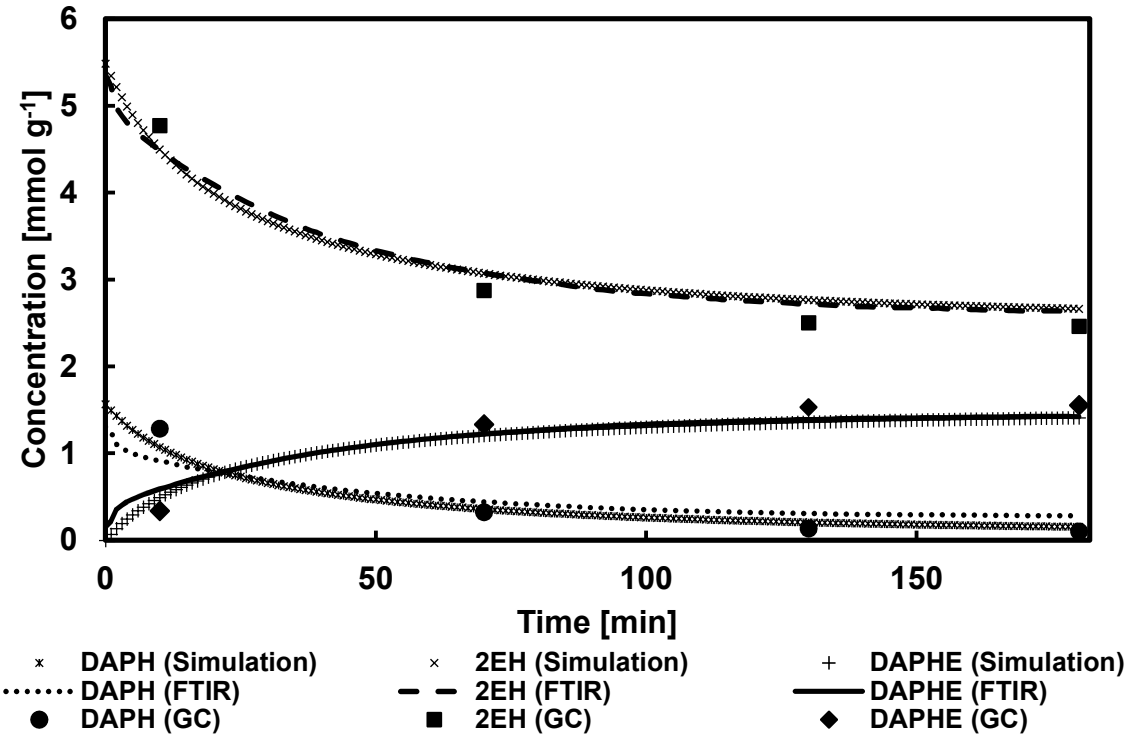

Figure 59: Concentration profile derived from Inline FTIR measurements along with offline samples and the kinetic model fitted to the inline data. Reaction conditions: T = 130°C, stirring rate: 1500rpm, molar ratio 2EH:DAPH = 3.5, m_{DAPH} = 2.3214 g, m_{2EH} = 5.810 g. 1 mol% H_2SO_4 (after acid addition, the measurement was started), One FTIR spectrum per minute recorded.

The point of time zero in this plot is the addition of the acid catalyst. Both, inline data and the kinetic model show a similar curve. Only in the beginning some deviations are present. Here, the kinetic model is underestimating the concentration of DAPHE to some extent, while the concentration of the anhydride DAPH is overestimated. Since there is probably some autocatalytic formation of DAPHE before the catalyst was added, the inline measurement "starts" here already with measuring some product. The overestimation of the anhydride DAPH, can also be explained by this earlier product formation. From this experiment, the kinetic parameters were determined, which are summarized in Table 11.

Table 11: Reaction rate constants and their confidence intervals determined from experimental data. Reaction conditions: T = 130°C, stirring rate: 1500rpm, molar ratio 2EH:DAPH = 3.5, m_{DAPH} = 2.3214 g, m_{2EH} = 5.810 g. 1 mol% H_2SO_4 (after acid addition, the measurement was started), One FTIR spectrum per minute recorded.

	Reaction rate constant	**Confidence interval**
$\mathbf{k_3}$ [$\cdot 10^{-3}$ g^2 mmol^{-2} min^{-1}]	1.502	0.034
$\mathbf{k_4}$ [$\cdot 10^{-3}$ min^{-1}]	0.693	0.143

Following the definition, reaction constant have the same unit for the forward and backwards reaction. This is the case, if the kinetics are determined based on thermodynamic activities, but not if a kinetic model is applied on data in standard chemical concentrations. Nevertheless, the kinetic model is valid, it just need to be taken into account that the equilibrium constant K_{eq} is then defined as $K_{eq,conc}$, which is then not dimensionless, but has a distinct unit. (Laidler, 1990).

The established kinetic parameters based on the inline measured data were tested on the applicability to varied reaction parameters. Therefore, the kinetic model is now applied for simulations. The simulations are compared to inline and offline data collected in respective experiments. First the influence of an increased reaction temperature was investigated. The kinetic model fitted on experimental data collected at 130 °C is used to simulate an experiment at 158 °C. To see the effects of only an increased reaction temperature, the ratio of 2EH to DAPH was kept constant in comparison to the models data at a ratio of 3.5. The results of the simulation along with the inline and offline data are summarized in Figure 60.

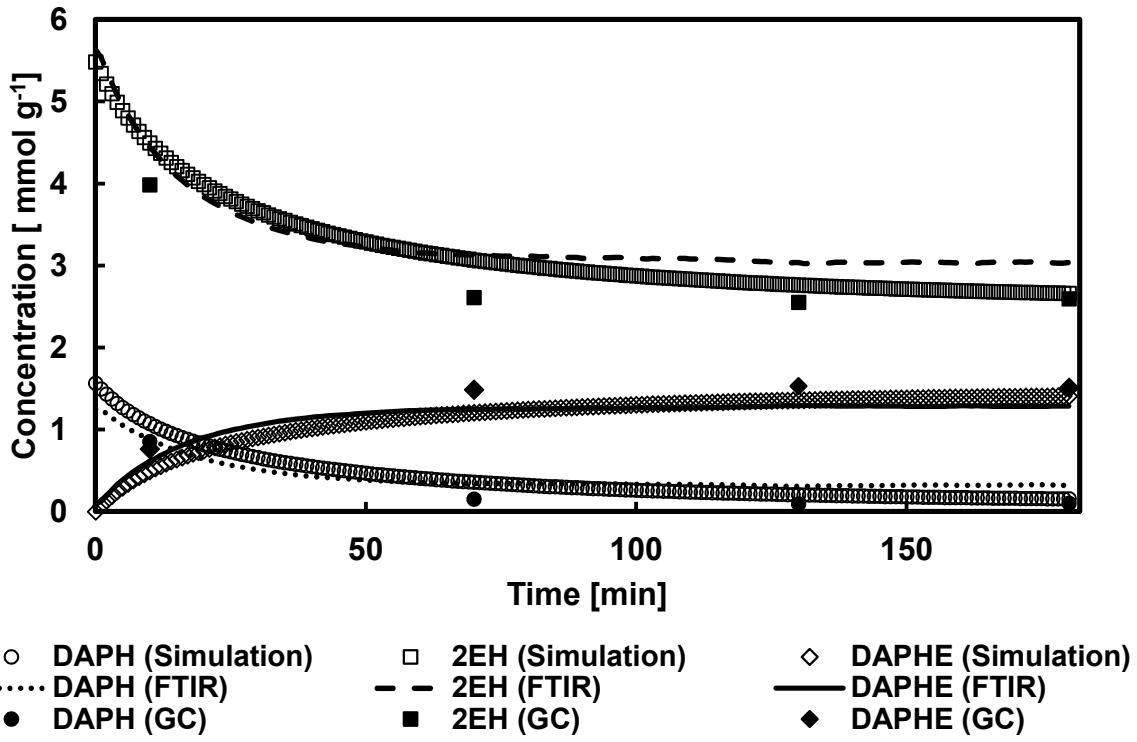

Figure 60: Concentration profile derived from Inline FTIR measurements along with offline samples and the simulation performed. Reaction conditions: T = 158°C, stirring rate: 1500 rpm, molar ratio 2EH:DAPH = 3.5, m_{DAPH} = 2.3220 g, m_{2EH} = 5.810 g. 1 mol% H_2SO_4 (after acid addition, the measurement was started), One FTIR spectrum per minute recorded.

In principle, the progress of the different curves depicts a similar trend. The DAPHE formation and the DAPH depletion are highly similar. Only in the beginning, a deviation of the anhydride concentration can be detected, the kinetic model displays a higher concentration compared to the inline analytic. Probably, this is attributed to a potential autocatalytic DAPHE formation, which was not considered. At higher conversion, the amount of 2EH determined by the kinetic model, is lower than measured by the inline analytic. Strikingly, for all offline GC measurements there is a clear tendency throughout the experiment. DAPHE content is higher in all samples, while the content of 2EH and DAPH is always lower compared to both, the inline analytic and also the kinetic model. This can be explained by the higher temperatures: the experiment was carried out at 158 °C and the boiling point of 2EH is at 184.7 °C. Despite the samples were weighed, afterwards some 2EH could be evaporated leading to lower final concentration, while DAPH and DAPHE were measured with higher content. Additionally, the effect of temperature shows some minor effects, which are not included into the kinetic model. The predictive capability, especially for DAPHE, is acceptable compared to the inline measurements.

Moreover, the kinetic model is tested to application on changes of the concentration range. An experiment carried out at the same temperature, like in the determination of the kinetic parameter (T = 130 °C), however, with changed ratio of 2EH to DAPH, was simulated. Here an excess of 5.6 equivalents of 2EH was chosen. As for the simulation shown before, again the concentration profiles calculated using the kinetic model are shown along with inline data and the offline GC measurements as well. These results are to be found in Figure 61. Compared to the inline measurements, the kinetic simulation estimates a faster progress of the reaction for all reaction components. The concentration of DAPH and 2EH is underestimated, while the DAPHE formation is overestimated. As expected, the offline data collected in the experiments are in good agreement with the simulation obtained using the determined kinetic paramters. A reason for the deviation of the inline data and the simulation could be that the IHM is calibrated in another concentration, and therefore, the deviation could be assigned to errors introduced by the chemometric model. This is supported by the offline data, which are in accordance with the simulation.

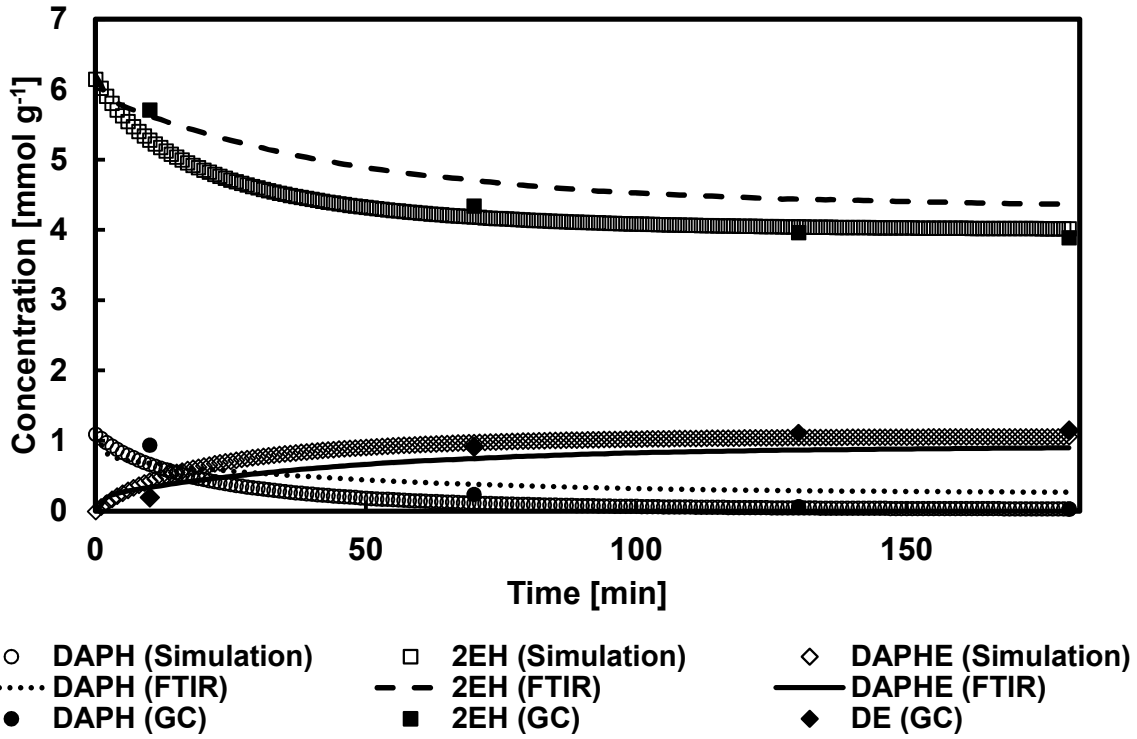

Figure 61: Concentration profile derived from Inline FTIR measurements along with offline samples and the simulation performed. Reaction conditions: T = 130°C, stirring rate: 1500 rpm, molar ratio 2EH:DAPH = 5.6, m_{DAPH} = 1.5830 g, m_{2EH} = 6.3379 g. 1 mol% H_2SO_4 (after acid addition, the measurement was started), One FTIR spectrum per minute recorded.

The presented kinetic was succesfully validated for the concentration range applied in the determination of the kinetic paramters. Changes of the reaction temperature showed only minor effects on the preciseness of the kinetic, despite the effect of temperature was not included into the kinetic model. For changes of the concentration of the starting materials, the kinetic is in good agreement with the offline samples. At high alcohol ratios, the inline measurement for 2EH shows an offset compared to the kinetic model. Since the offline samples are in accordance with the kinetic, here possibly further calibration data for the IHM are needed. To sum up, the kinetic model was validated in a temperature range from 130 °C to 158 °C and for molar ratios between 3 and 5.6 equivalents of 2EH.

7 Discussion and Outlook

In the following, the results for the single reaction steps presented in the last chapters are discussed in an overall discussion. The main focus is the interconnection of these three individual steps sketching an overall process scheme. Besides proposing suitable reactors and downstream units, an outlook for a further improvement of the inline analytics is provided.

7.1 Diels-Alder Reaction of 2-Methylfuran and Maleic Acid Anhydride

In chapter *4*, the results of the first step of the reaction sequence, the Diels-Alder reaction yielding DAP were presented. Both substrates, MAA and 2MF, can be derived on the basis of renewable resources in biorefinery approach. Compared to many other bio-based plasticizer, these substrates are not in a direct competition with the food sector, e.g. epoxidized vegetable oils (Hosney *et al.*, 2018).

For analyzing this reaction step, a suitable analytical method was developed. Since Diels-Alder cycloaddition reactions are reversible, traditional offline analytical methods were not applicable. Solubilizing a reaction sample prior to the analysis, or changing its temperature will result in different equilibrium conditions and thereby influencing the reaction progress (Solntsev *et al.*, 2001). This fact encourages the application of inline analytics for the characterization of this system. However, for establishing an inline analytical method, suitable reference data are necessary. Artificial mixtures are not applicable since the starting material will immediately start reacting. Additionally, during mixing, the equilibrium conditions are changing and, therefore influencing the measurement of the different components (Riechert *et al.*, 2015).

In this work, FTIR spectroscopy was applied, which was implemented with ATR probes. As described in *section 4.2 Chemometric Model Development,* a chemometric model for the analysis of the FTIR spectra was developed. Since these references cannot be produced by offline samples or by creating artificial mixtures, another inline analytical method was chosen. A series of experiments was conducted in NMR tubes, which were inline analyzed by ^{1}H-NMR spectroscopy (600 MHz). For a detailed investigation of the reaction system, the applicability of this approach is limited. Inside the NMR tubes, stirring is impossible and also temperature control of the sample is

limited. Hence, these data were employed as calibration data set for the IHM. Since solvation effects impacts the kinetic of chemical reactions, the described reaction is investigated as solvent free system.

For tuning the NMR device, however, a deuterated standard is necessary, which is usually the solvent. In the experiments carried out, acetone-d_6 was added as external standard within a closed glass capillary. This standard cannot be applied to derive the real concentration in mol L^{-1}, since the absolute number of molecules of acetone is unknown. Therefore, a method was developed to derive absolute concentration data from these relative measurements. The NMR data were projected on stoichiometric conversions and yields based on the initial weighs of the experiment. In a second, step this absolute number of molecules. To calculate the concentration, information of the reaction density are needed, which were obtained by modeling a mixer unit in Aspen Plus. To further improve the developed inline analytic, direct quantification via the external standard can be performed. By knowing the absolute number of molecules in the external standard, the projection of the data on the stoichiometric conversion is unnecessary and a direct quantification can be obtained. Another possibility is the implementation of a benchtop NMR enabling online measurements in a by-pass (Claaßen *et al.*, 2020).

The NMR data were converted into absolute concentrations and the chemometric model was calibrated and validated, before the reaction system was characterized with the inline measurements. For rising temperatures, an increase of the reaction rate was observed. However, for temperatures above 35 °C, polymerization of the reaction mixture was detected on the reactor wall as well as on the FTIR probe. The ratio of the starting material was investigated as second parameter. With increasing 2MF equivalents, the initial reaction rate is decreasing. This is in accordance with the expectation, that additional 2MF molecules reduce the probability that one MAA and one 2MF molecule are correctly orientated for the reaction. With low 2MF content, however, the DAP formation is enhanced and a potential crystallization is more likely to occur. Furthermore, the measured inline data are used for the determination of kinetic parameters for the establishment of a universal kinetic model. Interestingly, assuming an irreversible kinetic model resulted in a better fit obtained by the progress curve analysis. The kinetic model was successfully validated for a range of five to ten equivalents of 2MF in simulation experiments.

In an industrial scale, this first step of the reaction sequence is proposed to be carried out in a continuous operation mode in a combination of continuous stirred tank batch reactor and a cooling crystallizer. The reactor could be operated at a temperature between 20 and 30 °C, so the formation of polymeric side products is avoided. The ratio of 2MF and MAA, which should be maintained constant in this continuous operation, is depending on the crystallizing cooling profile as well on the residence time of the reaction solution inside the reactor as well as the crystallizer. Here, further investigations are necessary. The crystallizer needs to be cooled to reduce the solubility of DAP within the excess 2MF. This particular downstream unit was beyond the scope of this thesis. Here, a suitable temperature has to be evaluated. One criterion is the selectivity at which only the product DAP is crystallizing, while MAA is still soluble and can be pumped back into the reactor. In addition, cooling crystallization can be analyzed using inline analytics. In literature, examples are reported, in which FTIR was applied by monitoring the liquid phase in a crystallization process (Alatalo *et al.*, 2008). A cooling profile of succinic acid crystallization was determined without the exact knowledge about the kinetics itself (Feng, Berglund, 2002). In this unit operation a crucial parameter is the remaining MAA content within the DAP, which needs to be minimized. Otherwise, in the following process steps, the formation of side products is enhanced.

7.2 Hydrogenation of 4-methyl-3a,4,7,7a-tetrahydro-4,7-epoxyisobenzofuran-1,3-dione

The instable Diels-Alder intermediate DAP is transported to a further reactor, where the hydrogenation of the remaining double bond is carried out. For the hydrogenation, a suitable solvent is needed. For reasons of sustainability, the green solvent 2MeTHF is applied, which can be produced using renewable resources (Pace *et al.*, 2010).

Like in the step before, this reaction was characterized by ATR-FTIR inline analytical measurements. The chemometric model for the evaluation of the spectral data was established with the approach of IHM. Considering potential impurities from the previous reaction, possibly MAA would be found in the DAP feed. This will be hydrogenated yielding the side product BSA. Residues of 2MF are potentially hydrogenated to 2MeTHF (Kang *et al.*, 2017), which then acts as solvent. Since the amount of solvent formed in this side reaction is comparably small, 2MF is not

considered. The starting material DAP is not stable in solution and is, therefore, not accessible with offline reference analytics or by artificial mixtures. As a consequence, in this reaction step the main product DAPH and the side product BSA were quantified. For setting up the IHM, the pure components DAPH and BSA were measured as solutions in 2MeTHF to obtain FTIR spectra recorded in a liquid state. The pure components were fitted into a mixture spectrum from a reaction data set. The final model was further calibrated using artificial mixtures prepared from stock solutions of BSA and DAPH in 2MeTHF.

The chemometric model was applied for the characterization of the hydrogenation reaction. Evaluation of the stirring rate revealed a mass transfer limitation from the gaseous hydrogen phase into the liquid phase, thereby limiting the reaction at the palladium catalyst particle. The pitched-blade stirrer, along with the built-in motor of this Parr reactor system (Parr Instrument Company, Moline, USA), does not provide a sufficient energy input to overcome the mass transfer limitation. Here, different stirrers (or combinations) should to be investigated to further increase the mass transfer of hydrogen into the liquid phase. GIBANEL *et al.*, were investigating the solubility of hydrogen in 2MeTHF, however, only at ambient pressure (Gibanel *et al.*, 1993). Since pressure shows an influence on the solubility, further measurements in a pressurized systems are needed. By this means, the Henry constant can be determined providing a basis for the calculation of hydrogen solubility in the solvent at the respective hydrogen pressure. For the measurement of the hydrogen in the liquid phase, Pd-based sensors can be applied. H_2 dissociates at the Pd-surface and the atomic H is absorbed by Pd. Consequently, the volume of Pd is increasing, which is measured by strain sensors (Fisser *et al.*, 2018). A further possibility is the application of immersion probes for the measurement of dissolved hydrogen. Through a polymer film and a porous substrate the dissolved hydrogen is permeating. Inside the probe, the hydrogen is transported with a carrier gas to the analyzer, which is then measuring the gas composition (Meyberg, Roessler, 2005). Another research group measured the dissolved hydrogen content by NMR (Buser, McFarland, 2014).

Highly important for hydrogenation reactions is the determination of the reaction heat in order to avoid any thermal runaways of the reactor. A sufficiently large cooling power must be provided to ensure the necessary heat transfer (Westerterp *et al.*, 1997). With the temperature recorded over the course of a reaction, a first estimation was calculated to 139 kJ mol^{-1} considering different assumptions discussed in chapter *5.1*

Introduction: Heterogeneously Catalyzed Hydrogenation Reactions. However, it is clear that the Parr autoclave is not adiabatic. Additionally, regarding the observed mass transfer limitation, the assumption of ideal heat transfer from the reaction mixture to the reactor is not fully valid. Therefore, this estimated heat of reaction is definitively overestimated. For the proper design of the cooling process for the hydrogen autoclave, a more accurate value for the reaction heat is needed. This can be achieved by performing an experiment in a calorimeter, which provides an adiabatic behavior along with proper mixing (Landau *et al.*, 1995).

An important issue is a putative deactivation of the palladium catalyst. Since the starting material of the process are derived from ligno-cellulose, possibly low amounts of sulfur are contained therein. Sulfuric compounds are bound to the active site of the catalyst and thereby reduce the activity (Pinna *et al.*, 2001). For this reason, the purity of the starting materials should be checked in terms of any sulfur containing impurities. This could be achieved by the implementation of an online analytical method based on the chemiluminescence of sulfur, which could be established in a bypass stream. For this measurement technique, a low detection limit along with high sensitivity was shown (Calbry-Muzyka *et al.*, 2019).

The hydrogenation reaction can be carried out in different reactor setups. For example, a batch reaction vessel can be applied. Other possibilities are an oscillatory baffled reactor or a slurry/fixed bed reactor, which can be operated continuously. In addition, different operation modes are possible, either batch or continuous mode are able to be chosen. Depending on the reactor setup, different possibilities of recycling the Pd/C catalyst. Further experiments are necessary, especially, to investigate the mass transfer in the different reactor setups. Since the reaction is mass transfer limited, the suggested reaction conditions in this step are not focusing on maximized reaction rates, more on a maximized specific productivity. For the case of a batch reactor, the stirring rate need to be at maximum. The specific productivity is the highest, if catalyst loading is at 0.5% and if the hydrogen pressure is set to 2 bar. With these conditions, a specific productivity of 123 mmol L^{-1} min^{-1} $g_{(Pd/C)}^{-1}$ bar H_2^{-1} is achieved.

After the hydrogenation is finished, the reaction mixture undergoes downstream processing. For removing the catalyst, a filtration step need be introduced. The catalyst can be reused for the next reaction. Like in the Diels-Alder reaction, the reaction product DAPH is a solid. For its separation, another crystallizer can be applied. Since

the downstream was not in the scope of this process development, additional experiments have to be carried out for determining the crystallization kinetics. As proposed for the crystallization of DAP, the characterization of the crystallization of DAPH can be performed using an inline analytical approach. The solvent 2MeTHF can be recycled in this process step. A selective hydrogenation avoiding the formation of BSA is crucial for the following esterification step, since BSA will be esterified to di-2-ethylhexyl succinate. This complicates the downstream processing due to the high boiling point of the formed di-2-ethylhexyl succinate, which is estimated to be at about 360 °C.

7.3 Acid-catalyzed Esterification of 4-Methylhexahydro-4,7-epoxyisobenzofuran-1,3-dione

In the last step of the reaction sequence, the plasticizer building block DAPH is esterified leading to the corresponding diester. The alcohol 2EH, which also can be produced on the basis of renewable resources (Menne, 2015), was employed for the esterification. The latter occurs in two distinct reaction steps. The first, non-catalyzed opening of the anhydride with subsequent esterification yields two different monoesters. The monoesters further react in an acid-catalyzed, second esterification step to the final plasticizer molecule.

Prior to setting up the respective analytical methods, the diester was synthesized and purified. As in a similar system investigated within the project *Bio-Weichmacher*, also the monoesters were attempted to be isolated. A purified intermediate would allow for the detailed analysis of both reaction steps of the reaction system (Hiessl *et al.*, 2020). From the isolated intermediate, a pure component FTIR spectrum can be recorded and an offline analytic for the determination of their concentration established. However, this reaction system is totally different compared to the previously investigated methyl-phthalate system. The content of monoesters were found to be relatively low, independent from the presence or absence of any catalyst and also independent from the ratio of the starting materials. The monoester is suspected to catalyze its own esterification to DAPHE, yielding these low concentrations measured. Purification of this low content of monoesters was unsuccessful, therefore, both esterification steps were summarized into one. Since this reaction is planned to be carried out solvent-

free, it has to be ensured that the starting materials are in liquid state. Thus, the melting point of the anhydride DAPH was determined to 102.9 °C.

As for the previous reaction steps, ATR-FTIR in combination with IHM is applied for the inline analytic developed for the analysis and characterization of this esterification step. In contrast to the prior analytics, here, the calibration of the IHM was achieved using a suitable offline analytic. For this reason, a GC method was developed to quantify the concentration in offline samples. After being validated, the inline analytic was applied for the evaluation of the DoE experiments. The conversion of DAPH, which is determined *via* inline analytics, was chosen as the target value. The FTIR analytic provides a high data density, in principle every point of time recorded can be applied for the evaluation. The conversion after 90 min and 200 min were preferred as target values. At 90 min, the equilibrium was not reached. Therefore, the information obtained are more focusing on the product formation rate. The conversion at 200 min is at or near the equilibrium of the reaction.

From the DoE experiments, a correlation between the two parameters reaction temperature and ratio of starting materials are obtained, which is shown in chapter *6.3 Reaction Characterization by Design of Experiments*. For temperatures above 130 °C and above about three equivalents of 2EH, conversions higher than 70% were reached after 90 min. For the validation of the correlation found by the DoE, both target values were maximized. Additionally, the molar excess of 2EH was minimized. This minimization shows importance in terms of efficiency: the excess alcohol has to be heated to the applied temperature and in the end, it has to be separated from the reaction mixture. Both, heating and separation, are energy consuming, so by this minimization approach the consumed energy within the process is addressed. The DoE software provided a solution for the described minimization and maximization method, which then was verified experimentally. The temperature was determined to 142.5 °C and the excess of 2EH to 3.3 equivalents. For both target values, the conversions determined based on the inline analytical measurements are within the 95% confidence interval given by the DoE showing the correctness of the model.

The DoE method could be extended to also account for side product formation. In literature, different examples for such side product formations during esterification reactions are reported. First, the alcohol is putatively symmetrical etherified. Moreover, an alkyl sulfonic acid from 2EH can be formed during this acid-catalyzed esterification.

At higher temperatures (above 175 °C), ethylhexene can be a possible side product (Suter, 1969). In general, for experiments performed at higher temperatures, the reaction mixture showed a darker color indicating an increased amount of side products. The composition of these side products have to be determined either by using GC-MS, NMR or an indirect quantification approach is necessary. Here, for example a *UV/VIS* spectroscopic analysis could exhibit a correlation between the color and possible side product content. In the DoE, this color value as a further target indicator could be minimized during another validation experiment. The amount of side products can be reduced drastically by avoiding the application of mineral acids as catalyst. The autocatalytic approach was reported to be less prone to side product formation, however, it also needs more time to achieve similar conversions (Suter, 1969).

Besides further investigations on the autocatalytic approach, different catalyst can be tested in various concentrations. For the esterification presented in this thesis, only 1 and 2 mol% H_2SO_4 were investigated (not shown). For 2 mol%, the conversion of DAPH to DAPHE was faster, but leading to the same equilibrium, as expected. Here, the effect on the target value DAPH conversion at 90 min can be studied, here the influence of the catalyst is the highest. Different concentrations and also different catalyst can be tested using the inline analytical method developed. Especially, the application of zeolites is of interest, since these heterogeneous solid catalyst can be easily separated from the reaction mixture (Chung, Park, 2009).

Because esterification reactions are reversible reactions, they are limited by the position of the equilibrium. By application of excess amount of alcohol, this equilibrium can be shifted towards product formation, as shown for the results obtained in the DoE. Another option is to continuously remove one product from the mixture and thus pulling on the equilibrium position. In esterification reactions, usually the water is removed from the reactor. While in small scale reactors, the water can be removed by the addition of molar sieves, in an industrial scale, this is not feasible. Here, distillation can be applied. It is important to note that 2EH and water are forming a heterogeneous azeotrope. As pointed out by SUTER for the esterification of phthalic anhydride, the reaction can be operated continuously in a cascade of stirred tank reactors. The excess water is supposed to be withdrawn by azeotrope distillation along with the excess alcohol. The crude reaction mixture is transported to a first distillation column where the excess alcohol is removed, which can be reused after water removal. For the next

step of the downstream process, the type of catalyst applied is important. While a zeolite is separated from the mixture by a filtration unit, homogeneous acidic catalysts has to be neutralized and removed by a washing unit with water. In a second step, water and residuals of alcohol are removed by a further distillation step (Suter, 1969). Another possibility is a bubble column reactor. Here, by gassing nitrogen or air throughout the reaction mixture, the water is removed. In addition, this reactor is also highly suitable for high viscous systems (Hilterhaus *et al.*, 2008) as it is the case for the plasticizer investigated in this thesis.

According to the reactors and downstream units proposed, a simplified flow scheme for a continuous process is presented in Figure 62. 2MF and MAA are continuously fed in to a stirred tank reactor. The product DAP is removed in a cooling crystallizer, while the starting materials are returned to the reaction vessel. The purified DAP and the solvent 2MeTHF are transported in to the hydrogenation reactor, where the hydrogenation is carried out using Pd/C and H_2. A filtration unit maintains the catalyst within the reactor setup. DAPH is selectively crystallized in a second crystallizer before it is fed into the last reactor. Here, 2EH is added and the esterification is carried out acid-catalyzed by application of H_2SO_4. Finally, the plasticizer DAPHE is continuously purified in a distillation setup enabling a recycling of the starting material.

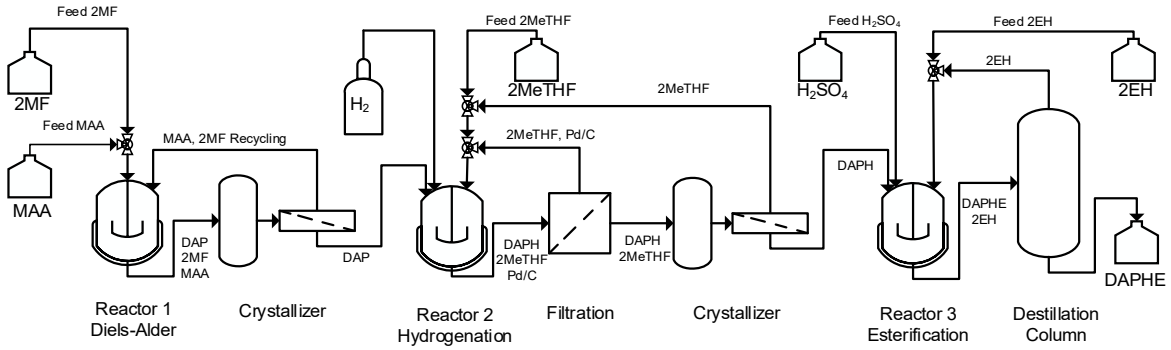

Figure 62: Proposed combined process for the production of DAPHE based on 2MF and MAA in a three step reaction sequence and respective unit operations for the downstream processing.

Neglecting the different steps to obtain 2MF and MAA from ligno-cellulosic biomass, the overall efficiency of the process is high. In the Diels-Alder reaction, a very high atom efficiency is achieved, since full conversion can be achieved and no side products are formed. In addition, the hydrogenation reaction is efficient, if the excess hydrogen pressure is not chosen unnecessarily high and if the crystallization step carried out before is highly selective avoiding MAA to be available for hydrogenation. The

esterification reaction as well as the respective distillation steps are the most energy consuming operations in the presented reaction sequence.

The novel plasticizer was evaluated towards applicability in PVC at the project partner BASF SE (not published). Additionally, within the frame of the Bio-Weichmacher project, different plasticizers were synthesized and investigated in performance assessments (Plass *et al.*, 2020). Further variations of the plasticizers core building block can be investigated. For instance, the remaining double bond after the Diels-Alder reaction can be epoxidized instead of hydrogenated. Another possibility is the application of different dienes, as for example furan, 3-methylfuran, dimethylfuran, or furfuryl alcohol leading to altered substitutions of the plasticizers cyclic backbone.

7.4 Inline Analytics and Process Control

The developed inline analytics applied for the process characterization can further be applied for establishing respective process control in the single reaction steps of the sequence. Their position within the sequence is shown in Figure 63.

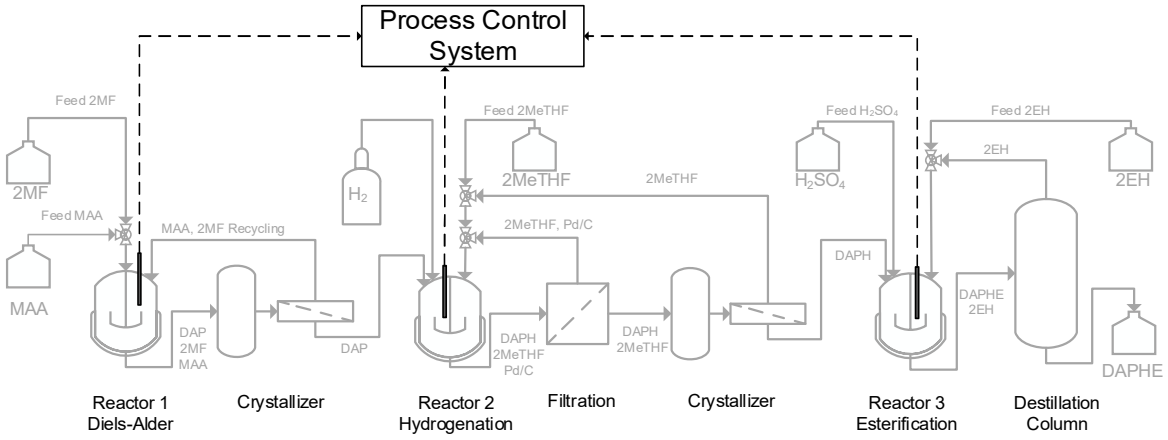

Figure 63: Proposed combined process for the production of DAPHE based on 2MF and MAA in a three step reaction sequence monitored by the developed inline analytics and the respective unit operations for the downstream processing.

Regarding the Diels-Alder reaction, the amount of additional substrates fed into the reactor can be controlled using the inline analytic implemented before. The measurement signal derived from the FTIR spectrometer is directly evaluated by the chemometric model. Now these values are fed into a process control system and forwarded to a pump or a respective solid transport system and thereby, starting the

addition. For the cooling crystallizer, another chemometric model can be set up enabling a continuous monitoring of this downstream processing step. By this approach, the concentrations can be measured at several locations and deviations detected swiftly.

In the hydrogenation step, the chemometric model is able to monitor the concentration of the main product DAPH as well the side product BSA. Since BSA cannot be recycled to the previous Diels-Alder reaction, its formation should be avoided. In the case of the reaction of MAA to BSA is suppressed or avoided, the remaining MAA can be recycled increasing the overall process efficiency. During the process characterization, the hydrogenation of MAA started only after the hydrogenation of the target DAP. This queue behavior is expected to be based on differences in their adsorption kinetics, which was also described for the hydrogenation of mixtures consisting of (poly-) cyclic aromatic compounds (Toppinen *et al.*, 1997). The observed queue effect along with the developed inline analytic enables a process control for this reaction step. From the concentrations measured in real-time, the point of time at which the hydrogenation of MAA to BSA starts can be deduced. In section *5.4 Selectivity Control*, from the inline concentration profiles, the apparent selectivity is calculated and plotted as function of the apparent conversion. The apparent selectivity approaches a value of one, before it decreases indicating the formation of BSA. Accordingly, criteria can be defined at which conversion the reaction is stopped. To achieve this, the inline measurement signal can be applied to control the residence time within a continuously operated reactor by adjusting the pump rate.

In the last reaction step, the esterification of DAPH to DAPHE, the inline analytical measurement can be applied for setting up a respective process control. The real-time data can be employed for controlling the feed of DAPH and 2EH to the continuous stirred tank reactor cascade or also in a bubble column reactor. Additionally, a further chemometric model can be designed for monitoring concentration profiles within the distillation unit (Hiessl, 2016), which is able control the heating and cooling power of the distillation column or the respective reflux ratio. To include the formation of monoester into the inline analytical process control, a different measurement technique is needed. For example, the application of a low-field benchtop NMR spectrometer enables the direct online measurement of the monoester. No pure components are necessary and without workup, the reaction mixture is analyzed in a bypass (Claaßen *et al.*, 2020).

7.5 Biocatalytic Esterification

The energy demand for heating could be drastically reduced by the application of enzymes for the catalysis of the esterification step. Lipases or esterases, examples from enzyme class 3 (EC 3 – hydrolases), catalyze a broad range of esterification reactions. Enzymes work in relatively mild conditions, therefore, the reaction temperature for the esterification reaction can be reduced drastically. Throughout the project "*Bio-Weichmacher*", more than 80 enzymes were screened, which catalyze the esterification of such anhydrides, respectively of the monoesters.

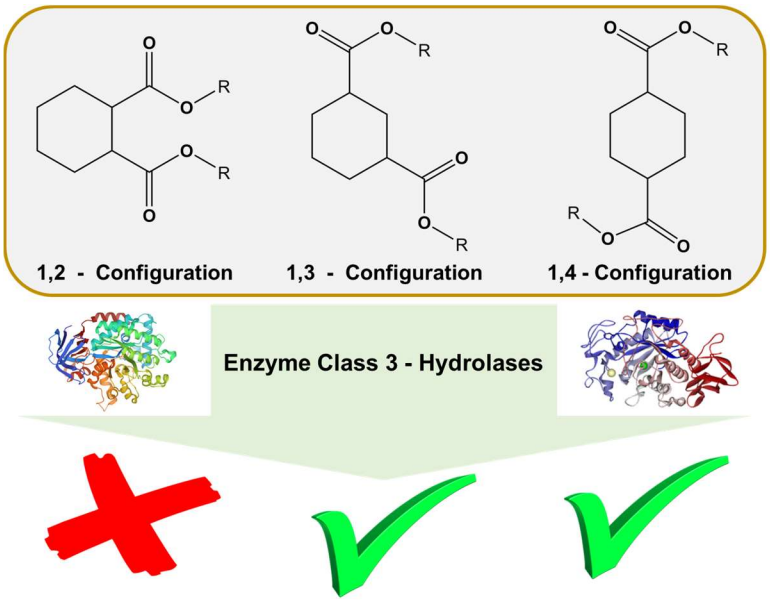

Figure 64: Screening for enzymes catalyzing the hydrolysis or esterification of cyclic components with different configurations of carboxylic acid groups (R = H) or the respective alkyl esters (R = CH_3).

In a first screening, commercial available enzyme preparations were tested on their capability of esterifying cyclohexane dicarboxylic acids with 2EH in 2MeTHF applied as solvent. In her bachelor thesis, SCHADE examined the effect of the position of the acid groups. Beside cyclohexane carboxylic acid, 1,2-, 1,3- and 1,4-cyclohexane dicarboxylic acid were investigated for being enzymatically esterified. While many enzymes were capable of converting cyclohexane carboxylic acid and 1,3-cyclohexane dicarboxylic acid, no enzyme was identified for the esterification of the target compound 1,2-cyclohexane dicarboxylic acid (Schade, 2018).

In a further approach, in the scope of his master thesis, KUNDOCH was investigating enzymes catalyzing the hydrolysis of short alkyl ester plasticizer analogues. These

analogues were chosen because these are soluble in water. In order to gather knowledge on the steric hindrance, here 1,2-, 1,3- and 1,4-cyclohexane dimethyl carboxylate were tested in parallel. This hydrolytic screening was performed in a plate reader to increase the through-put of the method. The conversion of the short chain alkyl esters was followed by the pH-shift evaluated by the absorbance of the indicator phenol red. Among others, the lipase BTL2 from *Geobacillus thermocatenulatus* (Martín *et al.*, 2008) and two newly isolated PETases (Danso *et al.*, 2018) were investigated. Similar to the findings before, 1,3-cyclohexane dimethyl carboxylate was found to be hydrolyzed by several enzymes, 1,4-cyclohexane dimethyl carboxylate only by few, here are the PETases to be mentioned (Kundoch, 2019).

Another screening focusing on extremophilic enzymes was carried out by LOPEZ HARO within his master thesis carried out in cooperation with the Institute of Technical Microbiology (TUHH). Different extremophiles and recombinant produced enzymes were tested in the plate assay based on the absorbance of phenol red. Additionally, enrichment cultures were investigated. The short chain alkyl-esters were supplemented as carbon source to environmental samples. However, this enrichment approach was unsuccessful. In this work, for the hydrolysis of 1,2-cyclohexane dimethyl carboxylate a lipase from *Thermoanaerobacter thermohydrosulfuricus* was identified. Though, the transfer to organic esterification was not successful. Possibly, the lyophilization step prior to the application in organic media is the reason that no activity could be shown in esterification experiments. Further experiments improving the lyophilization step are necessary (Lopez Haro, 2020). Alternatively, immobilization of enzymes can be applied for enabling the deployment in a pure organic system (Adlercreutz, 2013).

During all screening approaches, no enzyme being capable of the esterification of 1,2-cyclohexane dicarboxylic acid was identified, which possess a similar structure to the target plasticizers molecules. Potentially, the configuration of directly neighbored acid functions of the di-acid derived from the anhydride is disadvantageous in terms of a possible steric hindrance. To further investigate enzymatic esterification, insights in to this potential steric hindrance are necessary. Molecular docking simulations can be applied to gather insights in respect to the starting materials orientation within the enzymes active site (Udatha *et al.*, 2012). Additionally, by the employment of directed evolution, the enzymes 3D structure can be varied to enable a binding and conversion of diacids in 1,2-position (Arnold, 2018).

8 Summary

Scope of this thesis was the inline analytical aided process development towards alternative, bio-based plasticizers for application in PVC. For every reaction step, ATR-FTIR in combination with IHM was applied. The reaction sequence investigated consists of three distinct reaction steps.

The starting materials 2MF (Gandarias *et al.*, 2018) and MAA (Agirre *et al.*, 2020) can be produced on the basis of ligno-cellulosic biomass. In a first Diels-Alder reaction, 2MF and MAA are forming an intermediate (DAP), a cyclic precursor for the plasticizing central building block. Since DAP is not stable in solutions, GC and HPLC are not applicable underlining the need for a suitable inline analytic for the characterization of this reaction step. For the calibration of the chemometric model, ^{1}H-NMR experiments were carried out. The reaction was carried solvent free, therefore, acetone-d_6 was applied as external standard. To derive absolute concentration data from the obtained relative molar fractions measured in the NMR calibration, a projection on the stoichiometric conversion was carried out. Additionally, the density of the reaction mixture was modeled using a mixer unit operation in Aspen Custom Modeler. The chemometric model was successfully calibrated with the obtained absolute concentrations. Using the developed inline analytic, the reaction step was characterized and a kinetic model describing the reaction was established. An irreversible approach was found to deliver a better fit to the measured inline data. The kinetic constant was determined by progress curve analysis to $k_2 = (4.12 \pm 0.05) \cdot 10^{-3}$ L mol^{-1} min^{-1}. In additional simulations, the correctness of the kinetic model was shown.

Since the *retro*-Diels-Alder reaction will lead to a backwards reaction into the direction of the starting materials, the intermediate has to be stabilized. In the presented reaction sequence, the remaining double bond in the DAP is hydrogenated, yielding to the stabilized intermediate DAPH. As carried out before, an inline analytic was set up. However, in this step the chemometric model was calibrated with artificial mixtures. In this hydrogenation, a possible side reaction can occur: remaining MAA from the previous Diels-Alder reaction or resulting from *retro*-Diels-Alder reaction is hydrogenated to BSA, which should be avoided. Therefore, the inline analytic was designed for the measurement of both, the target product DAPH and as well as the side product BSA. Inline measurements showed a queue hydrogenation of both, which

can be attributed to differences in their adsorption kinetics on the catalyst particle Pd/C. The applied hydrogenation reactor was found to be severely mass transfer limited. Since a kinetic model is expected to describe a reaction system in a more general way, these mass transfer limited data were not applied for determining a kinetic model.

In the last step, the plasticizer precursor DAPH is esterified with 2EH using sulfuric acid as catalyst. (Bueschler, 2020). The calibration of the chemometric model was achieved by reference samples analyzed with GC. To obtain pure reference substances needed for the development of inline and offline analytic, the DAPHE was synthesized and purified with filtration by aluminum oxide and vacuum distillation. Additionally, for analyzing both reaction steps in detail, the monoesters are necessary. However, due to unfavorable equilibrium conditions, in all approaches only very low content of monoesters were found and purification was unsuccessful. Therefore, both steps are summarized and analyzed with the established inline analytic. The characterization of this reaction step was carried out using a DoE investigating reaction temperature and molar ratio of starting materials. Target value of the DoE was the conversion of DAPH after 90 and 200 min, which were maximized in the validation of the DoE. In parallel, the excess of 2EH and the reaction temperature were minimized. This optimum in the investigated range was determined by the DoE to 142.5 °C and a ratio of 3.3 equivalents, which was proven experimentally. A kinetic model describing the esterification as a simplified pseudo-third order reaction was established. The kinetic parameters were determined to $k_3 = (1.50 \pm 0.03) \cdot 10^{-3}$ g^2 mmol^{-2} min^{-1} and $k_4 = (0.69 \pm 0.14) \cdot 10^{-3}$ min^{-1} by fitting the inline data using progress curve analysis. In simulations, the correctness of the kinetic model for molar ratios between 3 and 5.6 equivalents of 2EH and at temperatures between 130 °C and 158 °C was shown. Additionally, enzymes were tested for application in the esterification reaction (Kundoch, 2019, Lopez Haro, 2020, Schade, 2018). However, no suitable enzyme was identified. Different model substrates were tested and the results suggest a steric hindrance of directly adjacent acid groups to be responsible.

Concluding, a combined three-step process, every step monitored by inline analytics, was established. By application of these inline measurements, the reaction steps were characterized and respective kinetic models set up. Additionally, possible unit operations for a potential downstream processing are discussed.

9 Supplemental Information

9.1 Calibration of Chemometric Models

- Diels-Alder reaction of MAA and 2MF to DAP

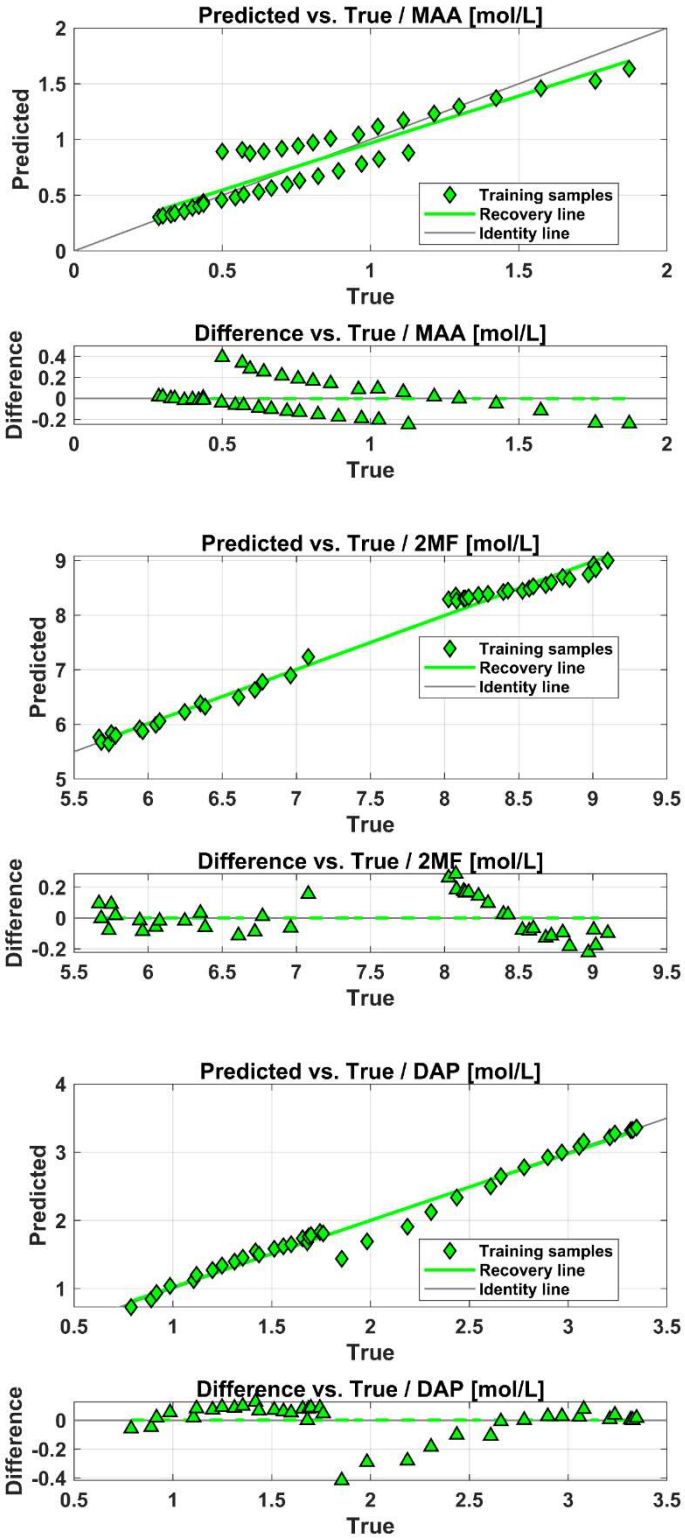

Figure 65: Calibration of MAA (top), 2MF (middle) and DAP (bottom) for the Indirect Hard Model for the Diels-Alder reaction of MAA and 2MF.

- Hydrogenation of DAP to DAPH

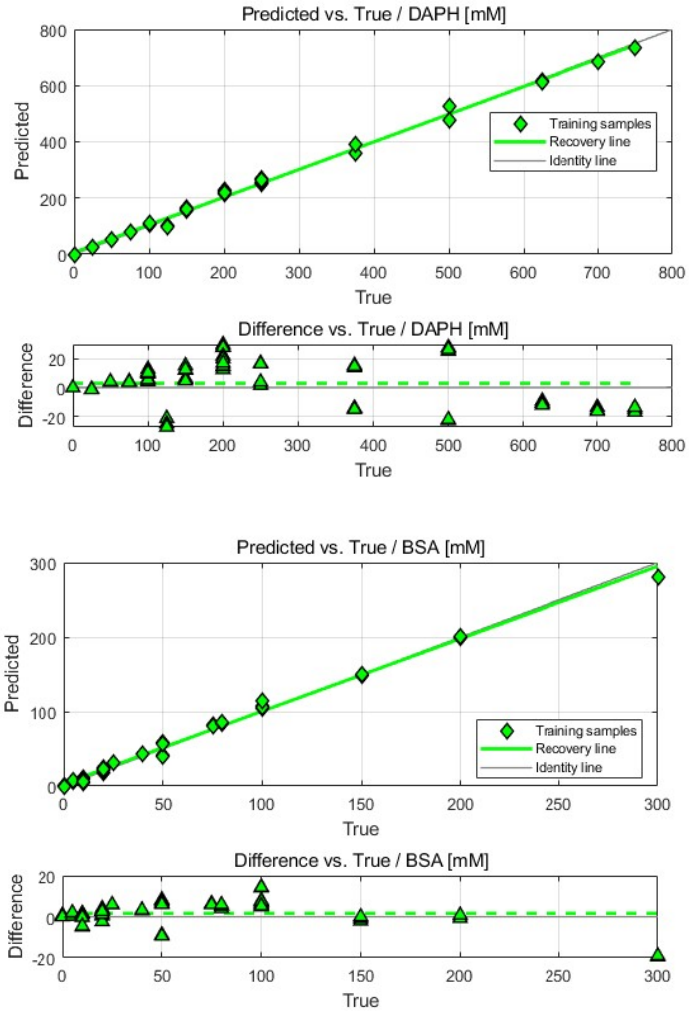

Figure 66: Calibration of DAPH (top) and BSA (bottom) used for the Indirect Hard Model with mixtures of DAPH and BSA in 2MeTHF.

- Esterification of DAPH and 2EH leading to diester DAPHE

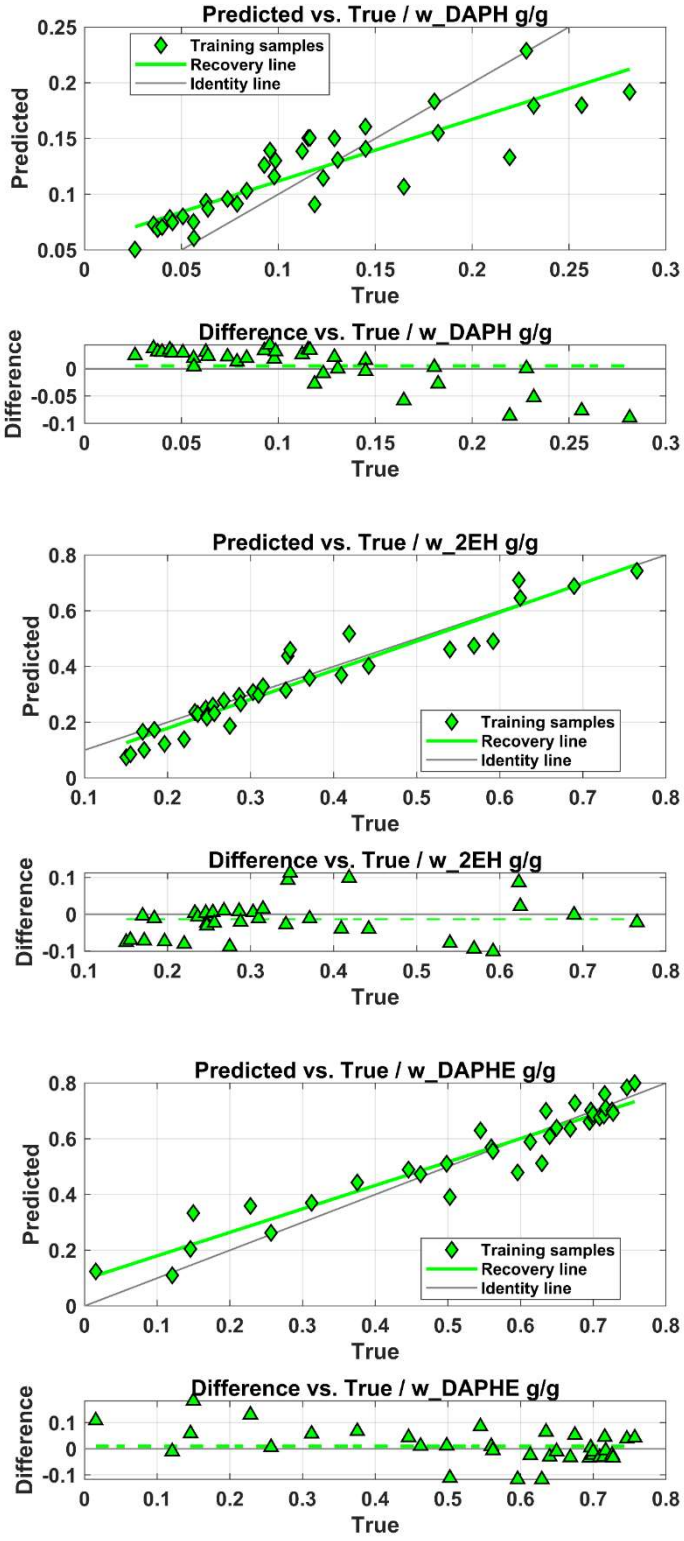

Figure 67: Calibration of DAPH (top), 2EH (middle) and DAPHE (bottom) for the Indirect Hard Model for the esterification reaction of DAPH and 2EH.

9.2 Design of Experiments

Table 12: Samples used for the calibration of the IHM for the analysis of FTIR spectra recorded during the esterification reaction.

Experiment	Samples / Points in time	Reaction conditions
Reaction 1	079, 099, 119, 139, 159, 179, 219, 299, 339, 419, 479	T = 130 °C 3 equivalents 2EH
ValIHM	079, 109, 139, 184, 244, 364	T = 130 °C 2.2 equivalents 2EH
Validation 2	030, 045, 060, 090, 150, 180, 199	T = 130 °C 3 equivalents 2EH
DoE Run1	030, 090, 150, 200	T = 130 °C 3.5 equivalents 2EH
DoE Run2	030, 150, 200	T = 150 °C 2 equivalents 2EH
DoE Run3	030, 090, 150, 200	T = 110 °C 5 equivalents 2EH

Table 13: Samples used for the validation of the IHM for the analysis of FTIR spectra recorded during the esterification reaction.

Experiment	Samples / Points in time	Reaction conditions
DoE Run4	010, 030, 090, 150, 200	T = 130 °C 5.6 equivalents 2EH
DoE Run5	010, 030, 090, 150, 200	T = 130 °C 3.5 equivalents 2EH
DoE Run6	010, 030, 090, 150, 200	T = 158 °C 3.5 equivalents 2EH
DoE Run7	010, 030, 090, 150, 200	T = 150 °C 5 equivalents 2EH
DoE Run8	010, 030, 090, 150, 200	T = 110 °C 2 equivalents 2EH
DoE Run9	010, 030, 090, 150, 200	T = 102 °C 3.5 equivalents 2EH
DoE Run10	010, 030, 090, 150, 200	T = 130 °C 1.4 equivalents 2EH
DoE Run11	010, 030, 090, 150, 200	T = 130 °C 3.5 equivalents 2EH

9.3 ^{1}H-NMR Spectra

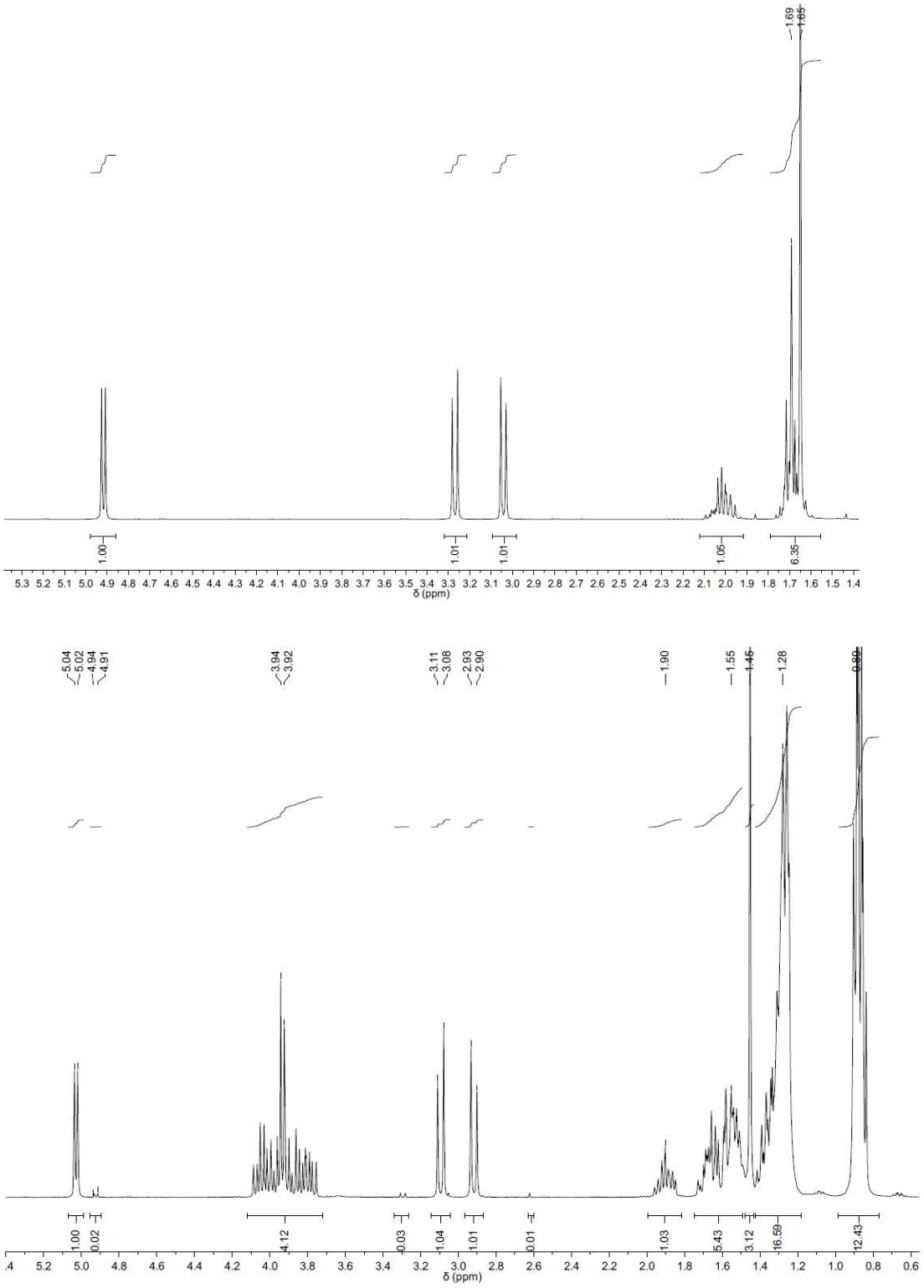

Figure 68: ^{1}H-NMR spectra of purified DAP (top) and DAPHE (bottom). Measured in $CDCl_3$ Bruker Avance II 400 MHz.

9.4 Determination of Kinetics

The kinetics in this work were determined using the progress curve fitting approach, which was kindly provided by Jannis A. Reich from the Institute of Technical Biocatalysis. Kinetic equations have been set up and implemented in the respective Matlab script. Matlab is reading the measurement data from the excel file and is then determining the parameters of the kinetic equations.

The Matlab scripts used are listed below.

9.4.1 Matlab script Diels-Alder reaction of 2MF and MAA

Curve_fit.m

```
%Param_fit_v5 works just like Param_fit_v4.
%Param_fit_v4 was meant to use different experiments (with differing
%numbers of samples) and caluclate kinetic parameters.
%Since all data is saved into one matrix, we need to fill the remaining
%data with 0 (or something). This changes the goodness of the fit and the
%confidence intervals - which is bad!
%For this reason, _v5 will save all data into one vector without the
%addition of zeros.

%What this script does:
%Take data found in excel-files
%turn all data into one big vector
%solve differential equations
%compare the solution to data
%change parameters within the ODE for a better fit
%???
%profit

global c_measured0 N_spec N_experiments N_max_exp N_data_points N_params
N_spec=3; %We have 3 species - will be used for the ode45-given matrix
N_params=1; %Number of kinetic parameters to fit.
param_names={'k1'};  %the fit result will be printed using these names.
units={'Unit1'};

%The name of your excel file that contains your measurments
filename='20200623_Diels-Alder Concentration_Normiert für Matlab';


N=5;
%Number of sheets (counting from 1) you want to use in your excel database

t_measured=cell(N,1); %time of measurement
c_measured=cell(N,1); %measured concentration
c_measured0=zeros(N,N_spec); %starting concentrations

%% Loading Data
disp('Reading excel files...')
%Reading an excel file named filename.
%Each different series of measurements is documented within it's own excel
%sheet.

for i=1:N
```

```
    t_measured{i}=xlsread(filename,i,'J8:J240')';
    %First we save our measurement times in a cell array.
    %Later we will converte it into a matrix since lsqcurvefit wants a vector
    %or matrix for the x_data.


    c_measured{i}=[xlsread(filename,i,'B8:B240')'; xlsread(filename,i,'C8:C240')';
xlsread(filename,i,'D8:D240')'];

    c_measured0(i,:)=[xlsread(filename,i,'E2'); xlsread(filename,i,'E3'); xlsread(filename,i,'E4')];

    fprintf('Loaded %2.0f out of %2.0f.\n',i,N)

end


disp('reading is done.')


N_experiments=size(c_measured0,1);
%Number of data points in each experiment. So N_data_points is a vector
%containing the lengths.


%% Pre-processing
disp('Staring preprocessing...Aka: Turning excel data into one vector');
%Order the data in a nice way so lsqcurvefit can compare two matrizes

C_cleared=cells2vec(c_measured);

t_measured_vector=cells2vec(t_measured);


disp('done preprocessing')


%% Now to the fitting:

disp('Starting fitting')
options = optimoptions('lsqcurvefit','Display','iter',...
    'MaxFunctionEvaluations',1e4,'FunctionTolerance',1e-16);

%You can add a for-loop here to test different starting parameters.
%The solver should arrive at the SAME result independent of the starting
%parameters!!
params0=[0.01]; % or use rand(1,N_params);

params_lb=zeros(1,N_params); %lower bounds for parameters
params_ub=[1000]; %upper bounts for parameters

[params_fit,~,residual,exitflag,~,~,jacobian]=...
    lsqcurvefit(@Conc_Curve_Model_v3,params0,...
     t_measured,C_cleared,params_lb,params_ub,options);

disp('done fitting')

%% Post processing
```

```
disp('Starting post-processing...')
CInt=nlparci(params_fit, residual, 'jacobian', jacobian);
CInt=abs((CInt(:,1)-CInt(:,2))/2);

disp('done post processing')

%% printing results

fprintf('Parameters:\n\t\t  Calculated\t Confi.Int\n')
formatSpec ='%s\t  %6.6f \t\t+- %6.6f \t%s\n';
for i=1:N_params
   fprintf(formatSpec,param_names{i},params_fit(i),CInt(i),units{i})
end



disp('done printing... baka')

%% Calculate using the found parameters

C_simulation=cell(N_experiments,1);
tout=cell(N_experiments,1);

figure

for i=1:N_experiments
   [tout{i},Ctemp]=ode45(@Kinetic,[0 1.1*t_measured{i}(end)],...
      [params_fit, c_measured0(i,:)]);
   C_simulation{i}(1:N_spec,:)=Ctemp(:,N_params+1:N_params+N_spec)';



   plot(tout{i},C_simulation{i});
   hold on
   plot(t_measured{i},c_measured{i},'.');

end
grid
xlabel('time [min]');
ylabel('concentration [mol/L]')

disp('Done and done')
%% Change History
% Jan 2020      - v4 is wrong. Fit results will be better because of the 0.
%               - v5 corrects this.
% November 2018 - Created the script and functions
% January 2019  - Removed typos and added a few comments
% August 2019   - Removed the generation of measurements and changed it so
% the script reads real data and fits those.
```

Kinetic.m

```
function [dx] = Kinetic(t,x)
%MM2SUB Kinetic is used by ode45 to solve differential equations.
%   x contains not only the concentration, but also the kinetic parameters
%   in its first positions.
global N_params N_spec

dx=zeros(size(x));
k1=x(1);
%k2=x(2);


c=x(N_params+1:N_params+N_spec); %c is now [MAA 2MF DAP]
% This way c(1)=cS1, c(2)=cS2 and c(3)=cP for easier rate expressions.

%Another methode:
% v_forward=vmaxf*c(1).*c(2)./(KMS1+c(1))./(KMS2+c(2));
% v_back=vmaxr*c(3)./(KMP+c(3));

%dx(N_params+1)=+v_forward-v_back; %Product
%dx(N_params+2)=-v_back+v_forward; %Substrate


dx(N_params+1)=-k1*c(1)*c(2)+k1*c(3); %Subsrate 1 MAA
dx(N_params+2)=-k1*c(1)*c(2)+k1*c(3); %Substrate 2 2MF
dx(N_params+3)=k1*c(1)*c(2)-k1*c(3); %product 3 DAP


end
```

Conc_Curve_Model_v3.m

```
function [C_to_compare] = Conc_Curve_Model_v3(params,t_measured)
%CONC_CURVE_MODEL is called by the main script curve_fit.
% It takes kinetic parameters and calls an ode-solver to calculate the
% concentration curves of different species. If you change the number of
% parameters make sure to also change the column-indecies that contain the
% relevant concentrations. Otherwise you will compare product-concentration
% curve with substrate-concentrations or parameters.
global c_measured0 N_data_points N_experiments N_max_exp N_spec N_params

%N_data_points is a vector with the number of data points for each
%experiment in each index.
%N_measurements: number of experiments

C_calced=cell(N_experiments,1);
for i=1:N_experiments
   [~,Ctemp]=ode45(@Kinetic,t_measured{i},[params, c_measured0(i,:)]);

   C_calced{i}=Ctemp(:,N_params+1:N_params+N_spec);
   C_calced{i}=C_calced{i}';



end


C_to_compare=cells2vec(C_calced);
%If you want to compare only certain species and not all, just change Line
%18.


end
```

9.4.2 Matlab script Esterification of DAPH and 2EH

Curve_fit.m

```
%Param_fit_v5 works just like Param_fit_v4.
%Param_fit_v4 was meant to use different experiments (with differing
%numbers of samples) and caluclate kinetic parameters.
%Since all data is saved into one matrix, we need to fill the remaining
%data with 0 (or something). This changes the goodness of the fit and the
%confidence intervals - which is bad!
%For this reason, _v5 will save all data into one vector without the
%addition of zeros.

%What this script does:
%Take data found in excel-files
%turn all data into one big vector
%solve differential equations
%compare the solution to data
%change parameters within the ODE for a better fit
%???
%profit

global c_measured0 N_spec N_experiments N_max_exp N_data_points N_params
N_spec=3; %We have 3 species - will be used for the ode45-given matrix
N_params=2; %Number of kinetic parameters to fit.
param_names={'k1' 'k2'};  %the fit result will be printed using these names.
units={'Unit1' 'Unit2'};%

%The name of your excel file that contains your measurments
filename='20200922_Inline Konzentrationen_Kinetik3';



N=3;
%Number of sheets (counting from 1) you want to use in your excel database

t_measured=cell(N,1); %time of measurement
c_measured=cell(N,1); %measured concentration
c_measured0=zeros(N,N_spec); %starting concentrations

%% Loading Data
disp('Reading excel files...')
%Reading an excel file named filename.
%Each different series of measurements is documented within it's own excel
%sheet.

for i=1:N
    t_measured{i}=xlsread(filename,i,'I26:I206')';
    %First we save our measurement times in a cell array.
    %Later we will converte it into a matrix since lsqcurvefit wants a vector
    %or matrix for the x_data.



    c_measured{i}=[xlsread(filename,i,'F26:F206')'; xlsread(filename,i,'G26:G206')';
xlsread(filename,i,'H26:H206')'];

    c_measured0(i,:)=[xlsread(filename,i,'E3'); xlsread(filename,i,'F3'); xlsread(filename,i,'G3')];
```

```
    fprintf('Loaded %2.0f out of %2.0f.\n',i,N)

end


disp('reading is done.')


N_experiments=size(c_measured0,1);
%Number of data points in each experiment. So N_data_points is a vector
%containing the lengths.


%% Pre-processing
disp('Staring preprocessing...Aka: Turning excel data into one vector');
%Order the data in a nice way so lsqcurvefit can compare two matrizes

C_cleared=cells2vec(c_measured);

t_measured_vector=cells2vec(t_measured);


disp('done preprocessing')


%% Now to the fitting:

disp('Starting fitting')
options = optimoptions('lsqcurvefit','Display','iter',...
    'MaxFunctionEvaluations',1e4,'FunctionTolerance',1e-16);

%You can add a for-loop here to test different starting parameters.
%The solver should arrive at the SAME result independent of the starting
%parameters!!
params0=[0.01 0.0002];
params_lb=zeros(1,N_params); %lower bounds for parameters
params_ub=[100 50]; %upper bounds for parameters

[params_fit,~,residual,exitflag,~,~,jacobian]=...
    lsqcurvefit(@Conc_Curve_Model_v3,params0,...
     t_measured,C_cleared,params_lb,params_ub,options);

disp('done fitting')

%% Post processing
disp('Starting post-processing...')
CInt=nlparci(params_fit, residual, 'jacobian', jacobian);
CInt=abs((CInt(:,1)-CInt(:,2))/2);

disp('done post processing')

%% printing results

fprintf('Parameters:\n\t\t  Calculated\t Confi.Int\n')
formatSpec ='%s\t  %6.6f \t\t+- %6.6f \t%s\n';
for i=1:N_params
```

```
    fprintf(formatSpec,param_names{i},params_fit(i),CInt(i),units{i})
end



disp('done printing... baka')

%% Calculate using the found parameters

C_simulation=cell(N_experiments,1);
tout=cell(N_experiments,1);

figure

for i=1:N_experiments
    [tout{i},Ctemp]=ode45(@Kinetic,[0 1.1*t_measured{i}(end)],...
        [params_fit, c_measured0(i,:)]);
    C_simulation{i}(1:N_spec,:)=Ctemp(:,N_params+1:N_params+N_spec)';



    plot(tout{i},C_simulation{i});
    hold on
    plot(t_measured{i},c_measured{i},'.');

end
grid
xlabel('time [min]');
ylabel('concentration [mmol/g]')

disp('Done and done')
%% Change History
% Jan 2020      - v4 is wrong. Fit results will be better because of the 0.
%               - v5 corrects this.
% November 2018 - Created the script and functions
% January 2019  - Removed typos and added a few comments
% August 2019   - Removed the generation of measurements and changed it so
% the script reads real data and fits those.
```

Kinetic.m

```
function [dx] = Kinetic(t,x)
%MM2SUB Kinetic is used by ode45 to solve differential equations.
%   x contains not only the concentration, but also the kinetic parameters
%   in its first positions.
global N_params N_spec

dx=zeros(size(x));
k1=x(1);
k2=x(2);
%k3=x(3);


c=x(N_params+1:N_params+N_spec); %c is now [DAPH 2EH DAPH-Ester]
% This way c(1)=cS1, c(2)=cS2 and c(3)=cP for easier rate expressions.

%Another methode:
% v_forward=vmaxf*c(1).*c(2)./(KMS1+c(1))./(KMS2+c(2));
% v_back=vmaxr*c(3)./(KMP+c(3));

%dx(N_params+1)=+v_forward-v_back; %Product
%dx(N_params+2)=-v_back+v_forward; %Substrate


dx(N_params+1)=-k1*c(1)*c(2)^2+k2*c(3);%Subsrate 1 DAPH
dx(N_params+2)=-k1*2*c(1)*c(2)^2+2*k2*c(3); %Substrate 2 2EH
dx(N_params+3)=k1*c(1)*c(2)^2-k2*c(3); %Product 3 DAPH-Ester




end
```

Conc_Curve_Model_v3.m

```
function [C_to_compare] = Conc_Curve_Model_v3(params,t_measured)
%CONC_CURVE_MODEL is called by the main script curve_fit.
% It takes kinetic parameters and calls an ode-solver to calculate the
% concentration curves of different species. If you change the number of
% parameters make sure to also change the column-indecies that contain the
% relevant concentrations. Otherwise you will compare product-concentration
% curve with substrate-concentrations or parameters.
global c_measured0 N_data_points N_experiments N_max_exp N_spec N_params

%N_data_points is a vector with the number of data points for each
%experiment in each index.
%N_measurements: number of experiments

C_calced=cell(N_experiments,1);
for i=1:N_experiments
   [~,Ctemp]=ode45(@Kinetic,t_measured{i},[params, c_measured0(i,:)]);

   C_calced{i}=Ctemp(:,N_params+1:N_params+N_spec);
   C_calced{i}=C_calced{i}';



end


C_to_compare=cells2vec(C_calced);
%If you want to compare only certain species and not all, just change Line
%18.


end
```

10 References

Adlercreutz, P., Immobilisation and application of lipases in organic media. *Chemical Society reviews* **2013,** *42* (15), 6406–6436.

Agirre, I.; Gandarias, I.; Granados, M. L.; Arias, P. L., Process design and techno-economic analysis of gas and aqueous phase maleic anhydride production from biomass-derived furfural. *Biomass Conv. Bioref.* **2020,** *10* (4), 1021–1033.

Alatalo, H.; Kohonen, J.; Qu, H.; Hatakka, H.; Reinikainen, S.-P.; Louhi-Kultanen, M.; Kallas, J., In-line monitoring of reactive crystallization process based on ATR-FTIR and Raman spectroscopy. *J. Chemometrics* **2008,** *22* (11-12), 644–652.

Allsopp, M. W.; Vianello, G., Poly(Vinyl Chloride). *Ullmann's encyclopedia of industrial chemistry*; Wiley: Chichester, **2010**.

Alsmeyer, F.; Koss, H.-J.; Marquardt, W., Indirect spectral hard modeling for the analysis of reactive and interacting mixtures. *Applied spectroscopy* **2004,** *58* (8), 975–985.

Anastas, P. T.; Zimmerman, J. B., Design through the 12 principles of green engineering. *Environmental science & technology* **2003,** *37* (5), 94A-101A.

Andrady, A. L.; Neal, M. A., Applications and societal benefits of plastics. *Philosophical transactions of the Royal Society of London. Series B, Biological sciences* **2009,** *364* (1526), 1977–1984.

Arnold, F. H., Directed Evolution: Bringing New Chemistry to Life. *Angewandte Chemie (International ed. in English)* **2018,** *57* (16), 4143–4148.

Audic, J.-L.; Lemiègre, L.; Corre, Y.-M., Thermal and mechanical properties of a polyhydroxyalkanoate plasticized with biobased epoxidized broccoli oil. *J. Appl. Polym. Sci.* **2014,** *131* (6), n/a-n/a.

Averett, L. A.; Griffiths, P. R.; Nishikida, K., Effective path length in attenuated total reflection spectroscopy. *Analytical chemistry* **2008,** *80* (8), 3045–3049.

Barnicki, S. D. *Synthetic Organic Chemicals*. *Handbook of industrial chemistry and biotechnology*, 12th ed. 2012; Springer: Boston, MA, **2012**.

BASF SE, Hexamoll® DINCH BMB. https://products.basf.com/global/en/cp/hexamoll-dinch-bmb.html (accessed March 13, **2021**).

Bocqué, M.; Voirin, C.; Lapinte, V.; Caillol, S.; Robin, J.-J., Petro-based and bio-based plasticizers: Chemical structures to plasticizing properties. *J. Polym. Sci. Part A: Polym. Chem.* **2016,** *54* (1), 11–33.

Bond, G. C., Platinum Metals as Hydrogenation Catalysts. *Platinum Metals Rev* **1957,** *1* (3), 87–93.

Bouchareb, B.; Benaniba, M. T., Effects of epoxidized sunflower oil on the mechanical and dynamical analysis of the plasticized poly(vinyl chloride). *J. Appl. Polym. Sci.* **2008,** *107* (6), 3442–3450.

Braun, D., Controlled free-radical polymerization of vinyl chloride. *J Vinyl Addit Technol* **2005,** *11* (3), 86–90.

Breitscheidel, B., Alternative to phthalates also for adhesives and sealants. *Adhes Adhes Sealants* **2013,** *10* (1), 19–21.

Búcsi, A.; Szőcs, F., Kinetics of radical generation in PVC with dibenzoyl peroxide utilizing high-pressure technique. *Macromol. Chem. Phys.* **2000,** *201* (4), 435–438.

Bueschler, V., Inline Process Analytics for Bio-based Plasticiser Synthesis. Masterthesis; Hamburg University of Technology, Hamburg, **2020**.

Buser, J. Y.; McFarland, A. D., Reaction characterization by flow NMR: quantitation and monitoring of dissolved H_2 via flow NMR at high pressure. *Chemical communications (Cambridge, England)* **2014,** *50* (32), 4234–4237.

Calbry-Muzyka, A. S.; Indlekofer, J.; Schneebeli, J.; Biollaz, S. M. A., Online Measurement of Sub-ppm v Total Sulfur in Biogas by Chemiluminescence. *Energy Fuels* **2019,** *33* (10), 9859–9869.

Carneiro de Oliveira, J.; Laborie, M.-P.; Roucoules, V., Thermodynamic and Kinetic Study of Diels-Alder Reaction between Furfuryl Alcohol and N-Hydroxymaleimides-An Assessment for Materials Application. *Molecules (Basel, Switzerland)* **2020,** *25* (2).

Casado, J.; Lopez-Quintela, M. A.; Lorenzo-Barral, F. M., The initial rate method in chemical kinetics: Evaluation and experimental illustration. *J. Chem. Educ.* **1986,** *63* (5), 450.

Casas, A.; Ramos, Maria Jesus, Rodriguez, Juan Francisco; Perez, A., Tin compounds as Lewis acid catalysts for esterification and transesterification of acid vegetable oils. *Fuel Processing Technology* **2013,** No. 106, 321–325.

Christen, V.; Crettaz, P.; Oberli-Schrämmli, A.; Fent, K., Antiandrogenic activity of phthalate mixtures: validity of concentration addition. *Toxicology and applied pharmacology* **2012,** *259* (2), 169–176.

Chung, K.-H.; Park, B.-G., Esterification of oleic acid in soybean oil on zeolite catalysts with different acidity. *Journal of Industrial and Engineering Chemistry* **2009,** *15* (3), 388–392.

Claaßen, C.; Mack, K.; Rother, D., Benchtop NMR for Online Reaction Monitoring of the Biocatalytic Synthesis of Aromatic Amino Alcohols. *ChemCatChem* **2020,** *12* (4), 1190–1199.

Daniels, P. H., A brief overview of theories of PVC plasticization and methods used to evaluate PVC-plasticizer interaction. *J Vinyl Addit Technol* **2009,** *15* (4), 219–223.

Danso, D.; Schmeisser, C.; Chow, J.; Zimmermann, W.; Wei, R.; Leggewie, C.; Li, X.; Hazen, T.; Streit, W. R., New Insights into the Function and Global Distribution of Polyethylene Terephthalate (PET)-Degrading Bacteria and Enzymes in Marine and Terrestrial Metagenomes. *Applied and environmental microbiology* **2018,** *84* (8).

Desimoni, G.; Faita, G.; Righetti, P. P.; Sfulcini, A.; Tsyganov, D., Solvent effect in pericyclic reactions. IX. The ene reaction. *Tetrahedron* **1994,** *50* (6), 1821–1832.

Diels, O.; Alder, K., Synthesen in der hydroaromatischen Reihe. *Justus Liebigs Ann. Chem.* **1928,** *460* (1), 98–122.

Diels, O.; Alder, K., Synthesen in der hydroaromatischen Reihe. III. Mitteilung: Synthese von Terpenen, Camphern, hydroaromatischen und heterocyclischen Systemen. *Justus Liebigs Ann. Chem.* **1929,** *470* (1), 62–103.

Dinç, E.; Ustündağ, O.; Baleanu, D., Simultaneous chemometric determination of pyridoxine hydrochloride and isoniazid in tablets by multivariate regression methods. *Drug testing and analysis* **2010,** *2* (8), 383–387.

Dong, F.; Zhu, Y.; Ding, G.; Cui, J.; Li, X.; Li, Y., One-step Conversion of Furfural into 2-Methyltetrahydrofuran under Mild Conditions. *ChemSusChem* **2015,** *8* (9), 1534–1537.

Eggelte, T. A.; Koning, H. de; Huisman, H. O., Synthesis and Some Reductions of Endo and Exo-3,6-epoxy-Tetrathydrophthalic Anhydride. *Tetrahedron* **1973,** *29* (16), 2445–2447.

Erickson, Britt E., EU members agree to restrict 4 phthalates. https://cen.acs.org/policy/chemical-regulation/EU-members-agree-restrict-4/96/i30.

Feng, L.; Berglund, K. A., ATR-FTIR for Determining Optimal Cooling Curves for Batch Crystallization of Succinic Acid. *Crystal Growth & Design* **2002,** *2* (5), 449–452.

Fenollar, O.; Garcia-Sanoguera, D.; Sanchez-Nacher, L.; Lopez, J.; Balart, R., Effect of the epoxidized linseed oil concentration as natural plasticizer in vinyl plastisols. *J Mater Sci* **2010,** *45* (16), 4406–4413.

Fischer, A.; Müller, K.; Arlt, W., Measurement of Micro Kinetics of Hydrogenation in Liquid Phase Using Raman Spectroscopy. *Chem. Eng. Technol.* **2017,** *40* (1), 56–63.

Fischer, E.; Speier, A., Darstellung der Ester. *Berichte der deutschen chemischen Gesellschaft* **1895,** *28* (3), 3252–3258.

Fischer, F.; Tropsch, H., Über die Herstellung synthetischer Olgemische (Synthol) durch Aufbau aus Kohlenoxyd und Wasserstoff. *Brennstoff-Chemie* **1923,** *4*, 276–285.

Fisser, M.; Badcock, R. A.; Teal, P. D.; Hunze, A., Optimizing the sensitivity of palladium based hydrogen sensors. *Sensors and Actuators B: Chemical* **2018,** *259*, 10–19.

Froidevaux, V.; Borne, M.; Laborbe, E.; Auvergne, R.; Gandini, A.; Boutevin, B., Study of the Diels–Alder and retro-Diels–Alder reaction between furan derivatives and maleimide for the creation of new materials. *RSC Adv.* **2015,** *5* (47), 37742–37754.

Fu, Q.; Long, Y.; Gao, Y.; Ling, Y.; Qian, H.; Wang, F.; Zhu, X., Synthesis and properties of castor oil based plasticizers. *RSC Adv.* **2019,** *9* (18), 10049–10057.

Funel, J.-A.; Abele, S., Industrial applications of the Diels-Alder reaction. *Angewandte Chemie (International ed. in English)* **2013,** *52* (14), 3822–3863.

Gandarias, I.; García-Fernández, S.; Obregón, I.; Agirrezabal-Telleria, I.; Arias, P. L., Production of 2-methylfuran from biomass through an integrated biorefinery approach. *Fuel Processing Technology* **2018,** *178*, 336–343.

Gandini, A.; Coelho, D.; Silvestre, A. J.D., Reversible click chemistry at the service of macromolecular materials. Part 1: Kinetics of the Diels–Alder reaction applied to furan–maleimide model compounds and linear polymerizations. *European Polymer Journal* **2008,** *44* (12), 4029–4036.

Geyer, R., Production, use, and fate of synthetic polymers. In *Plastic waste and recycling*: *Environmental impact, societal issues, prevention, and solutions*; Letcher, T. M., Ed.; Elsevier, **2020**; pp 13–32.

Gheneim, R.; Perez-Berumen, C.; Gandini, A., Diels−Alder Reactions with Novel Polymeric Dienes and Dienophiles: Synthesis of Reversibly Cross-Linked Elastomers. *Macromolecules* **2002,** *35* (19), 7246–7253.

Gibanel, F.; López, M. C.; Royo, F. M.; Pardo, J.; Urieta, J. S., Solubility of 13 non-polar gases (He, Ne, Ar, Kr, Xe, H2, D2, N2, CH4, C2H4, C2H6, CF4 and SF6) in 2-methyltetrahydrofuran at 273.15 to 303.15 K and 101.33 kPa partial pressure of gas. *Fluid Phase Equilibria* **1993,** *87* (2), 285–294.

Gold.de, Palladiumpreis aktuell in Euro und Dollar. https://www.gold.de/kurse/palladiumpreis/ (accessed October 5, **2020**).

Gomes Almeida, A.; Meneses, A. C. de; Araújo, P. H. H. de; Oliveira, D. de, A review on enzymatic synthesis of aromatic esters used as flavor ingredients for food, cosmetics and pharmaceuticals industries. *Trends in Food Science & Technology* **2017,** No. 69, 95–105.

Greco, A.; Maffezzoli, A., Cardanol derivatives as innovative bio-plasticizers for poly-(lactic acid). *Polymer Degradation and Stability* **2016,** *132*, 213–219.

Gregoritza, M.; Brandl, F. P., The Diels-Alder reaction: A powerful tool for the design of drug delivery systems and biomaterials. *European journal of pharmaceutics and biopharmaceutics : official journal of Arbeitsgemeinschaft fur Pharmazeutische Verfahrenstechnik e.V* **2015,** *97* (Pt B), 438–453.

Groot, W. J.; Borén, T., Life cycle assessment of the manufacture of lactide and PLA biopolymers from sugarcane in Thailand. *The International Journal of Life Cycle Assessment,* **2010,** *15* (9), 970–984.

Hamminga, G. M.; Mul, G.; Moulijn, J. A., Real-time in situ ATR-FTIR analysis of the liquid phase hydrogenation of γ -butyrolactone over Cu-ZnO catalysts: A mechanistic study by varying lactone ring size. *Chemical Engineering Science* **2004,** *59* (22-23), 5479–5485.

Hiessl, R., Development and Validation of a Space Resolved Inline Measurement Technique for Biocatalyzed Reactive Distillation. Master Thesis; Hamburg University of Technology, Hamburg, **2016**.

Hiessl, R.; Hennecke, L.; Plass, C.; Kleber, J.; Wahlefeld, S.; Otter, R.; Gröger, H.; Liese, A., FTIR based kinetic characterisation of an acid-catalysed esterification of 3-methylphthalic anhydride and 2-ethylhexanol. *Analytical methods : advancing methods and applications* **2020,** *12* (24), 3137–3144.

Hiessl, Robert, Liese, Andreas. *Inline analytical supported process development towards alternative bio-based plasticizers*. *Category 1 - Sustainability: How to improve a sustainable use plasticisers and/or flexible vinyl*, **2020**.

Hilterhaus, L.; Thum, O.; Liese, A., Reactor Concept for Lipase-Catalyzed Solvent-Free Conversion of Highly Viscous Reactants Forming Two-Phase Systems. *Org. Process Res. Dev.* **2008,** *12* (4), 618–625.

Ho A Kwie, F.; Baudoin-Dehoux, C.; Blonski, C.; Lherbet, C., Bismuth(III) Triflate: A Safe and Easily Handled Precursor for Triflic Acid: Application to the Esterification Reaction. *Synthetic Communications* **2010,** *40* (7), 1082–1087.

Hogue, C., U.S. to restrict 5 phthalates in children's products: Chemical industry criticizes agency for limiting DINP. https://cen.acs.org/articles/95/i43/US-restrict-5-phthalates-childrens.html?utm_source=YMAL&utm_medium=YMAL&utm_campaign=CEN&utm_content=pos1 (accessed August 20, **2020**).

Horiuti, I.; Polanyi, M., Exchange reactions of hydrogen on metallic catalysts. *Trans. Faraday Soc.* **1934,** *30*, 1164.

Hosney, H.; Nadiem, B.; Ashour, I.; Mustafa, I.; El-Shibiny, A., Epoxidized vegetable oil and bio-based materials as PVC plasticizer. *J. Appl. Polym. Sci.* **2018,** *135* (20), 46270.

Hu, Y.; Liu, C.; Wang, P.; Li, G.; Wang, A.; Cong, Y.; Liang, X.; Li, W.; Zhang, X.; Li, N., Sustainable Production of Safe Plasticizers with Bio-Based Fumarates and 1,3-Dienes. *Ind. Eng. Chem. Res.* **2020,** *59* (16), 7367–7374.

INOVYN. *INOVYN launches World's first commercially available grade of bio-attributed PVC*: London, **2019**.

Jackson, S. D. *Hydrogenation;* De Gruyter: Berlin, Boston, **2018**.

Jia, P.; Xia, H.; Tang, K.; Zhou, Y., Plasticizers Derived from Biomass Resources: A Short Review. *Polymers* **2018,** *10* (12).

Jia, P.; Zhang, M.; Hu, L.; Zhou, Y., Green plasticizers derived from soybean oil for poly(vinyl chloride) as a renewable resource material. *Korean J. Chem. Eng.* **2016,** *33* (3), 1080–1087.

Kamo, B.; Morita, I.; Horie, S.; Furusawa, S., Radical Polymerization of Furan with Maleic Anhydride through the Diels—Alder Adduct. *Polymer Journal* **1974,** *6* (2), 121–131.

Kang, J.; Liang, X.; Guliants, V. V., Selective Hydrogenation of 2-Methylfuran and 2,5-Dimethylfuran over Atomic Layer Deposited Platinum Catalysts on Multiwalled Carbon Nanotube and Alumina Supports. *ChemCatChem* **2017,** *9* (2), 282–286.

Kessler, W. *Multivariate Datenanalyse für die Pharma-, Bio- und Prozessanalytik*. *Ein Lehrbuch*, 1. Aufl., 1. Nachdr; WILEY-VCH: Weinheim, **2008**.

Killner, M. H.M.; Rohwedder, J. J.R.; Pasquini, C., A PLS regression model using NIR spectroscopy for on-line monitoring of the biodiesel production reaction. *Fuel* **2011,** *90* (11), 3268–3273.

Knöpke, L. R.; Nemati, N.; Köckritz, A.; Brückner, A.; Bentrup, U., Reaction Monitoring of Heterogeneously Catalyzed Hydrogenation of Imines by Coupled ATR-FTIR, UV/Vis, and Raman Spectroscopy. *ChemCatChem* **2010,** *2* (3), 273–280.

Koleske, J. V.; Tan, P.; Krauskopf, L. G., Plasticizers. *Paint and Coating Testing Manual*, **2012**, 136-139.

Kriesten, E.; Mayer, D.; Alsmeyer, F.; Minnich, C. B.; Greiner, L.; Marquardt, W., Identification of unknown pure component spectra by indirect hard modeling. *Chemometrics and Intelligent Laboratory Systems* **2008,** *93* (2), 108–119.

Kucherov, F. A.; Galkin, K. I.; Gordeev, E. G.; Ananikov, V. P., Efficient route for the construction of polycyclic systems from bioderived HMF. *Green Chem* **2017,** *19* (20), 4858–4864.

Kumar, S., Recent Developments of Biobased Plasticizers and Their Effect on Mechanical and Thermal Properties of Poly(vinyl chloride): A Review. *Ind. Eng. Chem. Res.* **2019,** *58* (27), 11659–11672.

Kundoch, J.-O., Charakterisierung und Identifizierung von Biokatalysatoren für die Hydrolyse und Synthese von zweifach-veresterten Cyclohexandiecarbonsäuren. Masterthesis; Hamburg University of Technology, Hamburg, **2019**.

Laidler, K. J., Units of an equilibrium constant. *J. Chem. Educ.* **1990,** *67* (1), 88.

Landau, R. N.; Singh, U.; Gortsema, F.; Sun, Y. K.; Gomolka, S. C.; Lam, T.; Futran, M.; Blackmond, D. G., A Reaction Calorimetric Investigation of the Hydrogenation of a Substituted Pyrazine. *Journal of Catalysis* **1995,** *157* (1), 201–208.

Li, J. J. *Name Reactions*. *A Collection of Detailed Mechanisms and Synthetic Applications;* Springer International Publishing Switzerland, **2014**.

Libardi, J.; Ravagnani, S. P.; Morais, A. M. F.; Cardoso, A. R., Study of plasticizer diffusion in a solid rocket motor's bondline. *JATM* **2009,** *1* (2), 223–229.

Lin, P.; Chen, Y.; He, Y., Identification of Geographical Origin of Olive Oil Using Visible and Near-Infrared Spectroscopy Technique Combined with Chemometrics. *Food Bioprocess Technol* **2012,** *5* (1), 235–242.

Littler, B. J.; Looker, A. R.; Blythe, T. A., Optimization of a Hydrogenation Process using Real-Time Mid-IR, Heat Flow and Gas Uptake Measurements. *Org. Process Res. Dev.* **2010,** *14* (6), 1512–1517.

Liu, X.; Du, P.; Liu, L.; Zheng, Z.; Wang, X.; Joncheray, T.; Zhang, Y., Kinetic study of Diels–Alder reaction involving in maleimide–furan compounds and linear polyurethane. *Polym. Bull.* **2013,** *70* (8), 2319–2335.

Lopez Haro, F., Hydrolysis of plasticizer analogues by thermophilic microorganisms and their enzymes. Masterthesis; Hamburg University of Technology, Hamburg, 2020.

Lozano, M.; Cid, J., DEHP plasticizer and blood bags: challenges ahead. *VOXS* **2013,** *8* (1), 127–130.

Machado, Reinaldo M. *Fundamentals of Mass Transfer and Kinetics for the Hydrogenation of Nitrobenzene to Aniline*, **2007**.

Mahmoud, E.; Watson, D. A.; Lobo, R. F., Renewable production of phthalic anhydride from biomass-derived furan and maleic anhydride. *Green Chem* **2014,** *16* (1), 167–175.

Martín, J. R.; Nus, M.; Gago, J. V. S.; Sánchez-Montero, J. M., Selective esterification of phthalic acids in two ionic liquids at high temperatures using a thermostable lipase of Bacillus thermocatenulatus: A comparative study. *Journal of Molecular Catalysis B: Enzymatic* **2008,** *52-53*, 162–167.

Martino-Andrade, A. J.; Chahoud, I., Reproductive toxicity of phthalate esters. *Molecular nutrition & food research* **2010,** *54* (1), 148–157.

Melzak, K. A.; Uhlig, S.; Kirschhöfer, F.; Brenner-Weiss, G.; Bieback, K., The Blood Bag Plasticizer Di-2-Ethylhexylphthalate Causes Red Blood Cells to Form Stomatocytes, Possibly by Inducing Lipid Flip-Flop. *Transfusion medicine and hemotherapy* **2018,** *45* (6), 413–422.

Menne, A., Fully bio-based plasticizers. *Adhes Adhes Sealants* **2015,** *12* (2), 14–15.

Menschutkin, N., Beiträge zur Kenntnis der Affinitätskoeffizienten der Alkylhaloide und der organischen Amine. *Zeitschrift für Physikalische Chemie* **1890a,** *5U* (1).

Menschutkin, N., Über die Affinitätskoeffizienten der Alkylhaloide und der Amine. *Zeitschrift für Physikalische Chemie* **1890b,** *6U* (1).

Meyberg, M.; Roessler, F., In Situ Measurement of Steady-State Hydrogen Concentrations during a Hydrogenation Reaction in a Gas-Inducing Stirred Slurry Reactor. *Ind. Eng. Chem. Res.* **2005,** *44* (25), 9705–9711.

Meyer-Kirschner, J.; Kather, M.; Pich, A.; Engel, D.; Marquardt, W.; Viell, J.; Mitsos, A., In-line Monitoring of Monomer and Polymer Content During Microgel Synthesis Using Precipitation Polymerization via Raman Spectroscopy and Indirect Hard Modeling. *Applied spectroscopy* **2016,** *70* (3).

Minnich, C.; Hardy, S.; Krämer, S., Stopping the Babylonian Confusion: An Updated Nomenclature for Process Analyzers in PAT Applications. *Chemie Ingenieur Technik* **2016,** *88* (6), 694–697.

Mueller, J. J.; Baum, S.; Hilterhaus, L.; Eckstein, M.; Thum, O.; Liese, A., Simultaneous determination of mono-, di-, and triglycerides in multiphase systems by online Fourier transform infrared spectroscopy. *Analytical chemistry* **2011,** *83* (24), 9321–9327.

Nagrockiene, D.; Pundienė, I.; Kicaite, A., The effect of cement type and plasticizer addition on concrete properties. *Construction and Building Materials* **2013,** *45*, 324–331.

Normann, W., Patent: Process for the Conversion of Unsaturated Fatty Acids or Their Glycerides into Saturated Compounds **1902,** No. 141,029.

O'Brien, D. F.; Gates, J. W., The Configurations of the 2,3-Epoxides of Some Diels-Alder Adducts of 1,4-Benzoquinones. *J. Org. Chem.* **1965,** *30* (8), 2593–2601.

Omar, B. M.; Bita, M.; Louafi, I.; Djouadi, A., Esterification process catalyzed by ZSM-5 zeolite synthesized via modified hydrothermal method. *MethodsX* **2018,** *5*, 277–282.

Otto, S.; Bertoncin, F.; Engberts, J. B. F. N., Lewis Acid Catalysis of a Diels−Alder Reaction in Water. *J. Am. Chem. Soc.* **1996,** *118* (33), 7702–7707.

Pace, V.; Hoyos, P.; Fernández, M.; Sinisterra, J. V.; Alcántara, A. R., 2-Methyltetrahydrofuran as a suitable green solvent for phthalimide functionalization promoted by supported KF. *Green Chem* **2010,** *12* (8), 1380.

Pinna, F.; Menegazzo, F.; Signoretto, M.; Canton, P.; Fagherazzi, G.; Pernicone, N., Consecutive hydrogenation of benzaldehyde over Pd catalysts: Influence of supports and sulfur poisoning. *Applied Catalysis A: General* **2001,** *219* (1), 195–200.

Plass, C. *Planned Dissertation*. *University of Bielefeld*, **2020**.

Plass, C.; Hiessl, R.; Kleber, J.; Grimm, A.; Langsch, A.; Otter, R.; Liese, A.; Gröger, H., Towards bio-based plasticizers with reduced toxicity: Synthesis and performance testing of a 3-methylphthalate. *Sustainable Chemistry and Pharmacy* **2020,** *18*, 100319.

Raj, K.; Partow, S.; Correia, K.; Khusnutdinova, A. N.; Yakunin, A. F.; Mahadevan, R., Biocatalytic production of adipic acid from glucose using engineered Saccharomyces cerevisiae. *Metabolic engineering communications* **2018,** *6*, 28–32.

Reinecke, H.; Navarro, R.; Pérez, M., Plasticizers. *Encyclopedia of polymer science and technology*; Wiley Interscience: Hoboken, NJ, **2004**.

Renon, H.; Prausnitz, J. M., Local compositions in thermodynamic excess functions for liquid mixtures. *AIChE J.* **1968,** *14* (1), 135–144.

Riechert, O.; Husham, M.; Sadowski, G.; Zeiner, T., Solvent effects on esterification equilibria. *AIChE J.* **2015,** *61* (9), 3000–3011.

Roberge, S.; Dubé, M. A., Inline monitoring of styrene/butyl acrylate miniemulsion polymerization with attenuated total reflectance/Fourier transform infrared spectroscopy. *J. Appl. Polym. Sci.* **2007,** *103* (1), 46–52.

Roelen, O., Verfahren zur Herstellung von sauerstoffhaltigen Verbindungen, **1938**.

Rueping, M.; Bootwicha, T.; Sugiono, E., Continuous-flow catalytic asymmetric hydrogenations: Reaction optimization using FTIR inline analysis. *Beilstein journal of organic chemistry* **2012,** *8*, 300–307.

Schade, Y., Systematische Untersuchung von Hydrolasen für die biokatalytische Synthese von Weichmachermolekülen. Bachelorthesis; Hamburg University of Technology, Hamburg, 2018.

Sears, J.; Touchette, N.; Darby, J., Applied Polymer Science: Plasticizers. *ACS Symposium Series*, **1985**, 611–641.

Sellin, D.; Hiessl, R.; Bothe, M.; Timmermann, J.; Becker, M.; Schlüter, M.; Liese, A., Simultaneous local determination of mass transfer and residence time distributions in organic multiphase systems. *Chemical Engineering Journal* **2017,** No. 321, 635–641.

Semeijn, V. P., Schur, K. M. *Decarbonisation options for the Dutch PVC industry*, **2020**.

Siracusa, V.; Blanco, I.; Romani, S.; Tylewicz, U.; Rocculi, P.; Rosa, M. D., Poly(lactic acid)-modified films for food packaging application: Physical, mechanical, and barrier behavior. Journal of Applied Polymer Science **2012,** *2* (125), 390–401.

Solntsev, K. M.; Huppert, D.; Agmon, N., Challenge in Accurate Measurement of Fast Reversible Bimolecular Reaction. *J. Phys. Chem. A* **2001,** *105* (24), 5868–5876.

Sparks, B. G.; Poling, B. E., Energy storage capacity of reversible liquid-phase Diels Alder reaction between maleic anhydride and 2-methyl furan. *AIChE J.* **1983,** *29* (4), 534–537.

Stirn, Z.; Rucigaj, A.; Krajnc, M., Characterization and kinetic study of Diels-Alder reaction: Detailed study on N-phenylmaleimide and furan based benzoxazine with potential self-healing application. *Express Polym. Lett.* **2016,** *10* (7), 537–547.

Suter, H., Kontinuierliche Herstellung von Phthalsäureestern aus Phthalsäureanhydrid und hochsiedenden Alkoholen. *Chemie Ingenieur Technik* **1969,** *41* (17), 971–974.

Thiyagarajan, S.; Genuino, H. C.; Śliwa, M.; van der Waal, J. C.; Jong, E. de; van Haveren, J.; Weckhuysen, B. M.; Bruijnincx, P. C. A.; van Es, D. S., Substituted Phthalic Anhydrides from Biobased Furanics: A New Approach to Renewable Aromatics. *ChemSusChem* **2015,** *8* (18), 3052–3056.

Tijssen, K. C. H.; van Weerdenburg, B. J. A.; Zhang, H.; Janssen, J. W. G.; Feiters, M. C.; van Bentum, P. J. M.; Kentgens, A. P. M., Monitoring Heterogeneously Catalyzed Hydrogenation Reactions at Elevated Pressures Using In-Line Flow NMR. *Analytical chemistry* **2019,** *91* (20), 12636–12643.

Toppinen, S.; Salmi, T.; Rantakylä, T.-K.; Aittamaa, J., Liquid-Phase Hydrogenation Kinetics of Aromatic Hydrocarbon Mixtures. *Ind. Eng. Chem. Res.* **1997,** *36* (6), 2101–2109.

Tullo, A. H., Plasticizer Makers Want A Piece Of The Phthalates Pie: Chemical firms makers see a big opportunity from the phaseout of phthalate esters. *Chemical & Engineering News*, **2015**. https://cen.acs.org/articles/93/i25/Plasticizer-Makers-Want-Piece-Phthalates.html (accessed August 18, 2020).

Udatha, D. B. R. K. G.; Sugaya, N.; Olsson, L.; Panagiotou, G., How well do the substrates KISS the enzyme? Molecular docking program selection for feruloyl esterases. *Scientific reports* **2012,** *2*, 323.

Umweltbundesamt, Stoffmonographie für 1,2-Cyclohexandicarbonsäure-di-isononylester (Hexamoll® DINCH®) - HBM-Werte für die Summe der Metabolite Cyclohexan-1,2-dicarbonsäure-mono-hydroxyisononylester (OH-MINCH) und Cyclohexan-1,2-dicarbonsäure-mono-carboxy-isooctylester (cx-MINCH) im Urin von Erwachsenen und Kindern: Stellungnahme der Kommission "Human-Biomonitoring" des Umweltbundesamtes. *Bundesgesundheitsblatt, Gesundheitsforschung, Gesundheitsschutz* **2014,** *57* (12), 1451–1461.

United Nations. *Transforming our World: The 2030 Agenda for Sustainable Development*. *A/RES/70/1*, 2015.

VinylPlus. *Progress Report 2020*. *Reporting on 2019 Activities*, **2020**.

Wadey, B. L., An innovative plasticizer for sensitive applications. *J Vinyl Addit Technol* **2003,** *9* (4), 172–176.

Westerterp, K. R.; Molga, E. J.; van Gelder, K. B., Catalytic hydrogenation reactors for the fine chemicals industries. Their design and operation. *Chemical Engineering and Processing: Process Intensification* **1997,** *36* (1), 17–27.

Wijnen, J. W.; Engberts, J. B. F. N., Retro-Diels-Alder Reaction in Aqueous Solution: Toward a Better Understanding of Organic Reactivity in Water. *The Journal of organic chemistry* **1997,** *62* (7), 2039–2044.

PVC handbook; Wilkes, C. E., Summers, J. W., Daniels, C. A., Berard, M. T., Eds., 1. ed.; Hanser; Hanser Gardner: München, Cincinnati, Ohio, **2005**.

Williams, C. L.; Chang, C.-C.; Do, P.; Nikbin, N.; Caratzoulas, S.; Vlachos, D. G.; Lobo, R. F.; Fan, W.; Dauenhauer, P. J., Cycloaddition of Biomass-Derived Furans for Catalytic Production of Renewable p -Xylene. *ACS Catal.* **2012,** *2* (6), 935–939.

Wisniak, J., The History of Catalysis. From the Beginning to Nobel Prizes. *Educación Química* **2010,** *21* (1), 60–69.

Wold, S.; Martens, H.; Wold, H., The multivariate calibration problem in chemistry solved by the PLS method. *Matrix Pencils* **1983,** *973*, 286–293.

Woodward, R. B.; Baer, H., The Reaction of Furan with Maleic Anhydride 1. Journal of the American Chemical Society, 70(3), 1161-1166 **1948**.

Woodward, R. B.; Sondheimer, F.; Taub, D.; Heusler, K.; McLamore, W. M., The Total Synthesis of Steroids 1. *J. Am. Chem. Soc.* **1952,** *74* (17), 4223–4251.

Wypych, G. *PVC Degradation and Stabilization;* Elsevier, **2015**.

Handbook of plasticizers; Wypych, G., Ed., 3rd edition; ChemTec Publishing: Toronto, **2017**.

Zientek, N.; Laurain, C.; Meyer, K.; Kraume, M.; Guthausen, G.; Maiwald, M., Simultaneous 19F-1H medium resolution NMR spectroscopy for online reaction monitoring. *Journal of magnetic resonance* **2014,** *249*, 53–62.